Doctoral Dissertation (Shinshu University)

Development of magnetic carbon nanomaterials for high performance microwave absorption
（高性能マイクロ波吸収用磁性カーボンナノ材料の創製）

September 2022

LI FENGYU

Contents

Abstract

The rapid development of communication technology not only brings convenience to life, but also brings electromagnetic radiation pollution, which affects the operation state of precision instruments and may threaten human health. Therefore, research and development on microwave absorption materials has become the focus of attention. Compared with other nanomaterials, carbon materials have become research focus of microwave absorption composites due to their special mechanism and simple synthesis method. But poor impedance results from high dielectric constant matching makes carbon materials remain difficult for preparing excellent microwave absorption materials. Meanwhile, multilayer composites also show potential to regulating microwave absorption performance. However, multilayer composite structure has complex parameters which makes it difficult to optimize properties with simple experimental methods. In order to improve performance of carbon materials and efficiently optimize the structural parameters of multilayer composites, high-performance magnetic carbon-based composites using biomass materials and metal organic framework are prepared, and structures of multilayer composites is optimized by genetic algorithm and finite element analysis. The significant work is as follows:

(1) Biomass derivatives are being extensively studied for microwave absorption because of their simple and environment-friendly preparation

process. Herein, we report a facile and low-cost method wherein egg white is used as a carbon and sulfur source for the first time. Meanwhile a trimetallic alloy derived from cobalt nitrate, ferric nitrate, and nickel nitrate is used as the magnetic component to fabricate microwave absorption materials. The amount of alloy can regulate the microwave absorption performance of egg-white-derived carbon. The strongest reflection loss (−47.09 dB) of the obtained composites can be achieved at 13.8 GHz with an ultrathin thickness (1 mm). The analysis of dielectric and magnetic constant reveals that the introduced alloy affects dielectric loss while increasing the amount of alloy affect magnetic loss more obviously. This study not only evidence that egg-white-derived carbon flakes can absorb microwaves but also reveals the role of alloy introduction in enhancing microwave attenuation capability.

(2) Template-free strategy has been widely used to prepare microwave absorption materials, but it still remains hard to achieve full X band (8.2-12.4 GHz) absorption at a thin thickness. Herein, NiCo alloy and N co-doped carbon with spontaneous three-dimensional network was obtained by preparing precursors using Ni^{2+} and Co^{2+} to be designed into zeolitic imidazolate frameworks (ZIF). The morphology of composites is able to be controlled by regulating Ni/Co ratios in crystallization. During pyrolysis, 3D network structure with N-doped carbon and NiCo alloy can be catalyzed to form under a specific Ni/Co ratio. Excellent microwave absorption performance, the minimum reflection loss is -41.9 dB at 1.5 mm and entire X band absorption at 2.6mm, is achieved. The 3D network

structure containing N-doped carbon and NiCo alloy not only provide favorable dielectric and magnetic loss, but also have a crucial impact on reflection and scattering of incident microwave. The mechanism of dielectric loss including polarization relaxation, conductive loss and magnetic loss derived from resonance also is investigated. The chemical components and network structure controlled by ZIF-derived strategy have practical research value to improve microwave absorption performance.

(3) Multilayer composites can be used to prepare controllable microwave absorption materials by using specific materials or structures. But calculation with complex parameters limits optimization efficiency. Genetic algorithm is used to overcome this problem. The EWC-1 and Ni_1Co_2@C are used as the database for optimizing multilayer composites, and the results are analyzed by COMSOL finite element method. Firstly, in the single factor variable experiment, multilayer composites composed of a single material is analyzed. Thickness of the single layer, number of layers, interval distance, layer and the total thickness of the multilayer composite material all show effect on microwave absorption properties of multilayer composites. Then genetic algorithm is used to optimize multilayer composites. When the number of layers is five and the surface layer is EWC-1, the composite exhibits C-band absorption at 4.71687mm. In analysis of finite element simulation, the result is consistent with the calculated one, which means validity of the model. From the simulation result, it can be seen that power loss of microwave is mainly concentrated in front part of the structure, which indicates that Ni_1Co_2@C play a more

important role in attenuating microwave. The successful optimization of multilayer composites provides a theoretical reference for development of novel microwave absorption materials.

In summary, referring characteristics of carbon materials, the egg white and metal organic framework are used to prepare ultra-thin and X-band absorbing materials, respectively. By analyzing the electromagnetic parameters, the effect of component and morphology on microwave absorption properties is systematically discussed. Then, combined with characteristics of two materials, the genetic algorithm is used to develop multilayer composites with C-band absorption. By finite element method, attenuation mechanism of the multilayer composite is figured out. We believe that this work can provide an important theoretical reference for the design and development of new microwave absorption composites.

Chapter 1: General introduction

1.1 Introduction

With the development of modern science and technology, various high-precision instruments, vehicles and smart devices have become an indispensable part of people's lives[1-3]. In order to deal with various complex situations, the working accuracy of equipment is constantly improving, while a large number of microwave is also generated at the same time[4-7]. These electromagnetic radiations not only affect their own performance and longevity, but also cause health problems to human bodies. Recently, studies have shown that, compared with microwave in other frequencies, microwave in the frequency band of 300MHz-300GHz has the greatest impact on human bodies[8]. Especially for people's daily information transmission tools such as mobile phones and computers, microwaves in the frequencies mentioned above are released by themselves all the time. For this reason, microwave existing around the environment in a form is not easy to prevent. It gradually becomes a new source of pollution after air pollution, soil and water pollution and noise pollution[9-13]. In addition, communication equipment will radiate microwave carrying information into the air because of the operation mode. If the information is intercepted by someone, it will cause serious information leakage. Due to above concerns, electromagnetic shielding materials have been developed for decades and the most common way to

control electromagnetic pollution[14-18]. The mechanism is to cut off the propagation route of the microwave by reflecting microwave, thereby suppressing the electromagnetic radiation intensity within a safe range. However, due to shielding mechanism, electromagnetic shielding materials is hard to eliminate harm of microwave fundamentally. Fortunately, microwave absorption materials can attenuate intensity of electromagnetic radiation efficiently and gradually have received extensive attention[19-22].

1.2 Development of microwave absorption materials

1.2.1 Mechanisms and evaluation of microwave absorption materials

When microwave arrive at surface of microwave absorption (MA) materials, it will undergo multiple refraction, transmission and reflection processes[23, 24]. To be specific, transmitted microwave is usually divided into three parts, namely incident waves, reflected waves and transmitted waves shown in Fig.1.1[25]. In order to improve absorbers' ability, two basic principles are usually required. One is the principle of impedance matching, which aims to control impedance of surface to make it closer to air impedance, thereby increasing the ability of microwave to penetrate the material[26]. The second is the principle of attenuation matching. Attenuation matching requires absorbers to have good loss capability, which can maximize the energy loss of microwave inside the material and

reduce amount of transmission.

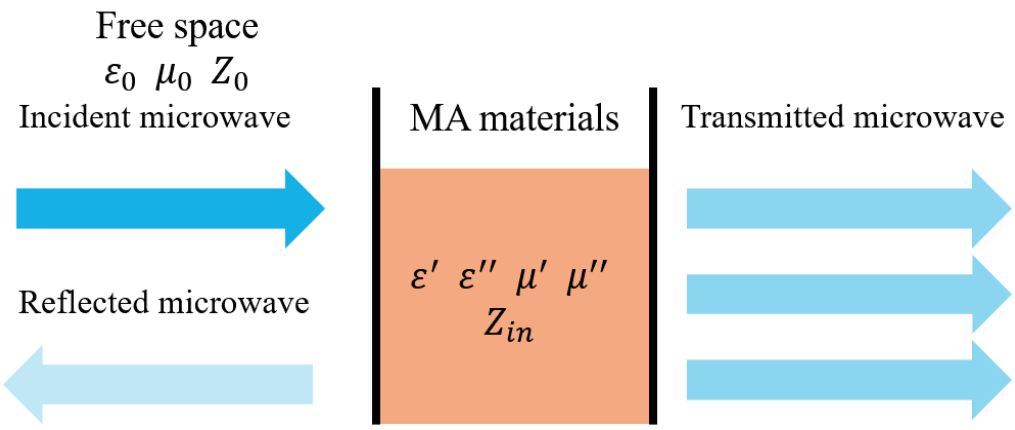

Fig. 1.1 Schematic chart of microwave propagation

Fig. 1.1 also exhibit necessary parameters for evaluating microwave absorption. It is generally accepted that reflection coefficient is used to evaluate microwave incident ability for materials, and its value depends on difference between input impedance Z_{in} and free space impedance Z_0. The relative permittivity $\varepsilon_r = \varepsilon' - j\varepsilon''$ and relative permeability $\mu_r = \mu' - j\mu''$ describe the microwave performance of the material. ε' and μ' represent the real part of the relative permittivity and permeability of the material and represent the energy storage capacity. ε'' and μ'' are imaginary parts of the relative permittivity and permeability, representing the attenuation ability [27].

1.2.2 Definition of electromagnetic parameters

The aforementioned relative permittivity ε_r and relative permeability μ_r is widely used in evaluating microwave absorption. To better understand microwave absorption, the origin of both parameters is introduced[28-30].

The physical meaning of complex permittivity (ε_r): The characteristic of dielectric is that positive and negative charge centers of gravity store and transfer influence of electricity action without overlap record. The basic process of electric polarization includes three processes, including distortion of electron cloud outside the electron nucleus, relative displacement polarization of positive and negative ions in molecules and steering polarization of molecular intrinsic chainsaws. In external electric field, the relative permittivity of the medium is a macroscopic physical quantity that reflects above three processes. Since establishment of these polarizations will be affected by frequency, the permittivity is a function of frequency.

According to relevant literature, when placed in an electrostatic field, the medium is polarized[28, 31]. the vector sum of molecular electric moments in a unit volume, denoted by P, is called the electric polarization intensity. For isotropic dielectrics, the relationship of P and external field strength E can be expressed by following:

$$P = \chi_e \varepsilon_0 E \tag{1-1}$$

χ_e is polarizability and ε_0 is vacuum dielectric constant. For electric displacement D, it can be expressed as following:

$$D = \varepsilon_0 E + P = (1 + \chi_e)\varepsilon_0 E = \varepsilon_r \varepsilon_0 E \tag{1-2}$$

When external field is an alternating field, with frequency of external field increases, polarization of the medium is hard to keep up with change of the external field. As a result, the dielectric constant is supposed to be represented as following:

$$\varepsilon_r = \varepsilon' - j\varepsilon'' \tag{1-3}$$

Then, the current and voltage with capacitor model can explain the equation (1-3) by following equation (1-4) and (1-5):

$$I = j\omega C_P U + \frac{U}{R_P} \tag{1-4}$$

$$I = j\omega(\varepsilon' - \varepsilon'')C_0 U \tag{1-5}$$

According to equation 1-4 and 1-5, the meaning of ε' and ε'' can be explained as below:

$$C_P = \varepsilon' C_0 \tag{1-6}$$

$$R_P = \frac{I}{\omega \varepsilon'' C_0} \tag{1-7}$$

The above equation 1-6 and 1-7 can demonstrate the physical meaning of the complex permittivity of the surface, that is, the real part is the same as the relative permittivity in static field, which represents the ability to store charge or energy while the imaginary part is equivalent to connecting an equivalent resistance in parallel with capacitors, representing energy loss.

As for physical meaning of complex permeability, similar to how dielectric is polarized in an external electric field, magnetic medium is magnetized in an external magnetic field[32-34]. The degree of magnetization M of a magnetic medium is described by the equation 1-8。In static magnetic field, the magnetization M at any point inside isotropic magnetic media is proportional to magnetic field strength H. The proportional coefficient χ_m is a constant, called magnetic susceptibility. The specific relationship can be expressed as following:

$$M = \chi_m H \tag{1-8}$$

The magnetic induction intensity B in the medium can be expressed as:

$$B = \mu_0(H + M) = \mu_0(1 + \chi_m)H = \mu_0\mu_r H \tag{1-9}$$

Here μ_0 is vacuum permeability while μ_r is relative permeability. When external magnetic field is an alternating field, due to the existence of hysteresis effect, eddy current effect, domain wall resonance and natural resonance, the change of magnetization state of the medium is hard to keep up with change of the external field in time. As a result, the time of magnetization needs to be taken into consideration. When the amplitude of the applied alternating magnetic field and angular frequency is H_m and ω, the relationship can be expressed by following equation:

$$H = H_m \cos \omega t \tag{1-10}$$

Then corresponding magnetic induction intensity B also changes periodically, but still fall behind H by a phase difference δ in time. When the amplitude is B_m, the function of B can be expressed as following:

$$B = B_m \cos(\omega t - \delta) \tag{1-11}$$

In the process of dynamic magnetization, in order to express the relationship between B and H in the alternating field, the concept of complex permeability is introduced, which is used to simultaneously reflect the relationship between the amplitude and phase between B and H. The related expression is as below:

$$\mu_r = \mu' - j\mu'' \tag{1-12}$$

According above equations the H and B can be expressed as following:

$$\widetilde{H} = H_m e^{j\omega t} \tag{1-13}$$

$$\tilde{B} = B_m e^{j(\omega t-\delta)} \tag{1-14}$$

Then the relative permeability in complex form can be obtained as following:

$$\mu_r = \frac{\tilde{B}}{\mu_0 \tilde{H}} = \frac{B_m}{\mu_0 \tilde{H}} e^{-j\omega} = \frac{B_m}{\mu_0 \tilde{H}} (\cos\delta - j\sin\delta) \tag{1-15}$$

To be more specific, the μ' and μ'' can be expressed as following:

$$\mu' = \frac{B_m}{\mu_0 \tilde{H}} \cos\delta \tag{1-16}$$

$$\mu'' = \frac{B_m}{\mu_0 \tilde{H}} \sin\delta \tag{1-17}$$

Finally, the magnetization P can be expressed as following:

$$P = \frac{1}{2} \mu_0 \mu'' H_m^2 \tag{1-18}$$

It can be seen external field energy consumption of the medium is caused by that magnetic induction intensity B falls behind external field H. Magnetic loss power is proportional to the imaginary number of the complex permeability, and the density of the stored energy inside the magnetic medium is:

$$w = \frac{1}{2} H * B = \frac{1}{2} \mu_0 \mu' H_m^2 \tag{1-19}$$

From the equation 1-19, it is also demonstrated that energy density stored in the magnetic medium in the alternating field is proportional to the real part of the complex permeability.

It can be seen from the above that the permittivity and permeability are intrinsic parameters that characterize the electromagnetic properties of absorbers. Under the action of alternating magnetic field, the two parameters are expressed by equations 1-3 and 1-12. Moreover,

Considering the equation 1-12 for attenuation constant and absorption of microwave in medium, there is a conclusion that while the values ε' and μ' are large enough, the ε'' and μ'' should be as large as possible. However, due to impedance matching of absorbers also needs to be considered in design, the values ε'' and μ'' should be designed in an optimal range of values. It is necessary to regulate impedance matching to reduce the reflection of microwave at incident interface, and to strengthen absorption capability of microwave to prevent incident microwave from being reflected back and transmitted.

$$\alpha = \omega\sqrt{\mu'\mu_0\varepsilon'\varepsilon_0}\sqrt{2(\frac{\varepsilon''\mu''}{\varepsilon'\mu'} - 1 + \sqrt{1 + \frac{\mu''^2}{\mu'^2} + \frac{\varepsilon''^2}{\varepsilon'^2} + \frac{\varepsilon''^2\mu''^2}{\varepsilon'^2\mu'^2}})} \quad (1\text{-}12)$$

1.2.3 Carbon-based microwave absorption materials

Due to dielectric properties, carbon materials can bring high dielectric loss through rational design and are often used to prepare high-performance microwave absorption materials[35-39]. At the same time, carbon material has the advantages of light weight, stable physical and chemical properties, and has irreplaceable advantages in design of lightweight materials. However, pure carbon material has exaggerated dielectric constant[40-45]. As a kind of microwave absorption materials, impedance matching is so bad that microwave is hard to be incident into materials. Consequently, carbon materials have difficulty in absorbing materials. For this reason, how to modify carbon materials in an appropriate way has become one of research point[46-50]. Adding

magnetic materials and adjusting dielectric properties are the main research directions at present.

Graphene, carbon nanotubes are widely used as microwave absorption materials because of their unique structure and excellent electronic properties[51-56]. The structure can provide abundant sites for scattering microwave while the current induced by alternating electromagnetic field can cause polarization loss for attenuating microwave. Huang et al.[57] developed ultralight foams containing CNT and graphene through a solvothermal method. The CGFs exhibit tunable microwave absorption properties by regulating ratio of CNT and graphene. For the optimized process, the foams show average absorption intensity exceeding 22.5 dB in both C and X bands. Then the synergetic effect of CNT and graphene and three-dimensional network are the main reasons attributing to microwave absorption excellent performance. Besides, due to excessive permittivity, magnetic metals and their alloy are used for regulating microwave absorption performance of CNT and graphene.

Recently, Mxene, as 2 two-dimensional materials, have been manipulated for developing microwave absorption composites[13, 43, 58]. Due to abundant functional group, special structure and full of carbon, the Mxene[59, 60] owe intrinsic conductivity and, native defects and surface chemical activity, which are all benefit to absorbing microwave[61-63]. However, pure Mxene is difficult to be used because of unpromising impedance matching. Therefore, it is always combined with other materials to absorb microwave. Wang et al.[13] develop promising Mxene-based

microwave absorption materials. By regulating ratio of Ni nanochain, a minimum reflection loss -49.9dB is achieved in 1.75mm. the results shows the dielectric, magnetic loss and impedance matching can be easily by content of Ni chains. The conclusion provides a simple but effective way for improving microwave absorption performance of Mxene-based materials.

Conductive polymers, such as polyacetylene, polypyrrole, polyaniline, polythiophene, have conjugated π electronic structure system[64-67]. Through chemical or electrochemical doping, conductive polymers with semiconductor properties can be obtained[17, 68]. Due to their dielectric properties, polymers are often used in combination with carbon materials to adjust the dielectric properties of composites. Duan et al.[55] prepare polyaniline/graphene oxide composites by a one-step intercalation polymerization of aniline in the presence of GO layers. The synthesis mechanism of the entire hierarchical sandwich-like structure is discussed by different mechanical agitation duration period. Meanwhile the composites generate an ultrawide effective absorbing bandwidth 4.825 GHz to 18 GHz by changing thickness from 2mm to 5.5 mm. It reveals that a hierarchical microstructure can be a potential way for preparing excellent microwave absorption materials.

Numerous literatures have proved that adding magnetic metal can improve the single loss mechanism of carbon materials and adjust the impedance matching to regulate microwave absorption performance. The common method is to mix metal salt with high specific surface area

carbon material then reduce the composite to metal/carbon composite for absorbing microwave[69-71]. However, such method often leads to uneven distribution of metal particles on surface of synthesized composites, resulting in weakened properties and uncontrollable sample preparation. In recent years, MOF can avoid the problem of uneven distribution in material preparation, and can be used as carbon and metal source to simplify the material preparation process, which are gradually applied to develop new microwave absorption materials[72-75]. Du et al.[76] use Prussian blue, known as a kind of Fe based-MOF, to prepare Fe/C composites by in-situ derivation. The resultant product is composed of cubic frameworks of amorphous carbon and uniformly dispersed core-shell Fe@graphitic carbon nanoparticles. By regulating pyrolysis temperature between 600-700℃, the composites show different microwave absorption responses due to the changing graphitization degree and microstructure. The conclusion is that synergetic effect of dielectric loss, magnetic loss, matched impedance, and dielectric resonances accounts for the improved microwave absorption properties of the Fe/C nano cubes.

1.2.4 Multilayer microwave absorption materials

Although nanostructures have characteristics of strong absorption, they still have the shortcoming of uncontrollable absorption frequency band, which results in narrow application surface as new absorbing materials[77-79]. The multilayer structures can adjust microwave transmission path from the macro level through the structural design, and then operate

absorbing frequency band, which has shown great potential in the development of high-performance microwave materials[24, 31, 80-82]. The study of multilayer microwave absorption structures can be carried out from two aspects. On the one hand, the database composed of different microwave absorption materials needs to be set[83-86]. By complementing absorption mechanism with various materials, the effectiveness of composites structures is improved, so as to improve absorption performance of multilayer composites. On the other hand, structural changes are used to optimize propagation path of microwave and explore influence of material structure on performance[87-89]. However, due to the design diversity of multilayer structures, there are too many experimental parameters need to be determined. How to adjust complex parameters and get the most optimal solution of multilayer materials also remains difficult。

1.2.5 Simulation of microwave absorption materials

Actual preparation of microwave absorption materials will cost a lot but application of simulation software can solve the problem and improve research efficiency in most cases[44, 90, 91]. At present, the main simulation software tested for microwave absorption materials is HFSS, CST and COMSOL[92-95].

Through the application of simulation software in microwave absorption[96-99], it can be concluded that software plays a role in calculate absorption performance according to given parameters such as

structures and materials, and adjust the parameters to obtain the structure with different wave absorption performance. Therefore, the simulation software is a irreplaceable way for research and development of microwave absorption structures. Combining simulation results and theory of multilayer microwave absorption composites, it provides a theoretical basis for designing excellent structures[100-103]. However, finite element simulation software has relatively high requirements on computer performance, and the solution process of a single parameter takes long time, which limits simulation process of multi-parameter research. How to improve the efficiency of electromagnetic simulation is also one of vital problems.

1.3 Purposes and significances of research

Considering the current application requirements of microwave absorption composites, this paper plans to use chemical synthesis, theoretical calculation of transmission lines, genetic algorithm and finite element analysis to design multilayer microwave absorption materials. According to experimental and theoretical analysis, new multilayer composites with C-band microwave absorption are developed.

At the beginning, egg white-derived magnetic carbon composite is synthesized for the first time. Egg white is used as carbon source while Iron, cobalt and nickel ions are magnetic metal sources. The physical properties of synthesized composites can be regulated by changing metal content. By controlling morphology and component ratio, composites with

excellent microwave absorption performance can be determined. Then effect of morphology and component ratio on the performance is discussed. Meanwhile, microwave absorption mechanism also is deeply investigated by obtained electromagnetic parameters.

Besides component, morphology is also a main factor effecting microwave absorption performance. Then concept of metal organic framework is manipulated to prepare magnetic carbon composites. Here the carbon and metal sources are ZIF-67 and nickel ion. By regulating ratio of nickel and cobalt, there are composites with different properties. The metal ratio on physical properties and microwave absorption performance are discussed. With help of transmission line theory, electromagnetic parameters are used to find out absorption mechanism.

Finally, according to two synthetic materials, the microwave absorption calculation formula of multilayer composites derived from the transmission line theory is used to find the structure parameters of composites. Based on global genetic algorithm, multilayer composites with broadband microwave absorption ability can be developed. With help of COMSOL, simulation results of electromagnetic fields and power loss can be used to analyze attenuation mechanism of multilayer composites. This is useful to extend development of multilayer composites for microwave absorption.

1.4 Outline of dissertation

In chapter 1, it mainly elaborates research background and

significance of microwave absorption. Microwave absorption theory and related composites are introduced in detail. Then recent simulation research situation about microwave absorption is discussed. Besides, the importance of microwave absorption composites with multilayer structure is emphasized. Finally, the existing problems is summarized and the main research content is put forward.

In chapter 2, a biomass-based nano magnetic carbon material was developed. The magnetic carbon composites with different microwave absorption were prepared by using egg white rich in sulfur as carbon and sulfur sources and iron, cobalt and nickel ions as magnetic source.

In chapter 3, a kind of magnetic carbon nanomaterial based on metal organic framework is developed. The morphology and component of the composites can be controlled by changing the synthetic process parameters, then microwave absorption properties also can be regulated.

In chapter 4, the optimization design of multilayer composites is developed based on the two materials above. According to two materials with different electromagnetic properties, the genetic algorithm is used to optimize the ordering, thickness and number of layers of the multilayer structure for developing composites with excellent microwave absorption performance. Besides, the optimized structures are simulated by finite element, and the absorption mechanism of the multilayer composite is discussed.

In chapter 5, a summary of the research and conclusion were presented.

References

[1] Y. Cheng, H. Zhao, Y. Zhao, J. Cao, J. Zheng, G. Ji, Structure-switchable mesoporous carbon hollow sphere framework toward sensitive microwave response. Carbon, 161 (2020) 870-879.

[2] Y. Qi, L. Qi, L. Liu, B. Dai, D. Wei, G.-M. Shi, Y. Qi, Facile synthesis of lightweight carbonized hydrochars decorated with dispersed ZnO nanocrystals and enhanced microwave absorption properties. Carbon, 150 (2019) 259-267.

[3] J.-C. Shu, X.-Y. Yang, X.-R. Zhang, X.-Y. Huang, M.-S. Cao, L. Li, H.-J. Yang, W.-Q. Cao, Tailoring MOF-based materials to tune electromagnetic property for great microwave absorbers and devices. Carbon, 162 (2020) 157-171.

[4] Y. Du, W. Liu, R. Qiang, Y. Wang, X. Han, J. Ma, P. Xu, Shell thickness-dependent microwave absorption of core-shell Fe3O4@C composites. ACS Appl Mater Interfaces, 6 (2014) 12997-13006.

[5] P. Liu, S. Gao, Y. Wang, Y. Huang, Y. Wang, J. Luo, Core-Shell CoNi@Graphitic Carbon Decorated on B,N-Codoped Hollow Carbon Polyhedrons toward Lightweight and High-Efficiency Microwave Attenuation. ACS Appl Mater Interfaces, 11 (2019) 25624-25635.

[6] H. Wang, F. Meng, F. Huang, C. Jing, Y. Li, W. Wei, Z. Zhou, Interface Modulating CNTs@PANi Hybrids by Controlled Unzipping of the Walls of CNTs To Achieve Tunable High-Performance Microwave Absorption. ACS Appl Mater Interfaces, 11 (2019) 12142-

12153.

[7] Q. Liu, Q. Cao, H. Bi, C. Liang, K. Yuan, W. She, Y. Yang, R. Che, CoNi@SiO2 @TiO2 and CoNi@Air@TiO2 Microspheres with Strong Wideband Microwave Absorption. Adv Mater, 28 (2016) 486-490.

[8] F. Wang, N. Wang, X. Han, D. Liu, Y. Wang, L. Cui, P. Xu, Y. Du, Core-shell FeCo@carbon nanoparticles encapsulated in polydopamine-derived carbon nanocages for efficient microwave absorption. Carbon, 145 (2019) 701-711.

[9] F. Wu, K. Yang, Q. Li, T. Shah, M. Ahmad, Q. Zhang, B. Zhang, Biomass-derived 3D magnetic porous carbon fibers with a helical/chiral structure toward superior microwave absorption. Carbon, 173 (2021) 918-931.

[10] Y. Zhao, W. Wang, J. Wang, J. Zhai, X. Lei, W. Zhao, J. Li, H. Yang, J. Tian, J. Yan, Constructing multiple heterogeneous interfaces in the composite of bimetallic MOF-derivatives and rGO for excellent microwave absorption performance. Carbon, 173 (2021) 1059-1072.

[11] S. Dong, P. Hu, X. Li, C. Hong, X. Zhang, J. Han, NiCo2S4 nanosheets on 3D wood-derived carbon for microwave absorption. Chem Eng J, 398 (2020).

[12] X. Liu, L.-S. Wang, Y. Ma, Y. Qiu, Q. Xie, Y. Chen, D.-L. Peng, Facile synthesis and microwave absorption properties of yolk-shell ZnO-Ni-C/RGO composite materials. Chem Eng J, 333 (2018) 92-100.

[13] L. Liang, G. Han, Y. Li, B. Zhao, B. Zhou, Y. Feng, J. Ma, Y. Wang, R. Zhang, C. Liu, Promising Ti3C2Tx MXene/Ni Chain Hybrid with Excellent Electromagnetic Wave Absorption and Shielding Capacity. ACS Appl Mater Interfaces, 11 (2019) 25399-25409.

[14] B. Wen, M. Cao, M. Lu, W. Cao, H. Shi, J. Liu, X. Wang, H. Jin, X. Fang, W. Wang, J. Yuan, Reduced graphene oxides: light-weight and high-efficiency electromagnetic interference shielding at elevated temperatures. Adv Mater, 26 (2014) 3484-3489.

[15] H. Lv, Z. Yang, S.J.H. Ong, C. Wei, H. Liao, S. Xi, Y. Du, G. Ji, Z.J. Xu, A Flexible Microwave Shield with Tunable Frequency - Transmission and Electromagnetic Compatibility. Advanced Functional Materials, 29 (2019).

[16] J.C. Shu, W.Q. Cao, M.S. Cao, Diverse Metal–Organic Framework Architectures for Electromagnetic Absorbers and Shielding. Advanced Functional Materials, 31 (2021).

[17] M.H. Al-Saleh, U. Sundararaj, Electromagnetic interference shielding mechanisms of CNT/polymer composites. Carbon, 47 (2009) 1738-1746.

[18] J. Hong, P. Xu, H. Xia, Z. Xu, Q.-Q. Ni, Electromagnetic interference shielding anisotropy enhanced by CFRP laminated structures. Compos Sci Technol, 203 (2021).

[19] H. Guo, Y. Chen, Y. Li, W. Zhou, W. Xu, L. Pang, X. Fan, S. Jiang,

Electrospun fibrous materials and their applications for electromagnetic interference shielding: A review. Composites Part A: Applied Science and Manufacturing, 143 (2021).

[20] J.-M. Thomassin, C. Jérôme, T. Pardoen, C. Bailly, I. Huynen, C. Detrembleur, Polymer/carbon based composites as electromagnetic interference (EMI) shielding materials. Materials Science and Engineering: R: Reports, 74 (2013) 211-232.

[21] P. Liu, S. Gao, W. Huang, J. Ren, D. Yu, W. He, Hybrid zeolite imidazolate framework derived N-implanted carbon polyhedrons with tunable heterogeneous interfaces for strong wideband microwave attenuation. Carbon, 159 (2020) 83-93.

[22] W.-L. Song, K.-L. Zhang, M. Chen, Z.-L. Hou, H. Chen, X. Yuan, Y. Ma, D. Fang, A universal permittivity-attenuation evaluation diagram for accelerating design of dielectric-based microwave absorption materials: A case of graphene-based composites. Carbon, 118 (2017) 86-97.

[23] W. Li, L. Xu, X. Zhang, Y. Gong, Y. Ying, J. Yu, J. Zheng, L. Qiao, S. Che, Investigating the effect of honeycomb structure composite on microwave absorption properties. Composites Communications, 19 (2020) 182-188.

[24] Y. Huang, Q. Fan, J. Chen, L. Li, M. Chen, L. Tang, D. Fang, Optimization of flexible multilayered metastructure fabricated by dielectric-magnetic nano lossy composites with broadband microwave absorption. Compos Sci Technol, 191 (2020).

[25] Z. Zhang, C. Wang, H. Yang, P. Wang, M. Chen, H. Lei, D. Fang, Broadband radar absorbing composites: Spatial scale effect and environmental adaptability. Compos Sci Technol, (2020).

[26] Z. Meng, C.H. Tian, C.L. Xu, J.F. Wang, S.N. Huang, X.H. Li, B.Y. Yang, Q. Fan, S.B. Qu, Multi-spectral functional metasurface simultaneously with visible transparency, low infrared emissivity and wideband microwave absorption. Infrared Physics & Technology, 110 (2020).

[27] N. Kumar, S. Somay, Multiwall carbon nanotube enhance the invisibility effect from radar. Results Phys, 18 (2020).

[28] M.S. Cao, X.X. Wang, M. Zhang, W.Q. Cao, X.Y. Fang, J. Yuan, Variable-Temperature Electron Transport and Dipole Polarization Turning Flexible Multifunctional Microsensor beyond Electrical and Optical Energy. Adv Mater, 32 (2020) e1907156.

[29] S.J. Yan, C.Y. Xu, J.T. Jiang, D.B. Liu, Z.Y. Wang, J. Tang, L. Zhen, Strong dual-frequency electromagnetic absorption in Ku-band of C@FeNi3 core/shell structured microchains with negative permeability. J Magn Magn Mater, 349 (2014) 159-164.

[30] X. Sun, J. He, G. Li, J. Tang, T. Wang, Y. Guo, H. Xue, Laminated magnetic graphene with enhanced electromagnetic wave absorption properties. J. Mater. Chem. C, 1 (2013) 765-777.

[31] J. Ning, S.F. Dong, X.Y. Luo, K. Chen, J.M. Zhao, T. Jiang, Y.J. Feng, Ultra-broadband microwave absorption by ultra-thin metamaterial with stepped structure induced multi-resonances.

Results Phys, 18 (2020).

[32] B. Quan, X. Liang, G. Ji, Y. Zhang, G. Xu, Y. Du, Cross-Linking-Derived Synthesis of Porous CoxNiy/C Nanocomposites for Excellent Electromagnetic Behaviors. ACS Appl Mater Interfaces, 9 (2017) 38814-38823.

[33] S. Dong, W. Tang, P. Hu, X. Zhao, X. Zhang, J. Han, P. Hu, Achieving Excellent Electromagnetic Wave Absorption Capabilities by Construction of MnO Nanorods on Porous Carbon Composites Derived from Natural Wood via a Simple Route. Acs Sustain Chem Eng, 7 (2019) 11795-11805.

[34] Q. Liu, D. Zhang, T. Fan, Electromagnetic wave absorption properties of porous carbon/Co nanocomposites. Appl Phys Lett, 93 (2008).

[35] D. Liu, Y. Du, F. Wang, Y. Wang, L. Cui, H. Zhao, X. Han, MOFs-derived multi-chamber carbon microspheres with enhanced microwave absorption. Carbon, 157 (2020) 478-485.

[36] Q. Zeng, L. Wang, X. Li, W. You, J. Zhang, X. Liu, M. Wang, R. Che, Double ligand MOF-derived pomegranate-like Ni@C microspheres as high-performance microwave absorber. Appl Surf Sci, 538 (2021).

[37] X. Li, W. Dong, C. Zhang, W. Guo, C. Wang, Y. Li, H. Wang, Leaf-like Fe/C composite assembled by iron veins interpenetrated into amorphous carbon lamina for high-performance microwave absorption. Composites Part A: Applied Science and Manufacturing,

140 (2021).

[38] Y. Li, R. Liu, X. Pang, X. Zhao, Y. Zhang, G. Qin, X. Zhang, Fe@C nanocapsules with substitutional sulfur heteroatoms in graphitic shells for improving microwave absorption at gigahertz frequencies. Carbon, 126 (2018) 372-381.

[39] H. Xu, X. Yin, M. Zhu, M. Li, H. Zhang, H. Wei, L. Zhang, L. Cheng, Constructing hollow graphene nano-spheres confined in porous amorphous carbon particles for achieving full X band microwave absorption. Carbon, 142 (2019) 346-353.

[40] J. Chen, J. Zheng, F. Wang, Q. Huang, G. Ji, Carbon fibers embedded with FeIII-MOF-5-derived composites for enhanced microwave absorption. Carbon, 174 (2021) 509-517.

[41] J. Li, K. Han, D. Wang, Z. Teng, Y. Cao, J. Qi, M. Li, M. Wang, Fabrication of high performance structural N-doped hierarchical porous carbon for supercapacitor. Carbon, 164 (2020) 42-50.

[42] X. Xu, G. Wang, G. Wan, S. Shi, C. Hao, Y. Tang, G. Wang, Magnetic Ni/graphene connected with conductive carbon nano-onions or nanotubes by atomic layer deposition for lightweight and low-frequency microwave absorption. Chem Eng J, 382 (2020).

[43] X.P. Han, Y. Huang, S. Gao, G.Z. Zhang, T.H. Li, P.B. Liu, A hierarchical carbon Fiber@MXene@ZnO core-sheath synergistic microstructure for efficient microwave absorption and photothermal conversion. Carbon, 183 (2021) 872-883.

[44] R. Tan, F. Zhou, P. Chen, B. Zhang, J. Zhou, PANI/FeCo@C

composite microspheres with broadband microwave absorption performance. Compos Sci Technol, 218 (2022).

[45] X.J. Zeng, X.Y. Cheng, R.H. Yu, G.D. Stucky, Electromagnetic microwave absorption theory and recent achievements in microwave absorbers. Carbon, 168 (2020) 606-623.

[46] D. Micheli, C. Apollo, R. Pastore, M. Marchetti, X-Band microwave characterization of carbon-based nanocomposite material, absorption capability comparison and RAS design simulation. Compos Sci Technol, 70 (2010) 400-409.

[47] F. Luo, D. Liu, T. Cao, H. Cheng, J. Kuang, Y. Deng, W. Xie, Study on broadband microwave absorbing performance of gradient porous structure. Advanced Composites and Hybrid Materials, 4 (2021) 591-601.

[48] X. Guan, Z. Yang, Y. Zhu, L. Yang, M. Zhou, Y. Wu, L. Yang, T. Deng, G. Ji, The controllable porous structure and s-doping of hollow carbon sphere synergistically act on the microwave attenuation. Carbon, 188 (2022) 1-11.

[49] W. Chu, K. Wang, H. Li, Y. Chen, H. Liu, Harvesting yolk-shell nanocomposites from Fe-MIL-101 self-template in NaCl/KCl molten salt environment for high-performance microwave absorber. Chem Eng J, (2021).

[50] P.B. Liu, S. Gao, Y. Wang, F.T. Zhou, Y. Huang, J.H. Luo, Metal-organic polymer coordination materials derived Co/N-doped porous carbon composites for frequency-selective microwave absorption.

Compos Part B-Eng, 202 (2020).

[51] W. Feng, Y. Wang, J. Chen, L. Wang, L. Guo, J. Ouyang, D. Jia, Y. Zhou, Reduced graphene oxide decorated with in-situ growing ZnO nanocrystals: Facile synthesis and enhanced microwave absorption properties. Carbon, 108 (2016) 52-60.

[52] P. Liu, Y. Zhang, J. Yan, Y. Huang, L. Xia, Z. Guang, Synthesis of lightweight N-doped graphene foams with open reticular structure for high-efficiency electromagnetic wave absorption. Chem Eng J, 368 (2019) 285-298.

[53] W.-L. Song, X.-T. Guan, L.-Z. Fan, Y.-B. Zhao, W.-Q. Cao, C.-Y. Wang, M.-S. Cao, Strong and thermostable polymeric graphene/silica textile for lightweight practical microwave absorption composites. Carbon, 100 (2016) 109-117.

[54] Y. Zhang, Y. Huang, T. Zhang, H. Chang, P. Xiao, H. Chen, Z. Huang, Y. Chen, Broadband and tunable high-performance microwave absorption of an ultralight and highly compressible graphene foam. Adv Mater, 27 (2015) 2049-2053.

[55] J. Liu, Y. Duan, L. Song, J. Hu, Y. Zeng, Heterogeneous nucleation promoting formation and enhancing microwave absorption properties in hierarchical sandwich-like polyaniline/graphene oxide induced by mechanical agitation. Compos Sci Technol, 182 (2019).

[56] Y. Zhang, Y. Huang, H. Chen, Z. Huang, Y. Yang, P. Xiao, Y. Zhou, Y. Chen, Composition and structure control of ultralight graphene foam for high-performance microwave absorption. Carbon, 105 (2016)

438-447.

[57] H. Chen, Z. Huang, Y. Huang, Y. Zhang, Z. Ge, B. Qin, Z. Liu, Q. Shi, P. Xiao, Y. Yang, T. Zhang, Y. Chen, Synergistically assembled MWCNT/graphene foam with highly efficient microwave absorption in both C and X bands. Carbon, 124 (2017) 506-514.

[58] G. Zhao, H. Lv, Y. Zhou, X. Zheng, C. Wu, C. Xu, Self-Assembled Sandwich-like MXene-Derived Nanocomposites for Enhanced Electromagnetic Wave Absorption. ACS Appl Mater Interfaces, 10 (2018) 42925-42932.

[59] A. Sotiropoulos, S. Koulouridis, A. Masouras, V. Kostopoulos, H.T. Anastassiu, Carbon nanotubes films in glass fiber polymer matrix forming structures with high absorption and shielding performance in X-Band. Composites Part B: Engineering, 217 (2021).

[60] Y. Jiao, J. Li, A. Xie, F. Wu, K. Zhang, W. Dong, X. Zhu, Confined polymerization strategy to construct polypyrrole/zeolitic imidazolate frameworks (PPy/ZIFs) nanocomposites for tunable electrical conductivity and excellent electromagnetic absorption. Compos Sci Technol, 174 (2019) 232-240.

[61] H. Li, M. Lu, W. Han, H. Li, Y. Wu, W. Zhang, J. Wang, B. Zhang, Employing MXene as a matrix for loading amorphous Si generated upon lithiation towards enhanced lithium-ion storage. Journal of Energy Chemistry, 38 (2019) 50-54.

[62] Z.-K. Li, Y. Liu, L. Li, Y. Wei, J. Caro, H. Wang, Ultra-thin titanium carbide (MXene) sheet membranes for high-efficient

oil/water emulsions separation. Journal of Membrane Science, 592 (2019).

[63] J. Shao, J.-W. Wang, D.-N. Liu, L. Wei, S.-Q. Wu, H. Ren, A novel high permittivity percolative composite with modified MXene. Polymer, 174 (2019) 86-95.

[64] M. Green, A.T.V. Tran, X.B. Chen, Maximizing the microwave absorption performance of polypyrrole by data-driven discovery. Compos Sci Technol, 199 (2020).

[65] A. Peyravi, F. Ahmadijokani, M. Arjmand, Z. Hashisho, Graphene oxide enhances thermal stability and microwave absorption/regeneration of a porous polymer. J Hazard Mater, 433 (2022) 128792.

[66] J. Xu, Y. Cui, J. Wang, Y. Fan, T. Shah, M. Ahmad, Q. Zhang, B. Zhang, Fabrication of wrinkled carbon microspheres and the effect of surface roughness on the microwave absorbing properties. Chem Eng J, 401 (2020).

[67] G. Kulkarni, P. Kandesar, N. Velhal, V. Phadtare, A. Jatratkar, S.K. Shinde, D.-Y. Kim, V. Puri, Exceptional electromagnetic interference shielding and microwave absorption properties of room temperature synthesized polythiophene thin films with double negative characteristics (DNG) in the Ku-band region. Chem Eng J, 355 (2019) 196-207.

[68] Y. Lu, H. Zhang, J.Y. Chan, R. Ou, H. Zhu, M. Forsyth, E.M. Marijanovic, C.M. Doherty, P.J. Marriott, M.M.B. Holl, H. Wang,

Homochiral MOF-Polymer Mixed Matrix Membranes for Efficient Separation of Chiral Molecules. Angew Chem Int Ed Engl, 58 (2019) 16928-16935.

[69] H. Ning, G. Li, Y. Chen, K. Zhang, Z. Gong, R. Nie, W. Hu, Q. Xia, Porous N-Doped Carbon-Encapsulated CoNi Alloy Nanoparticles Derived from MOFs as Efficient Bifunctional Oxygen Electrocatalysts. ACS Appl Mater Interfaces, 11 (2019) 1957-1968.

[70] S. Saha, A.K. Ganguli, FeCoNi Alloy as Noble Metal-Free Electrocatalyst for Oxygen Evolution Reaction (OER). ChemistrySelect, 2 (2017) 1630-1636.

[71] Z. Li, L. Cai, M. Song, Y. Shen, X. Wang, J. Li, J. Wang, P. Wang, L. Tian, Ternary FeCoNi alloy nanoparticles embedded in N-doped carbon nanotubes for efficient oxygen evolution reaction electrocatalysis. Electrochimica Acta, 339 (2020).

[72] Z. Li, X. Han, Y. Ma, D. Liu, Y. Wang, P. Xu, C. Li, Y. Du, MOFs-Derived Hollow Co/C Microspheres with Enhanced Microwave Absorption Performance. Acs Sustain Chem Eng, 6 (2018) 8904-8913.

[73] M.D. Walle, M. Zhang, K. Zeng, Y. Li, Y.-N. Liu, MOFs-derived nitrogen-doped carbon interwoven with carbon nanotubes for high sulfur content lithium–sulfur batteries. Appl Surf Sci, 497 (2019).

[74] X.C. Xie, K.J. Huang, X. Wu, N. Wu, Y.Y. Xu, S.K. Zhang, C.H. Zhang, Binding hierarchical MoSe2 on MOF-derived N-doped carbon dodecahedron for fast and durable sodium-ion storage. Carbon, 169 (2020) 1-8.

[75] J. Gu, L. Sun, Y. Zhang, Q. Zhang, X. Li, H. Si, Y. Shi, C. Sun, Y. Gong, Y. Zhang, MOF-derived Ni-doped CoP@C grown on CNTs for high-performance supercapacitors. Chem Eng J, 385 (2020).

[76] R. Qiang, Y. Du, H. Zhao, Y. Wang, C. Tian, Z. Li, X. Han, P. Xu, Metal organic framework-derived Fe/C nanocubes toward efficient microwave absorption. J Mater Chem A, 3 (2015) 13426-13434.

[77] D. Zhi, T. Li, J. Li, H. Ren, F. Meng, A review of three-dimensional graphene-based aerogels: Synthesis, structure and application for microwave absorption. Composites Part B: Engineering, 211 (2021).

[78] S. Ren, H. Yu, L. Wang, Z. Huang, T. Lin, Y. Huang, J. Yang, Y. Hong, J. Liu, State of the Art and Prospects in Metal-Organic Framework-Derived Microwave Absorption Materials. Nanomicro Lett, 14 (2022) 68.

[79] F. Peng, M. Dai, Z. Wang, Y. Guo, Z. Zhou, Progress in graphene-based magnetic hybrids towards highly efficiency for microwave absorption. J Mater Sci Technol, 106 (2022) 147-161.

[80] X. Sun, Y. Pu, F. Wu, J. He, G. Deng, Z. Song, X. Liu, J. Shui, R. Yu, 0D-1D-2D multidimensionally assembled Co9S8/CNTs/MoS2 composites for ultralight and broadband electromagnetic wave absorption. Chem Eng J, 423 (2021).

[81] M. Green, A.T. Tran, X. Chen, Obtaining Strong, Broadband Microwave Absorption of Polyaniline Through Data - Driven

Materials Discovery. Adv Mater Interfaces, (2020).

[82] W. Zheng, Y. Li, Z. Xie, M. Liu, A. Zhang, X-band full absorbing multi-layer foam with lightweight and flexible performance. Composites Part B: Engineering, 231 (2022).

[83] A.A. Heidari, H. Faris, I. Aljarah, S. Mirjalili, An efficient hybrid multilayer perceptron neural network with grasshopper optimization. Soft Computing, 23 (2018) 7941-7958.

[84] Z. Alameer, M.A. Elaziz, A.A. Ewees, H. Ye, Z. Jianhua, Forecasting gold price fluctuations using improved multilayer perceptron neural network and whale optimization algorithm. Resources Policy, 61 (2019) 250-260.

[85] L.S. Guerras, D. Sengupta, M. Martin, M.M. El-Halwagi, Multilayer Approach for Product Portfolio Optimization: Waste to Added-Value Products. Acs Sustain Chem Eng, 9 (2021) 6410-6426.

[86] X. Shen, P. Bai, L. Chen, S. To, F. Yang, X. Zhang, Q. Yin, Development of thin sound absorber by parameter optimization of multilayer compressed porous metal with rear cavity. Applied Acoustics, 159 (2020).

[87] M. Kim, J. Seo, S. Yoon, H. Lee, J. Lee, B.J. Lee, Optimization and performance analysis of a multilayer structure for daytime radiative cooling. Journal of Quantitative Spectroscopy and Radiative Transfer, 260 (2021).

[88] K.S. Amorim, G.S. Pavani, Ant Colony Optimization-based distributed multilayer routing and restoration in IP/MPLS over optical

networks. Computer Networks, 185 (2021).

[89] K. Shi, G. Jin, R. Liu, T. Ye, Y. Xue, Underwater sound absorption performance of acoustic metamaterials with multilayered locally resonant scatterers. Results Phys, 12 (2019) 132-142.

[90] L. Huang, Y. Duan, X. Dai, Y. Zeng, G. Ma, Y. Liu, S. Gao, W. Zhang, Bioinspired Metamaterials: Multibands Electromagnetic Wave Adaptability and Hydrophobic Characteristics. Small, 15 (2019) e1902730.

[91] G. Shen, M. Xu, Z. Xu, Double-layer microwave absorber based on ferrite and short carbon fiber composites. Materials Chemistry and Physics, 105 (2007) 268-272.

[92] A. Kasgoz, M. Korkmaz, A. Durmus, Compositional and structural design of thermoplastic polyurethane/carbon based single and multi-layer composite sheets for high-performance X-band microwave absorbing applications. Polymer, 180 (2019).

[93] K. Peng, C. Liu, Y. Wu, G. Fang, G. Xu, Y. Zhang, C. Wu, M. Yan, Understanding the efficient microwave absorption for FeCo@ZnO flakes at elevated temperatures a combined experimental and theoretical approach. J Mater Sci Technol, 125 (2022) 212-221.

[94] J. Chen, J. Zheng, Q. Huang, F. Wang, G. Ji, Enhanced Microwave Absorbing Ability of Carbon Fibers with Embedded FeCo/CoFe2O4 Nanoparticles. ACS Appl Mater Interfaces, 13 (2021) 36182-36189.

[95] J. Lin, S. Sun, D. Xu, C. Cui, R. Ma, J. Luo, L. Fang, H. Li,

Microwave directional pyrolysis and heat transfer mechanisms based on multiphysics field stimulation: Design porous biochar structure via controlling hotspots formation. Chem Eng J, 429 (2022).

[96] X. Fan, Z. Pan, S. Chen, Y. Li, Z. Zhao, T. Pan, 3D Flexible Frequency Selective Surface with Stable Electromagnetic Transmission Properties. Advanced Materials Technologies, (2022).

[97] R. Mishra, R. Panwar, Investigation of graphene fractal frequency selective surface loaded terahertz absorber. Optical and Quantum Electronics, 52 (2020).

[98] A. Bhattacharya, B. Dasgupta, R. Jyoti, Design and analysis of ultrathin X - band frequency selective surface structure for gain enhancement of hybrid antenna. International Journal of RF and Microwave Computer-Aided Engineering, 31 (2020).

[99] V.P. Silva Neto, A.G. D'Assunção, Reconfigurable and stable frequency selective surfaces on nonuniform and finite arrays. Microwave and Optical Technology Letters, 60 (2018) 508-514.

[100] M.A. Belen, Performance enhancement of a microstrip patch antenna using dual-layer frequency-selective surface for ISM band applications. Microwave and Optical Technology Letters, 60 (2018) 2730-2734.

[101] Q. Zhou, P. Liu, K. Wang, H. Liu, D. Yu, Absorptive frequency selective surface with switchable passband. AEU - International Journal of Electronics and Communications, 89 (2018) 160-166.

[102] M. Rahzaani, G. Dadashzadeh, M. Khorshidi, New technique for designing wideband one layer frequency selective surface in X-band with stable angular response. Microwave and Optical Technology Letters, 60 (2018) 2133-2139.
[103] S. Kundu, A. Chatterjee, A compact super wideband antenna with stable and improved radiation using super wideband frequency selective surface. AEU - International Journal of Electronics and Communications, 150 (2022).

Chapter 2: Egg-white-derived magnetic carbon flakes with enhanced microwave absorption properties

2.1 Introduction

The rapid development of electronic equipment, and wireless communication has caused severe electromagnetic pollution, which not only damages human lives but also interferes with the reliability and security of electronic components [1, 2]. To address the issues associated with microwaves, enormous efforts have been taken to minimize electromagnetic radiation. Traditional shielding materials can partially block microwaves; however, contamination could be occurred due to secondary reflected microwaves [3]. Therefore, efficient microwave absorbers must be developed for attenuating microwaves rather than reflecting them.

Carbonaceous materials such as graphene, carbon nanotubes, and hollow carbon spheres [4, 5] exhibit tremendous potential as microwave absorption materials owing to their chemical stability, light weight, and electrical properties. However, pure carbon materials suffer from single loss mechanism and poor impedance matching. N, S, and P co-doping in carbon composites is a valid method for improving the performance of

carbon microwave absorption materials [6-8]. Owing to the difference in electronegativity between carbon and heteroatoms, doping heteroatoms can act as polarization centers in alternating electromagnetic fields to generate dipole polarization and electronic polarization. These polarizations can enhance the attenuation of incident microwaves. Although these carbon materials possess suitable microwave absorption properties, their attenuation ability primarily originates from single dielectric loss and heteroatom sources, such as urea and sulfur. This renders the preparation process more cumbersome. Hence, there remains a huge scope for improving the microwave absorption performance of carbon materials.

In addition to heteroatom doping, transition metal deposition (such as Fe, Co, Ni, and their derivatives) in the carbon matrix is a common method for improving microwave absorption properties [9]. The introduced magnetic metal component can regulate the impedance matching, ensuring that more incident waves penetrate the composites. Therefore, the coupling of a heteroatom-doped carbon matrix with transition metal elements is deemed an effective approach for promoting microwave absorption performance. Although several doped carbon-based microwave absorption materials have been reported [10-12], some disadvantages such as the requirement of expensive raw materials and the complexity of the synthetic process still remain; these disadvantages restrict the large-scale practical

application of such carbon-based materials. Hence, novel carbonaceous materials with low-cost, eco-friendly, and simple fabrication processes need to be explored [13].

Biomass is abundant in nature, and biomass-based carbon materials can be formed through simple carbonization; this has been widely exploited in the fields of microwave absorption [14-16], oxygen reduction reaction [17], and supercapacitors [18]. Particularly in microwave absorption, biomass primarily has the following two advantages over traditional synthetic precursors. On the one hand, biomass naturally possesses necessary heteroatoms, a small quantity of which act as polarization centers for attenuating microwaves and can be retained post calcination. On the other hand, biomass comprises unique structures such as walnut shells [19], woods [20], and loofah [21]. When biomass is converted into carbon materials, its native structure can be relatively reserved and the organic matter can be annealed to form a carbon matrix. Consequently, the approach of deriving biomass-based carbon materials is well-founded, eco-friendly, high-producing, low-cost, and easy-to-perform when preparing carbon-based microwave absorption materials. Egg white is a sustainable biomaterial that can be easily obtained. The main constituents of egg white are water and proteins including C, S, O, and N. These elements can work as doping sites to form S/N-doping carbon during carbonization processing. Besides, the protein in egg white has abundant sites which is easy to

capture metal ions by chelation[22]. Compared with traditional chemical synthesis, protein-assisted method is simpler to obtain precursors of alloy-carbon composites. The reduced alloy also can play a catalyst to carbonize egg white to form graphitic carbon in high temperature. However, less attention has been given to egg white a raw material for absorbing microwaves so far. According to the above-listed literature and some relevant research conducted by our study group [23], we infer that egg-white-derived carbon (EWC) is a potential microwave-absorbing material.

Herein, we aim to develop a biomass-based nano magnetic carbon material and to explore a simple and low-energy method for fabricating egg-white-derived microwave absorption materials for use in two main steps: mixture and pyrolysis. This study is the first to consider Egg white as a source for carbon and sulfur; in addition, Co^{2+}, Ni^{2+}, and Fe^{3+} are chosen as additives to form magnetic components at high temperature. Sulfur doping (S-doping) and modification using magnetic alloys are potential strategies for optimizing the microwave absorption performance of carbon-based materials. In pyrolysis, the sulfur remains in carbon flakes, causing abundant defects to enhance polarization relaxation while the reduced FeCoNi alloy generates extra magnetic loss. Then, the influence of alloy content on graphitization degree, morphology and elemental composition, and the microwave absorption coefficient are systematically investigated. Detailed analysis reveals the mechanism of dielectric and

magnetic loss are generated by the S-doped carbon and trimetallic alloy composites. These conclusions can be used as a reference for preparing sustainable and low-cost microwave absorption materials to some extent.

2.2 Experimental

2.2.1 Materials

The eggs were bought from a local supermarket. All chemicals including $Ni(NO_3)_2•6H_2O$, $Co(NO_3)_2•6H_2O$, and $Fe(NO_3)_3•9H_2O$ are of analytical grade and purchased from Wako Pure Chemical Indus-tries Ltd., Japan. Deionized water was used throughout the experiments.

2.2.2 Preparation of EWC composites

50 mL egg white obtained from two eggs was extracted by droppers then diluted with 100 mL water, and then stirred for 30 min to form a protein solution. To prepare multiple samples, differing amounts (3.9 mmol, 7.8 mmol, 15.6 mmol) of $Ni(NO_3)_2•6H_2O$, $Co(NO_3)_2•6H_2O$, and $Fe(NO_3)_3•9H_2O$ are dissolved in the protein solution at a molar ratio of 1:1:1 and stirred for 2 h. Next, this precursor solution is freeze dried, followed by calcination at 800℃ for 2 h at a heating rate of 5℃/min. The black bulks thus obtained labeled as EWC-1, EWC-2, and EWC-3 based on the amount of added metal salts: 3.9 mmol, 7.8 mmol, and 15.6 mmol, respectively. The pristine biomass-based carbon material is also prepared

via a similar process without adding $Ni(NO_3)_2•6H_2O$, $Co(NO_3)_2•6H_2O$, and $Fe(NO_3)_3•9H_2O$; this reference sample is labeled EWC-0. All the samples were uniformly ground with an agate mortar.

2.2.3 Characterization

The morphology and microstructure of the prepared samples are analyzed via scanning electron microscopy (SEM; SU1510, Hitachi Co., Ltd., Japan). The samples' crystal structure is studied via X-ray diffraction (XRD; MiniFlex 300, Rigaku Corporation, Japan). Raman spectroscopy is used to investigate the samples' existing phase using a HoloLab series 5000 Raman spectroscopy system (514-nm laser excitation). Fourier-transform infrared spectroscopy (ATR-FTIR, Shimadzu Co., Ltd., Japan) is applied to identify the chemical function groups, The electromagnetic parameters are tested using a vector network analyzer (37247D Anritsu Co., Ltd., Japan) at 2–14.2 GHz. The toroidal ring samples are prepared by mixing 40% of the obtained EWC composites and 60% of paraffin, followed by pressing into a mold with a φ_{out} = 7.0 mm and φ_{in} = 3.04 mm. The thickness of ring samples is 1.5mm.

2.3 Results and discussion

Fig. 2.1 shows the preparation process, where cobalt nitrate, ferric nitrate, and nickel nitrate act as trimetallic sources while egg white serves as the

carbon and sulfur source for fabricating EWC composites. When mixing metal ions and egg white, the protein in egg white can seize the metal ions to form protein–metal complexes. Further, the egg white solution turns from semitransparent to opaque. Freeze drying can remove the moisture in solution while calcination can convert Co^{2+}, Fe^{3+}, and Ni^{2+} to metallic Co, Fe, and Ni particles, and subsequently form the FeCoNi alloy under the alloy reaction. Simultaneously, the protein is carbonized into S-doped carbon flakes. The specimen's color thus changes from yellow to black, and finally, dielectric and magnetic EWC composites are obtained.

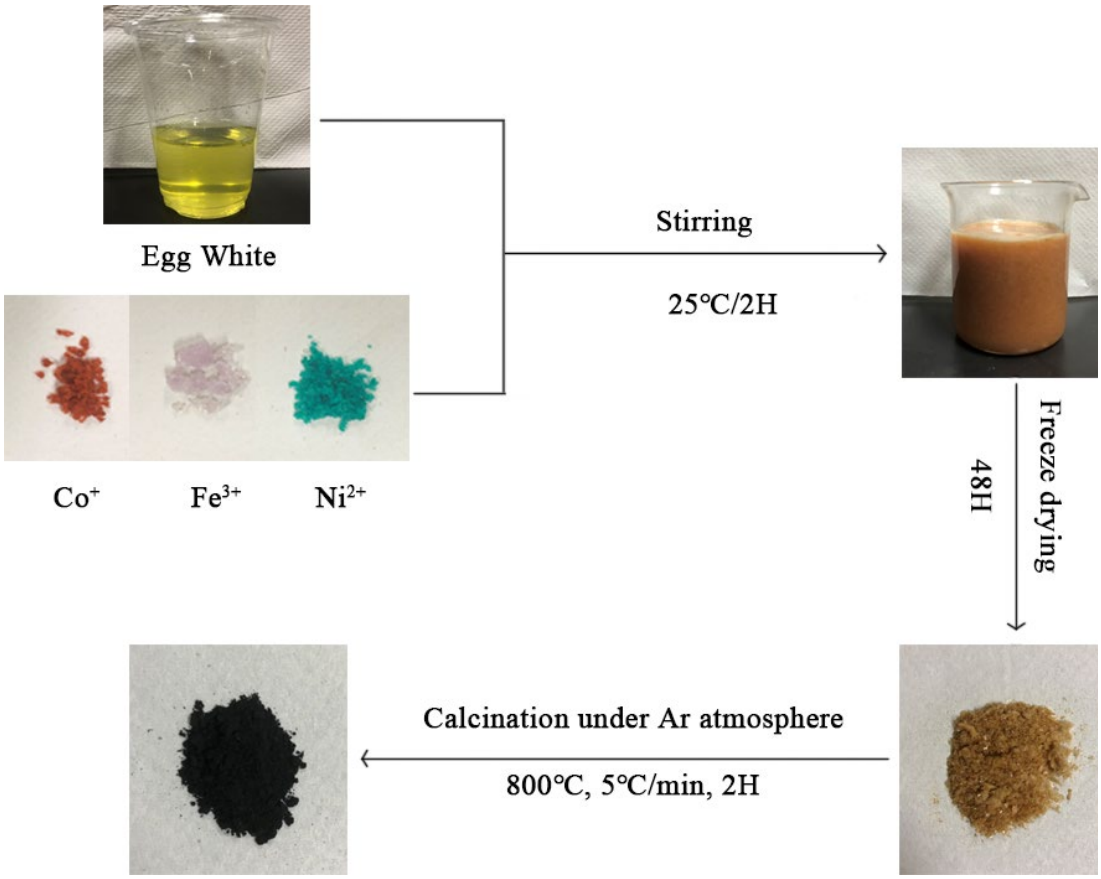

Fig. 2.1. Schematic illustration of sample preparation.

2.3.1 Morphology and composition analysis

Fig. 2.2 shows SEM images of the composites. Both the pristine EWC and alloy-containing EWC samples contain irregular flakes of submillimeter size. The microstructure of the samples reveals two types of morphologies. The morphologies of EWC-1 and EWC-2 are similar to that of EWC-0, whereas the morphology of EWC-3 markedly differs. That is to say, the FeCoNi alloy derived from small number (3.9, 7.8mmol) of metal salt (Fe^{3+}, Co^{2+}, Ni^{2+}) has less impact on morphology of EWC composites while the FeCoNi alloy derived from 15.6 mmol metal salt changes the flakes' surface morphologies more easily. The variation in the samples' morphology can be attributed to the aggregation of the trimetallic alloy during calcination. The aggregation of magnetic alloy is inevitable in template-free method, such phenomenon has been discussed in published literatures.[24-26]. Due to over-added metal salt, a mass of reductive FeCoNi particles aggregates on the surface of EWC-3. The SEM elemental mapping of EWC-2 reveals that C, S, Fe, Co, and Ni are randomly distributed in its carbon flake. Nitrogen is not detected in the flake, this may be due to the occurrence of nitrogen elimination during calcination at a high temperature[27].

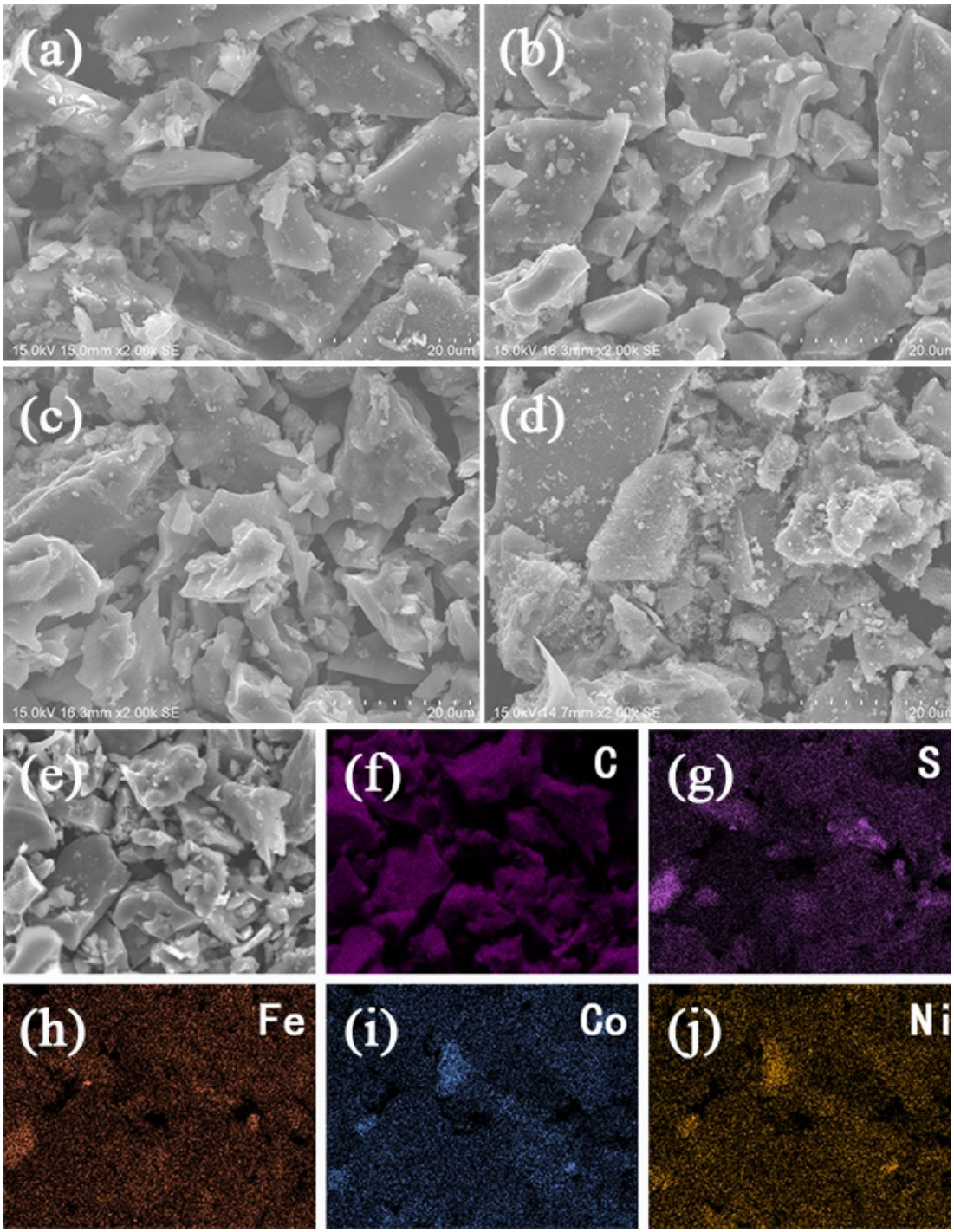

Fig. 2.2. SEM images of (a) EWC-0, (b) EWC-1, (c) EWC-2, and (d) EWC-3 as well as (e-j) the elemental mappings of C, S, Fe, Co, and Ni.

The crystal structures and constituents of the composites were measured via XRD; the corresponding results are shown in Fig. 2.3a. The diffraction peaks at 28°, 31°, 41°, and 45° can be attributed to the inorganic salt such

as KCl, NaCl existing in the egg-white-derived carbon. The three diffraction peaks located at 44°, 51°, and 75° of as-prepared materials are in compliance with the (111), (200), and (222) planes of the face-centered-cubic FeCoNi alloys, indicating the formation of FeCoNi alloy [28]. Due to relative portion of Fe^{3+}, Co^{2+}, Ni^{2+} is not changed in all samples, so XRD results show the same phase of FeCoNi alloy in three samples. Moreover, each diffraction peak of the FeCoNi alloy is a single peak, implying that the composites exist in the form of an alloy rather than a compound of elemental cobalt, nickel, and iron. Furthermore, the peak located 26° can be regarded as the diffraction (002) plane of graphitic carbon (PDF#4187), verifying the successful preparation of the carbon-based matrix after pyrolysis. The weak carbon peak observed for EWC-2 and EWC-3 may result from the presence of the alloy; hence, it is hard to be recognize. To better investigate the graphitization of carbon materials, Raman spectroscopy was performed. The obtained Raman spectrum is presented in Fig. 2.3b, showing two recognizable peaks at about 1350 cm^{-1} (D-band) and 1580 cm^{-1} (G-band). Typically, the ratio of D-band and G-band (I_D/I_G) is used to evaluate the graphitic degree of the composites [29]. The I_D/I_G values of the alloy-added EWCs are slightly lower than that of EWC-0, implying a higher degree of graphitization compared with EWC-0. However, the I_D/I_G values of EWC-1, EWC-2, and EWC-3 show little difference relative to each other, indicating a similar graphitization

between the doped samples. This finding suggests that catalysis of excessive alloy is limited to affect graphitization, which has been discussed in literatures[30, 31]. Furthermore, the intensities of the D- and G-bands for EWC-3 are weakened to a certain degree; this may be caused by the low content of carbon in EWC-3 relative to the other samples. The FT-IR spectra of EWC-0 and EWC-2 are presented in Fig. 2.3c to verify functional groups. Peaks at ~3450 cm^{-1}, 2920cm^{-1}, 1573cm^{-1}, 1182cm^{-1} are assigned to O-H, C-H, C=O, O-C-O stretching vibrations, respectively. Under the reduction of FeCoNi alloys in EWC-2, these peaks become weak or disappeared due to the formation of graphite carbon. The adsorption peaks observed at around 617 cm^{-1} in both EWC-0 and EWC-2 spectra can be attributed to thiophenic sulfur [32, 33], evidencing the successful S-doping in egg-white-derived carbon.

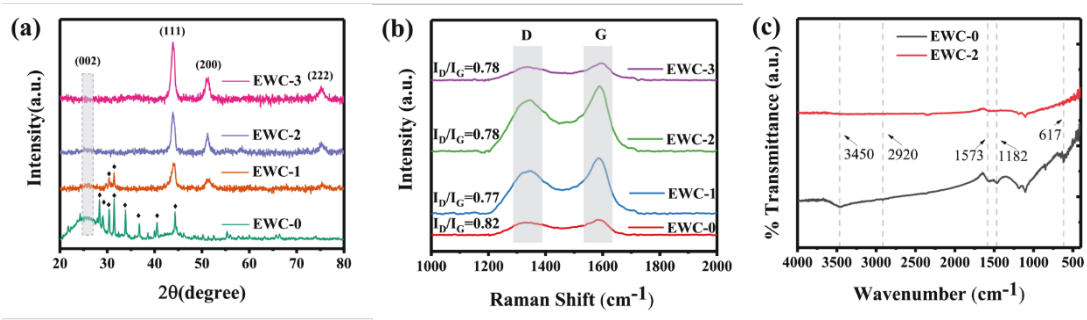

Fig. 2.3. XRD patterns (a), Raman spectra, (b) and FT-IR spectra (c) of the samples.

The chemical states of FeCoNi alloy in EWC-2 were characterized by XPS and displayed in Fig. 2.4. In general, it can be seen C, O, S, Fe, Co, Ni elements exist in full spectrum. Fig. 2.4b shows Fe 2p core level spectra which can be divided into three distinct peaks at 712.3eV, 726.2eV,

721.3eV. These peaks are related to, $2p_{1/2}$ and satellite peaks of metallic Fe. The Co $2p_{3/2}$, Co $2p_{1/2}$ can be observed at 780.9eV and 797.1eV with two satellites at 787.1eV and 803.4eV in Fig. 2.4c. Meanwhile, the Ni 2p spectrum also shows four peaks in Fig. 2.4d. Two main peaks in 855.7eV and 873.1eV are corresponding to the spin-orbit coupling peak of Ni $2p_{3/2}$ and spin-orbit splitting peak of Ni $2p_{1/2}$, while 862.4eV and 880.3eV are accordance with satellite peaks. These XPS results indicate there is little passivation reaction on the surface of synthetic FeCoNi alloy, which demonstrates the FeCoNi interface is connected with egg white derived carbon by van der waals interplanar interaction[24].

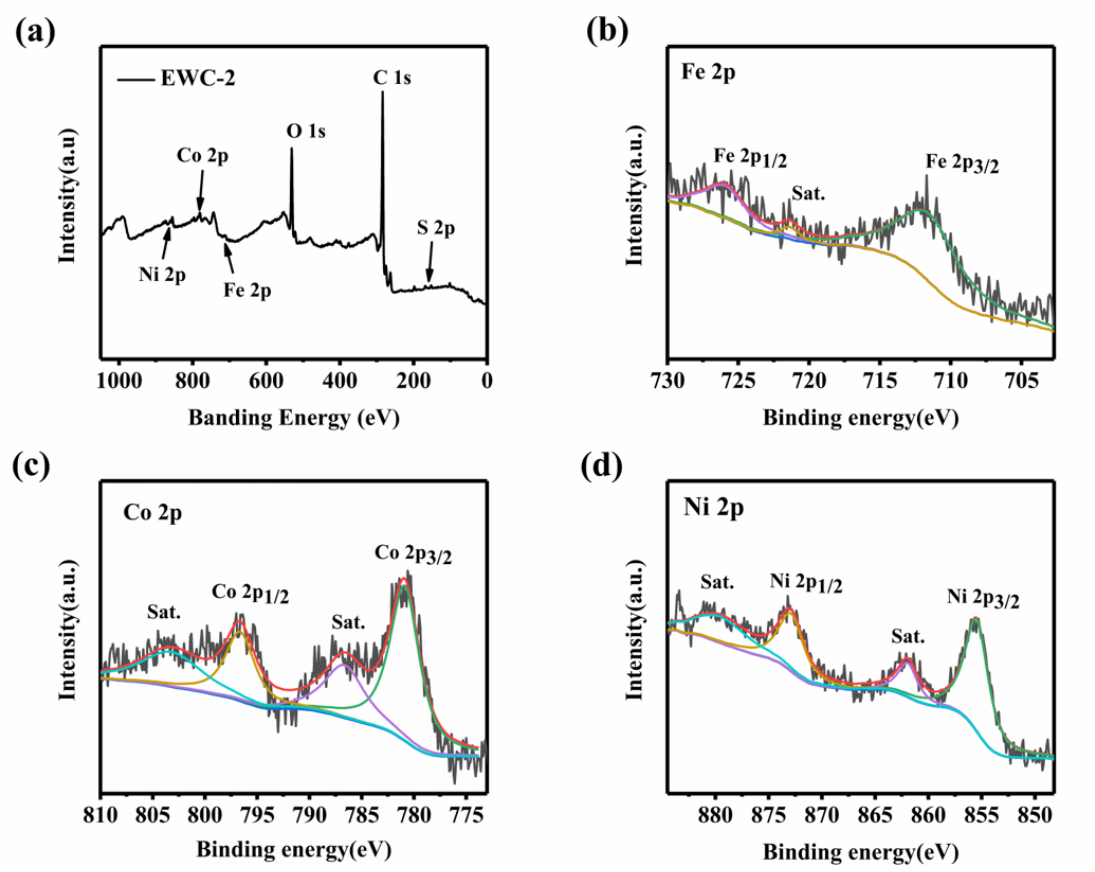

Fig. 2.4. XPS spectrum of EWC-2. (a)survey spectrum, (b) Fe 2p, (c) Co 2p, (d) Ni 2p.

2.3.2 Microwave absorption properties of EWC composites

To study the microwave absorbing properties, RL (reflection loss) values calculated through the transmission line theory [34] are widely used to assess the microwave absorption performance of composites. The specific equations are as follows.

$$Z_{\text{in}} = Z_0\sqrt{\mu_r/\varepsilon_r}\tanh[j(2\pi fd/c)\sqrt{\mu_r\varepsilon_r}] \quad (2\text{-}1)$$

$$RL(dB) = 20\,log|(Z_{in} - Z_0)/(Z_{in} + Z_0)| \quad (2\text{-}2)$$

Here, Z_{in} represents the input impedance of the composite, and Z_0 represents the impedance of free space. *d* represents the thickness of the composite, and *c* is the velocity of light. ε_r and μ_r are the complex permittivity and permeability, respectively, of the composite. An RL value of −10 dB implies 90% attenuation of the incident microwave, which is suitable for practical application. Moreover, the effective absorption bandwidth (EAB) is attained in the frequency range wherein RL values < −10 dB.

The RL values of composites at frequencies of 2–14.2 GHz and a thickness of 0.8–3 mm are calculated, and presented as three- and two-dimensional color maps in Fig. 2.5. Obviously, the amount of added alloy significantly affects microwave absorption performance. The minimum RL value (RL_{min}) of EWC-0 is −6.4 dB at a thickness of 3 mm. Such performance is insufficient for practical application. When the alloy is

added to S-doped carbon flakes, all alloy-added EWCs exhibit enhanced microwave absorption properties. EWC-1 exhibits an RL_{min} of −17.61 dB at a thickness of 3 mm and the EAB is 5.45 GHz. By comparing simulated different thicknesses from 1 to 3 mm, the EAB covers almost the whole X-band (8–12 GHz) at a thickness of 2.6 mm. As the amount of alloy increases, EWC-2 exhibits stronger absorption capacity with an RL_{min} of −47.09 dB at a thickness of 1 mm. However, the widest EAB of 2.8 GHz was attained at a thickness of 1.8 mm, which is narrower than that of EWC-1. Further increasing the amount of alloy, the microwave absorption performance of EWC-3 shows no improvement. The RL_{min} of EWC-3 is merely −20.33 dB at a thickness of 1 mm and the EAB is 2.64 GHz at a thickness of 1.4 mm. According to the trend of this curve, more ideal absorbing peaks are supposed to be exhibited at a high-frequency regime, i.e., 14.2–18 GHz. However, that performance could not be showed here because of the device limitations. Thus, alloy loading could affect the electromagnetic wave absorption performance of as-obtained composites and optimal alloy loading occurs. Notably, the absorption peaks of alloy-added EWCs exhibit the trend of shifting to a lower frequency with increasing thickness. This observation can be explained using the quarter wavelength model [35].

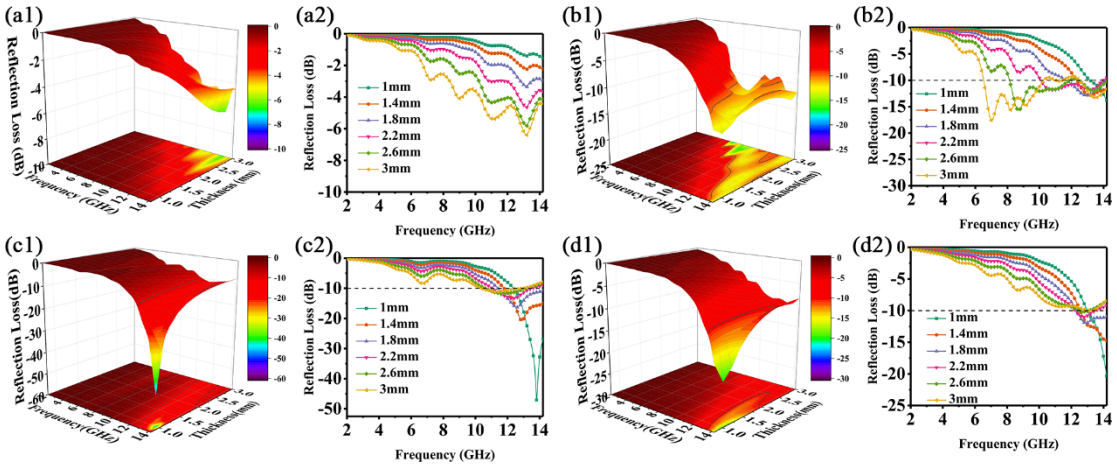

Fig. 2.5. RL values of samples. (a1–a2) EWC-0, (b1–b2) EWC-1, (c1–c2) EWC-2, and (d1–d2) EWC-3.

To better understand the reasons causing the variant microwave absorption performance of the series of EWC composites, the corresponding electromagnetic parameters are further discussed. The complex permittivity ($\varepsilon_r = \varepsilon' - j\varepsilon''$) and the complex permeability ($\mu_r = \mu' - j\mu''$) of the samples are presented in Fig. 2.6. The real part ε' and imaginary part ε'' of the complex permittivity are related to the storage and dissipation of the electric energy in electromagnetic energy, whereas the real part μ' and imaginary part μ'' of the complex permeability are related to the storage and dissipation of the magnetic energy. Figs. 2.6a–b displays the complex permittivity of the series EWC composites. The ε' values of EWC-0, EWC-1, EWC-2, and EWC-3 are in the range of 9.46–2.54, 17.95–2.99, 11.43–2.26, and 9.63–2, respectively. Furthermore, the ε'' values of EWC-0, EWC-1, EWC-2, and EWC-3 are in the range of 1.66–0.22, 7.23–0.24, 3.65–0.09, and 3.08–0.11, respectively. Obviously,

the complex permittivity of EWC-1 is higher than the others. This could be explained from conductivity of EWC composites. There is a positive correlation between the complex permittivity and conductivity[36-38]. Compared with EWC-0, carbon in EWC-1 has higher graphitization degree due to the catalysis of the FeCoNi alloy, which leads to higher conductivity. Among EWC-1, EWC-2, EWC-3, the highest conductivity of EWC-1 results from the high carbon content. Though the FeCoNi alloy is highly conductive, but the alloy particles is easily to aggregate then destroy the conductive structure[30]. Both ε' and ε'' values of samples exhibit a decreasing trend with increasing frequency, which can be explained through frequency dispersion behavior [39, 40]. Notably, such frequency dispersion behavior can also be observed in pristine carbon materials, graphene, carbon nanotubes, and carbon fibers, which improve microwave absorption performance [41-43].

Figs. 2.6c–d presents the complex permeability of all EWC composites. Compared with EWC-0, the EWC-1, EWC-2, and EWC-3 has larger μ' and μ'' which can be mainly attributed to formation of magnetic matter[44], here the magnetic matter is synthetic FeCoNi alloy. For EWC-2, another fluctuation occurs at around 13.8 GHz, indicating a better magnetic loss capacity than EWC-1 and EWC-3. Magnetic loss can be attributed to domain-wall resonance, natural resonance, hysteresis loss, exchange resonance, and the eddy current effect. In particular, the domain-

wall resonance (1–100 MHz) occurs in the frequency range of less than 2 GHz and hysteresis loss occurs in a strong magnetic field because of the irreversible magnetization. Hence, the composites' magnetic loss mainly results from the synergistic effect of natural resonance, exchange resonance, and eddy current in the measured frequency band.

The dielectric loss tangent ($tan\,\delta_\varepsilon = \varepsilon''/\varepsilon'$) and magnetic loss tangent ($tan\,\delta_\mu = \mu''/\mu'$) represent the intensity of dielectric loss and magnetic loss, respectively, where a greater value signifies stronger loss ability. In Figs. 2.6e–f, the dielectric and magnetic losses of EWC-1, EWC-2, and EWC-3 are almost all greater than those of EWC-0 in the measured frequency band. This suggests that addition FeCoNi alloy enhance either the dielectric or magnetic losses of the composites. The EWC-0 has little magnetic particles producing the lowest magnetic loss. The EWC-2 exhibits the highest magnetic loss, which is the same as the trend of μ''. From Figs. 2.6e–f, the tan ε value is higher than that of tan μ in the low frequency range (2–5.6 GHz), whereas the tan ε value is lower than the tan μ value in the relatively high frequency range (>5.6 GHz), indicating the dominant role would change from dielectric loss to magnetic loss with increasing frequency. The dielectric and magnetic losses are discussed based on the above analysis.

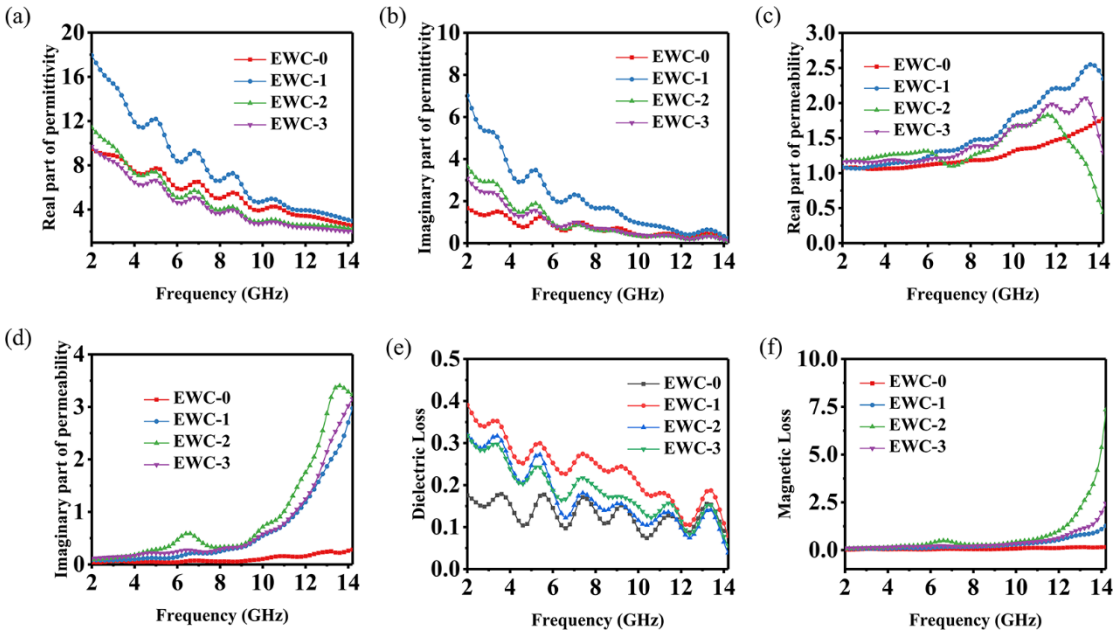

Fig. 2.6. (a) Real parts of the complex permittivity (ε') and (b) imaginary parts of the complex permittivity (ε''), (c) real parts of the complex permittivity (μ'')and (d) imaginary parts of the complex permittivity (μ''), (e) dielectric loss, and (f) magnetic loss of samples.

Dielectric loss includes polarization relaxation and conductive loss. Ionic and electric polarization occurring at a higher frequency (10^3–10^6 GHz) can be excluded [45, 46]. Debye theory is a useful approach for understanding the dielectric loss mechanism [47]. Debye relaxation can be expressed using the following equations.

$$\varepsilon_r = \varepsilon_\infty + \frac{\varepsilon_s - \varepsilon_\infty}{1 + j2\pi f\tau} = \varepsilon' - j\varepsilon'' \tag{2-3}$$

$$\varepsilon' = \varepsilon_\infty + \frac{\varepsilon_s - \varepsilon_\infty}{1 + (2\pi f)^2\tau^2} \tag{2-4}$$

$$\varepsilon'' = \frac{2\pi f\tau(\varepsilon_s - \varepsilon_\infty)}{1 + (2\pi f)^2\tau^2} \tag{2-5}$$

As inferred from Eqs. (2-4) and (2-5), the association between ε' and ε'' can be given as

$$\left(\varepsilon' - \frac{\varepsilon_s + \varepsilon_\infty}{2}\right)^2 + \left(\varepsilon''\right)^2 = \left(\frac{\varepsilon_s - \varepsilon_\infty}{2}\right)^2 \quad (2\text{-}6)$$

The curve of $\varepsilon'-\varepsilon''$ will appear as a semicircle when Debye relaxation occurs, which is known as the classical Cole–Cole semicircle. Further, the straight lines in the Cole–Cole curve represents the existence of conductive loss. Figs. 2.7a–d shows the relationships between ε' and ε'' of each sample. EWC-0 shows four Cole-Cole semicircles while EWC-1, EWC-2, EWC-3 show two Cole-Cole semicircles, suggesting that multiple relaxation processes occur to attenuate microwave energy. EWC-0 shows the most semicircles, implying that the largest number of Debye relaxation processes occurred in S-doped carbon. Referring to existing literature [7, 48], the incorporation of S into the carbon matrix causes substantial lattice defects. Lattice defects, evaluated by the degree of carbon disorder, can act as polarization centers and enhance polarization relaxation. The Raman spectra reveals that EWC-0 has the largest value of I_D/I_G, which represents the largest disorder degree as well as lattice defects in EWC-0. After adding the alloy, the EWC-1, EWC-2, and EWC-3 shows same number of semicircles implying increasing alloy content has no contribution to affect the Debye relaxation. In Debye's theory, relaxation occurs through dipole and interfacial polarizations. The former is generated from the defects in the S-doped carbon matrix and the latter is derived from the multiple interfaces between carbon and alloy [49]. EWC-1, EWC-2 and EWC-3 show similar results in terms of I_D/I_G values; hence, similar dipole

polarization can be generated when the heterogenous interfaces between S-doped carbon and alloy are not changed. To further investigate the polarization process, the relaxation time is evaluated. Through the correlation of Eqs. (4) and (5), the function relationship between ε' and ε'' can be deduced as follows:

$$\varepsilon' = \frac{1}{2\pi\tau}\frac{\varepsilon''}{f} + \varepsilon_{\infty}. \quad (2\text{-}7)$$

Theoretically, the expressed curves of ε' versus ε''/f should follow a linear relation when single polarization relaxation occurs because of dielectric loss [50]. Further, the slope of the linear function $(1/2\pi\tau)$ can be transformed into the following formation:

$$\tau = \frac{1}{2\pi k'}, \quad (2\text{-}8)$$

where k is the slope of the linear function. τ, the defined relaxation time, can be calculated using Eq. (2-8). The function relationship of ε' versus ε''/f is determined via linear regression and shown in Fig. 2.7e. Notably, every sample's curve cannot be fitted into a single line. Thus, the phenomenon evidence that multiple polarization relaxation occurs during microwave absorption. A potential explanation is as follows: on the one hand, when microwaves in the measured frequency band are attenuated, different types of polarization occur with disparate relaxation times. The intrinsic distinctions have respective responses to dielectric loss. On the other hand, the different condition of dipoles generated from lattice defects in the carbon matrix result in variable orientation. Under the

abovementioned actions, the EWC composites possess a relaxation spectrum that generates several slopes in the curves of ε' versus ε''/f. Each curve of the samples can be divided into three fitting lines in linear regression, labeled as Line1, Line2, and Line3. The slopes of the lines are used in the calculation of relaxation times, the results of which are presented in Fig. 2.7f. Typically, a shorter relaxation time implies that the direction of the dipoles needs less time to be corrected in the added electromagnetic field. Compared with the alloy-added EWC samples, EWC-0 exhibits the shortest relaxation time. In the alloy-added EWC samples, EWC-2 and EWC-3 exhibit similar relaxation times, implying that their dipoles spend similar time on direction adjustment in the electromagnetic field. This situation is also consistent with the Raman spectra because the similar degree of graphitization results in a similar relaxation time. The degree of graphitization of EWC-2 and EWC-3 is considerably close to each other.

Regarding conductive loss, as shown in Figs. 7a–d, the alloy-added EWC composites exhibit more and longer straight lines compared with EWC-0, whereas no evident distinction can be detected among them. However, the conductive loss of the alloy-added EWCs is difficult to compare because of the similar curves. The dielectric conductivity is an integral part of influencing the conductive loss, consequently impacting the microwave absorption performance [46, 50]. The conductive loss will be

discussed further as follows. According to Maxwell's equation, the conductivity can be obtained using the following equation.

$$\sigma = \omega \varepsilon_0 \varepsilon'' \tag{2-9}$$

Here, ω and ε_0 represent the angular frequency and permittivity of free space. The calculated conductivity of EWC composites is shown in Fig. 2.7g. Obviously, EWC-1 has the largest value, demonstrating the best conductivity and the largest conductive loss in dielectric loss. EWC-0, EWC-2, and EWC-3 possess close conductivity, probably because the alloy's dielectric conductivity differs from carbon and excessive alloy addition can negatively affect the dielectric conductivity.

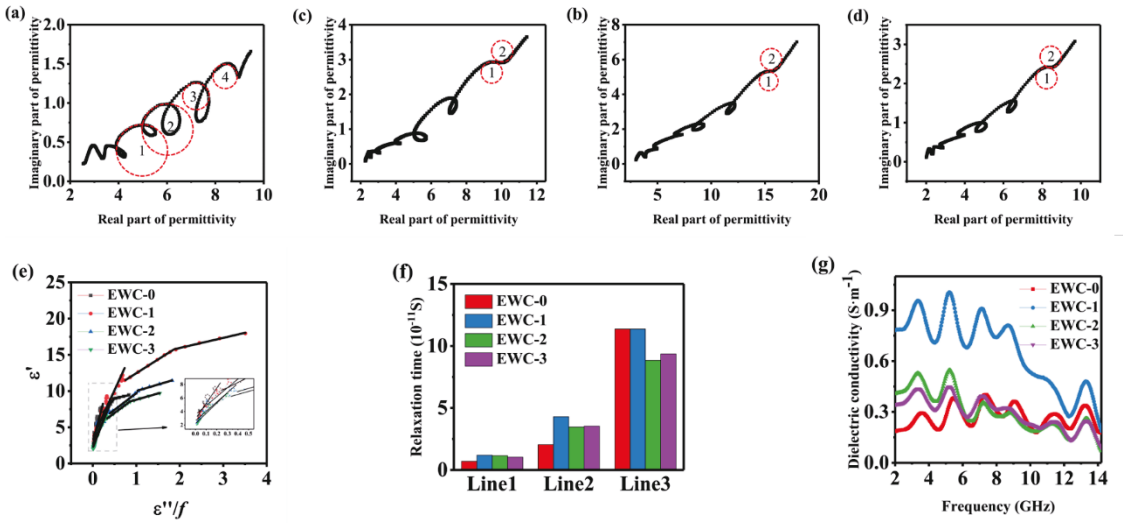

Fig. 2.7. (a) EWC-0, (b) EWC-1, (c) EWC-2, and (d) EWC-3 of Cole–Cole plots; (e) the curves of ε' versus ε''/f; (f) the relaxation time; and (g) the dielectric conductivity of samples.

The sources of magnetic loss also are analyzed herein. The tendency of C_0 $(C_0 = \mu''(\mu')^{-2}f^{-1} = 2\pi\mu_0 d^2\sigma)$ reveals the source of magnetic loss.

If the magnetic loss originates from eddy current loss, the value of C_0 would be a constant with changing frequency. As shown in Fig. 2.8, the tendencies of all samples' C_0 values initially remains constant in the range of 2–5.4 and 5.56–9.6, and then falls and rises in the remaining range. Analyzing the overall C_0 values, it is found that the magnetic loss of samples not only originates from eddy current loss but also from magnetic resonance (natural resonance and exchange resonance) in the measured frequency band. Meanwhile, the amount of FeCoNi alloy is the only variate among four samples, so the different magnetic loss may result from the eddy current loss induced by FeCoNi alloy.

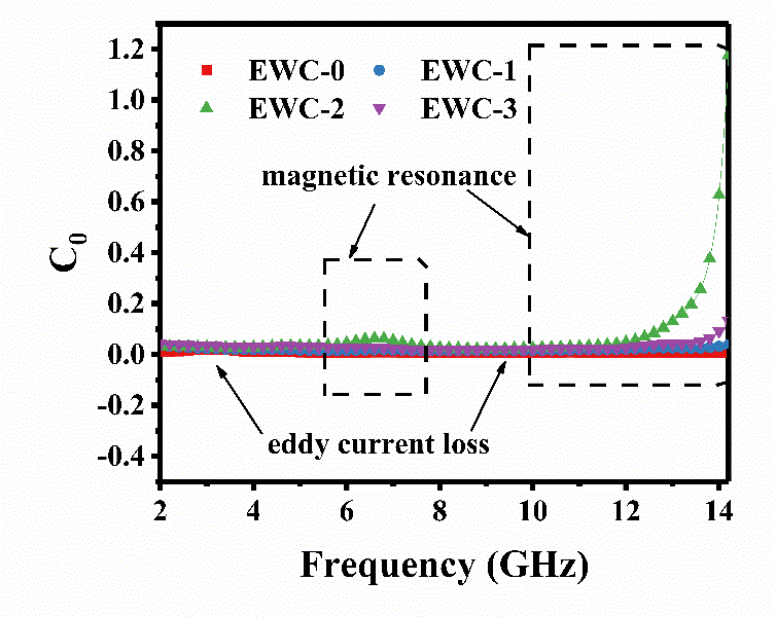

Fig. 2.8. C_0 of EWC-0, EWC-1, EWC-2, and EWC-3.

From Fig. 2.9a, RL_{min} of EWC-2 moved into low-frequency region when thickness of composites increased. This experimental phenomenon can be explained by quarter-wave matching model. The detail equation is as

follows:

$$t_m = \frac{n\lambda}{4} = \frac{nc}{4f_m\sqrt{|\varepsilon_r||\mu_r|}} \quad (n = 0, 1, 2, \cdots) \tag{2-10}$$

Where t_m is the theoretical matching thickness, λ is the wavelength of the incident microwave, c is the light velocity in free space, f_m is the corresponding frequency of the absorption peak. As shown in Fig. 2.9a, the black circles are got from Fig. 2.4 and fall around the t_m curve. This result means the excellent microwave absorption performance of EWC-2 well match the quarter-wave theory.

Based on transmission line theory, the attenuation constant α, which reveals comprehensive microwave absorption capability, can be calculated using the following Equation[51].

$$\alpha = \frac{\sqrt{2}\pi f}{c}\sqrt{(\mu''\varepsilon' - \mu'\varepsilon') + \sqrt{(\mu''\varepsilon'' - \mu'\varepsilon') + (\mu'\varepsilon'' + \mu''\varepsilon')}} \tag{2-11}$$

As illustrated in Fig. 2.9b, the attenuation constant greatly increased with addition of FeCoNi alloy , which means the α can be regulated by FeCoNi alloy. The value of α for EWC-2 is larger than that of other samples in the frequency range of 11.3–14.2 GHz. This trend is similar to that of magnetic loss, which can be attributed to the magnetic loss being dominant rather than dielectric loss in the hybrid. However, strong microwave absorption ability is partially dependent on α. Impedance matching is also a crucial factor, described as

$$Z = \left|\frac{Z_{in}}{Z_0}\right| = \sqrt{|\mu_r/\varepsilon_r|}\, tanh\left[j(2\pi f d/c)\sqrt{\mu_r\varepsilon_r}\right] \tag{2-12}$$

When Z was close to 1, the electromagnetic waves could penetrate the

composite's surface with little reflection then to be attenuated[52]. Fig. 9c shows the calculated Z of different samples at a thickness of 1 mm. In Fig. 2.9c, the FeCoNi alloy loading also has an obvious effect on Z initially, and then remains almost unchanged with increasing alloy content. All alloy-decorated EWC samples show Z values close to 1 in the frequency range of ~13–14.2 GHz; however, EWC-2 possesses the largest RL value owing to the highest attenuation constant in this frequency range. That is to say, the synergetic effect of attenuation constant and impedance matching determines the final microwave absorption. And magnetic FeCoNi alloy plays a vital role in regulating attenuation constant and impedance matching, similar function derived from magnetic alloy also is demonstrated in the literature[53].

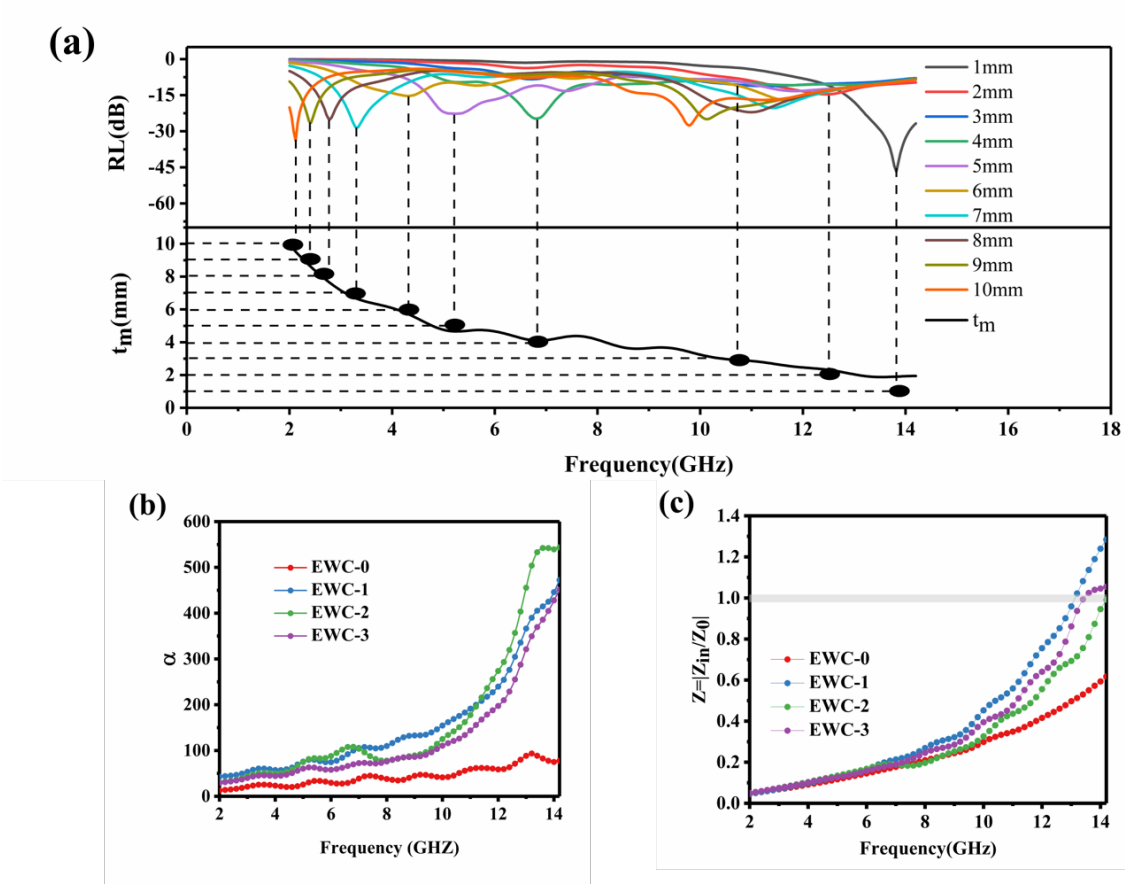

Fig. 2.9. (a) Dependence of λ/4 matching thickness and reflection loss peak of EWC-2, (b) Attenuation constant and (c) Impedance matching of samples at a thickness of 1 mm.

Comparation with the correlative biomass-derived microwave absorption materials listed in Table 2.1. Although EWC-2 has a higher packing content than other composites, the EWC-2 composite exhibits preferable microwave absorption performance in the minimum thickness. In brief, the EWC composite shows expecting potential for attenuating electromagnetic energy.

Table 2.1

RL_{min}, t_{RL} and content of relevant literature.

Samples	RL_{min}/dB	t_{RL}/mm	Content/%	Ref.
Spinach stem	–−62.2 dB	2.71	30	[54]
Rice husk	−43 dB	1.5	35	[55]
Cotton	−51.2 dB	1.65	25	[56]
Pomelo peel	−50.8 dB	2.5	30	[57]
Coconut shell	−32.4 dB	2	30	[58]
EWC-2	−47.09 dB	1	40	This work

The mechanism is illustrated in Fig. 2.10. The microwaves reach the surface of the composite and propagate into the inside under the precondition of suitable impedance matching. Then the trapped wave is dispersed through scattering and converted to other forms of energy such as heat. The excellent attenuation of microwaves can be explained as follows. First, the egg-white-derived carbon has considerable defects in the structure and the added alloy can regulate it to produce different polarization relaxations (interfacial and dipole polarization) and conductive loss, such that the dielectric loss is adjusted. Secondly, the alloy can improve impedance matching and regulate the magnetic loss for composites. The synergetic effect between dielectric and magnetic losses further enhances the microwave absorption performance. Finally, irregular flakes provide numerous paths for the propagation of the microwaves;

hence, the multiple reflection and scattering naturally increase within the composites, helping to attenuate some microwave energy.

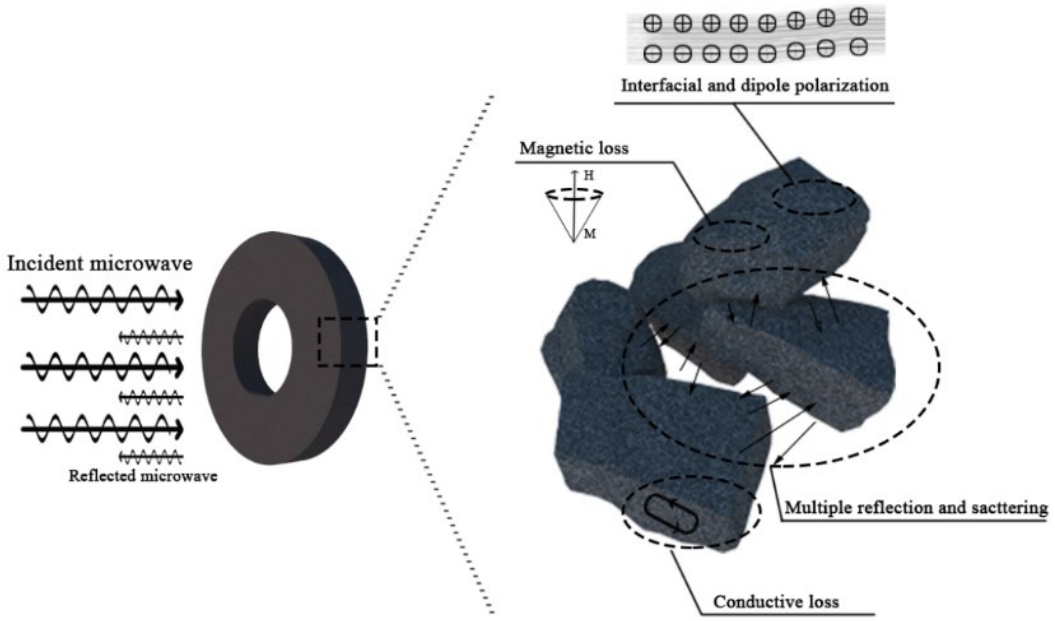

Fig. 2.10. Microwave absorption mechanism of samples.

2.4 Conclusions

In this chapter, we fabricated egg-white-derived S-doped carbon and alloy composites through simple mixing and pyrolysis processes. The S-doped carbon flake possesses multiple polarization relaxations but poor impedance matching, leading to low microwave absorption performance with an RL value of less than −10 dB. After introducing FeCoNi alloy in S-doped carbon, the microwave absorption performance of composites markedly improved. Compared with the other two samples, EWC-2 exhibits a stronger microwave absorption intensity (−47.09 dB at 13.8 GHz)

at a thinner thickness (1 mm). The impact of different contents of the alloy on absorption performance was investigated via the mechanism of dielectric and magnetic losses. The moderate polarization relaxation and conductive loss in dielectric and obvious natural resonance in magnetic loss result in the enhanced absorption performance. Through the synergetic effect of dielectric loss contributed by S-carbon and magnetic loss provided by FeCoNi alloy, the composites own appropriate impedance matching for the incidence of the microwaves and generate powerful attenuation capacity for consuming incident microwaves. Except for the alloy, the S-doped carbon derived from egg white assembled with more advanced components and its structure has promising applications in preparing microwave absorption materials.

References

[1] Y. Cheng, H. Zhao, Y. Zhao, J. Cao, J. Zheng, G. Ji, Structure-switchable mesoporous carbon hollow sphere framework toward sensitive microwave response. Carbon, 161 (2020) 870-879.

[2] Y. Huang, Q. Fan, J. Chen, L. Li, M. Chen, L. Tang, D. Fang, Optimization of flexible multilayered metastructure fabricated by dielectric-magnetic nano lossy composites with broadband microwave absorption. Compos Sci Technol, 191 (2020).

[3] P. Gahlout, V. Choudhary, Microwave shielding behaviour of polypyrrole impregnated fabrics. Composites Part B: Engineering, 175 (2019).

[4] X. Li, L. Yu, W. Zhao, Y. Shi, L. Yu, Y. Dong, Y. Zhu, Y. Fu, X. Liu, F. Fu, Prism-shaped hollow carbon decorated with polyaniline for microwave absorption. Chem Eng J, 379 (2020).

[5] Y. Wang, W. Zhou, G. Zeng, H. Chen, H. Luo, X. Fan, Y. Li, Rational design of multi-shell hollow carbon submicrospheres for high-performance microwave absorbers. Carbon, 175 (2021) 233-242.

[6] X. Sun, J. He, Z. Song, J. Pan, Y. He, J. He, R. Yu, X. Liu, Sodiumphosphinate-assisted synthesis of P-doped FeCo microcubes and their electromagnetic scattering characteristics. J Alloy Compd, 820 (2020).

[7] Y. Li, R. Liu, X. Pang, X. Zhao, Y. Zhang, G. Qin, X. Zhang, Fe@C nanocapsules with substitutional sulfur heteroatoms in graphitic shells for improving microwave absorption at gigahertz frequencies. Carbon, 126 (2018) 372-381.

[8] N. Yang, Z.X. Luo, G.R. Zhu, S.C. Chen, X.L. Wang, G. Wu, Y.Z. Wang, Ultralight Three-Dimensional Hierarchical Cobalt Nanocrystals/N-Doped CNTs/Carbon Sponge Composites with a Hollow Skeleton toward Superior Microwave Absorption. ACS Appl Mater Interfaces, 11 (2019) 35987-35998.

[9] J. Ouyang, Z. He, Y. Zhang, H. Yang, Q. Zhao, Trimetallic FeCoNi@C Nanocomposite Hollow Spheres Derived from Metal-Organic Frameworks with Superior Electromagnetic Wave Absorption Ability. ACS Appl Mater Interfaces, 11 (2019) 39304-39314.

[10] P. Liu, S. Gao, Y. Wang, F. Zhou, Y. Huang, W. Huang, N. Chang, Core-shell Ni@C encapsulated by N-doped carbon derived from nickel-organic polymer coordination composites with enhanced microwave absorption. Carbon, (2020).

[11] M. Huang, L. Wang, K. Pei, W. You, X. Yu, Z. Wu, R. Che, Multidimension-Controllable Synthesis of MOF-Derived Co@N-Doped Carbon Composite with Magnetic-Dielectric Synergy toward Strong Microwave Absorption. Small, 16 (2020) e2000158.

[12] L. Wang, M. Huang, X. Yu, W. You, J. Zhang, X. Liu, M. Wang, R. Che, MOF-Derived Ni1−xCox@Carbon with Tunable Nano–Microstructure as Lightweight and Highly Efficient Electromagnetic Wave Absorber. Nano-Micro Letters, 12 (2020).

[13] Q. Hu, R. Yang, Z. Mo, D. Lu, L. Yang, Z. He, H. Zhu, Z. Tang, X. Gui, Nitrogen-doped and Fe-filled CNTs/NiCo2O4 porous sponge with tunable microwave absorption performance. Carbon, 153 (2019) 737-744.

[14] Y.Q. Fan, Y.H. Li, Y.L. Yao, Y. Sun, B.H. Tong, J. Zhan, Hierarchically porous carbon sheets/Co nanofibers derived from corncobs for enhanced microwave absorbing properties. Appl Surf Sci, 534 (2020).

[15] J. Fang, Y. Shang, Z. Chen, W. Wei, Y. Hu, X. Yue, Z. Jiang, Rice husk-based hierarchically porous carbon and magnetic particles composites for highly efficient electromagnetic wave attenuation. J Mater Chem C, 5 (2017) 4695-4705.

[16] L. Huang, J. Li, Z. Wang, Y. Li, X. He, Y. Yuan, Microwave absorption enhancement of porous C@CoFe2O4 nanocomposites derived from eggshell membrane. Carbon, 143 (2019) 507-516.

[17] S. Gao, X. Li, L. Li, X. Wei, A versatile biomass derived carbon material for oxygen reduction reaction, supercapacitors and oil/water separation. Nano Energy, 33 (2017) 334-342.

[18] X. Kong, Y. Zhang, P. Zhang, X. Song, H. Xu, Synthesis of natural nitrogen-rich soybean pod carbon with ion channels for low cost and large areal capacitance supercapacitor. Appl Surf Sci, 516 (2020).

[19] Z. Li, H. Lin, S. Ding, H. Ling, T. Wang, Z. Miao, M. Zhang, A. Meng, Q. Li, Synthesis and enhanced electromagnetic wave absorption performances of Fe3O4@C decorated walnut shell-derived porous carbon. Carbon, (2020).

[20] J. Xi, E. Zhou, Y. Liu, W. Gao, J. Ying, Z. Chen, C. Gao, Wood-based straightway channel structure for high performance microwave absorption. Carbon, 124 (2017) 492-498.

[21] Q. Yang, Y. Shi, Y. Fang, Y. Dong, Q. Ni, Y. Zhu, Y. Fu, Construction of polyaniline aligned on magnetic functionalized biomass carbon giving excellent microwave absorption properties. Compos Sci Technol, 174 (2019) 176-183.

[22] C.B. Godiya, S.M. Sayed, Y. Xiao, X. Lu, Highly porous egg white/polyethyleneimine hydrogel for rapid removal of heavy metal ions and catalysis in wastewater. Reactive and Functional Polymers, 149 (2020).

[23] Y.F. Zhu, L. Zhang, T. Natsuki, Y.Q. Fu, Q.Q. Ni, Facile synthesis of BaTiO3 nanotubes and their microwave absorption properties. ACS Appl Mater Interfaces, 4 (2012) 2101-2106.

[24] Y. Li, J. Zhai, L. Zhao, J. Chen, X. Shang, C. Song, J. Chen, S. Liu, F. Meng, FeCoNi alloy-encapsulated graphene nanoplatelets with excellent magnetic properties, thermal stability and electrochemical performances. Journal of Solid State Chemistry, 276 (2019) 19-29.

[25] L. Xu, B. Fu, Y. Sun, P. Jin, X. Bai, X. Jin, X. Shi, Y. Wang, S. Nie, Degradation of organic pollutants by Fe/N co-doped biochar via peroxymonosulfate activation: Synthesis, performance, mechanism and its potential for practical application. Chem Eng J, 400 (2020).

[26] L. Chen, S. Yang, K. Qian, W. Wei, C. Sun, J. Xie, In situ growth of N-doped carbon coated CoNi alloy with graphene decoration for enhanced HER performance. Journal of Energy Chemistry, 29 (2019) 129-135.

[27] M. Sevilla, P. Valle-Vigón, A.B. Fuertes, N-Doped Polypyrrole-Based Porous Carbons for CO2Capture. Advanced Functional Materials, 21 (2011) 2781-2787.

[28] Z. Li, L. Cai, M. Song, Y. Shen, X. Wang, J. Li, J. Wang, P. Wang, L. Tian, Ternary FeCoNi alloy nanoparticles embedded in N-doped carbon nanotubes for efficient oxygen evolution reaction electrocatalysis. Electrochimica Acta, 339 (2020).

[29] J. He, D. Zhang, Y. Wang, J. Zhang, B. Yang, H. Shi, K. Wang, Y. Wang, Bioamss-derived porous carbons with tailored graphitization degree and pore size distribution for supercapacitors with ultra-high

rate capability. Appl Surf Sci, (2020).

[30] W. Chu, Y. Wang, Y. Du, R. Qiang, C. Tian, X. Han, FeCo alloy nanoparticles supported on ordered mesoporous carbon for enhanced microwave absorption. J Mater Sci, 52 (2017) 13636-13649.

[31] H. Ning, G. Li, Y. Chen, K. Zhang, Z. Gong, R. Nie, W. Hu, Q. Xia, Porous N-Doped Carbon-Encapsulated CoNi Alloy Nanoparticles Derived from MOFs as Efficient Bifunctional Oxygen Electrocatalysts. ACS Appl Mater Interfaces, 11 (2019) 1957-1968.

[32] W. Si, J. Zhou, S. Zhang, S. Li, W. Xing, S. Zhuo, Tunable N-doped or dual N, S-doped activated hydrothermal carbons derived from human hair and glucose for supercapacitor applications. Electrochimica Acta, 107 (2013) 397-405.

[33] Q. Xu, Y. Liu, C. Gao, J. Wei, H. Zhou, Y. Chen, C. Dong, T.S. Sreeprasad, N. Li, Z. Xia, Synthesis, mechanistic investigation, and application of photoluminescent sulfur and nitrogen co-doped carbon dots. J Mater Chem C, 3 (2015) 9885-9893.

[34] D.T. Kuang, L.Z. Hou, S.L. Wang, H. Luo, L.W. Deng, J.L. Mead, H. Huang, M. Song, Large-scale synthesis and outstanding microwave absorption properties of carbon nanotubes coated by extremely small FeCo-C core-shell nanoparticles. Carbon, 153 (2019) 52-61.

[35] F. Wen, F. Zhang, Z. Liu, Investigation on Microwave Absorption

Properties for Multiwalled Carbon Nanotubes/Fe/Co/Ni Nanopowders as Lightweight Absorbers. The Journal of Physical Chemistry C, 115 (2011) 14025-14030.

[36] J. Kuang, P. Jiang, F. Ran, W. Cao, Conductivity-dependent dielectric properties and microwave absorption of Al-doped SiC whiskers. J Alloy Compd, 687 (2016) 227-231.

[37] D. Liu, R. Qiang, Y. Du, Y. Wang, C. Tian, X. Han, Prussian blue analogues derived magnetic FeCo alloy/carbon composites with tunable chemical composition and enhanced microwave absorption. J Colloid Interface Sci, 514 (2018) 10-20.

[38] W. Zhou, Y. Li, L. Long, H. Luo, Y. Wang, High-temperature electromagnetic wave absorption properties of Cf/SiCNFs/Si3N4 composites. Journal of the American Ceramic Society, 103 (2020) 6822-6832.

[39] J. Xu, Y. Cui, J. Wang, Y. Fan, T. Shah, M. Ahmad, Q. Zhang, B. Zhang, Fabrication of wrinkled carbon microspheres and the effect of surface roughness on the microwave absorbing properties. Chem Eng J, 401 (2020).

[40] W. Xu, G.-S. Wang, P.-G. Yin, Designed fabrication of reduced graphene oxides/Ni hybrids for effective electromagnetic absorption and shielding. Carbon, 139 (2018) 759-767.

[41] D. Estevez, F.X. Qin, L. Quan, Y. Luo, X.F. Zheng, H. Wang, H.X.

Peng, Complementary design of nano-carbon/magnetic microwire hybrid fibers for tunable microwave absorption. Carbon, 132 (2018) 486-494.

[42] L. Liu, L. Wang, Q. Li, X. Yu, X. Shi, J. Ding, W. You, L. Yang, Y. Zhang, R. Che, High - Performance Microwave Absorption of MOF - Derived Core - Shell Co@N - doped Carbon Anchored on Reduced Graphene Oxide. ChemNanoMat, 5 (2019) 558-565.

[43] Y. Cheng, J. Cao, H. Lv, H. Zhao, Y. Zhao, G. Ji, In situ regulating aspect ratio of bamboo-like CNTs via CoxNi1−x-catalyzed growth to pursue superior microwave attenuation in X-band. Inorganic Chemistry Frontiers, 6 (2019) 309-316.

[44] R.C. Che, L.M. Peng, X.F. Duan, Q. Chen, X.L. Liang, Microwave Absorption Enhancement and Complex Permittivity and Permeability of Fe Encapsulated within Carbon Nanotubes. Advanced Materials, 16 (2004) 401-405.

[45] X. Xu, F. Ran, Z. Fan, Z. Cheng, T. Lv, L. Shao, Z. Xie, Y. Liu, Acidified Bimetallic MOFs Constructed Co/N Co-doped Low Dimensional Hybrid Carbon Networks for High-Efficiency Microwave Absorption. Carbon, (2020).

[46] X.J. Zeng, X.Y. Cheng, R.H. Yu, G.D. Stucky, Electromagnetic microwave absorption theory and recent achievements in microwave absorbers. Carbon, 168 (2020) 606-623.

[47] X. Zhou, B. Wang, Z. Jia, X. Zhang, X. Liu, K. Wang, B. Xu, G. Wu, Dielectric behavior of Fe3N@C composites with green synthesis and their remarkable electromagnetic wave absorption performance. J Colloid Interface Sci, 582 (2020) 515-525.

[48] H. Zhang, Z. Jia, A. Feng, Z. Zhou, C. Zhang, K. Wang, N. Liu, G. Wu, Enhanced microwave absorption performance of sulfur-doped hollow carbon microspheres with mesoporous shell as a broadband absorber. Composites Communications, 19 (2020) 42-50.

[49] T. Liu, N. Liu, L. Gai, Q. An, Z. Xiao, S. Zhai, W. Cai, H. Wang, Z. Li, Hierarchical carbonaceous composites with dispersed Co species prepared using the inherent nanostructural platform of biomass for enhanced microwave absorption. Micropor Mesopor Mat, 302 (2020).

[50] Y. Duan, Z. Liu, H. Jing, Y. Zhang, S. Li, Novel microwave dielectric response of Ni/Co-doped manganese dioxides and their microwave absorbing properties. Journal of Materials Chemistry, 22 (2012).

[51] M. Li, X. Fan, H. Xu, F. Ye, J. Xue, X. Li, L. Cheng, Controllable synthesis of mesoporous carbon hollow microsphere twined by CNT for enhanced microwave absorption performance. J Mater Sci Technol, 59 (2020) 164-172.

[52] M. Li, X. Yin, H. Xu, X. Li, L. Cheng, L. Zhang, Interface

evolution of a C/ZnO absorption agent annealed at elevated temperature for tunable electromagnetic properties. Journal of the American Ceramic Society, 102 (2019) 5305-5315.

[53] Q. Liu, Q. Cao, H. Bi, C. Liang, K. Yuan, W. She, Y. Yang, R. Che, CoNi@SiO2 @TiO2 and CoNi@Air@TiO2 Microspheres with Strong Wideband Microwave Absorption. Adv Mater, 28 (2016) 486-490.

[54] Z. Wu, K. Tian, T. Huang, W. Hu, F. Xie, J. Wang, M. Su, L. Li, Hierarchically Porous Carbons Derived from Biomasses with Excellent Microwave Absorption Performance. ACS Appl Mater Interfaces, 10 (2018) 11108-11115.

[55] Q. Li, J. Zhu, S. Wang, F. Huang, Q. Liu, X. Kong, Microwave absorption on a bare biomass derived holey silica-hybridized carbon absorbent. Carbon, 161 (2020) 639-646.

[56] H. Zhao, Y. Cheng, J. Ma, Y. Zhang, G. Ji, Y. Du, A sustainable route from biomass cotton to construct lightweight and high-performance microwave absorber. Chem Eng J, 339 (2018) 432-441.

[57] Y. Wang, X. Gao, H. Zhou, X. Wu, W. Zhang, Q. Wang, C. Luo, Fabrication of biomass-derived carbon decorated with NiFe2O4 particles for broadband and strong microwave absorption. Powder Technol, 345 (2019) 370-378.

[58] Q. Huang, C. Bao, Q. Wang, C. Dong, H. Guan, Tuning the

microwave absorption capacity of TiP2O7 by composited with biomass carbon. Appl Surf Sci, 515 (2020).

Chapter 3: CoNi and N co-doped carbon networks with a template-free strategy for excellent microwave absorption performance

3.1 Introduction

Egg white derived carbon can achieve excellent microwave absorption performance at a low thickness by regulating magnetic alloys, but the performance has no advantage in low frequency band, especially in X band and below (~12.4 GHz)[1]. Expect for magnetic component, morphology is also an important factor in enhancing performance. Recent studies have come up with a variety of potential microstructure for absorbing microwave to relieve electromagnetic pollution. Structure design such as 3D networks[2], nanoflakes[3], nanotubes[4], hollow spheres[5] and porous structures[6] for microwave absorbers is able to enhance microwave absorption performance to some extent. Rational design of structure can regulate interfacial polarization and change microwave propagation path to produce stronger attenuation capacity[7]. However, these processes regulating components and morphology are suffering from particles aggregation, complex synthesis and low productivity and final products are hard to reach the goal of full X band absorption with a single

thickness in most case. More rational methods are supposed to be carried out to solve these problems.

The concept of metal-organic frameworks (MOFs) was first defined by Yaghi and his group in 1995[8]. After decades of development, MOFs based composites have proved possible application in research directions of microwave absorption materials owing to various structures and good chemical homogeneity[9]. Zeolitic Imidazolate Framework (ZIF) as a typical subclass of MOFs, named by similar structure of zeolites, gradually become hot precursor for preparing composites in various fields[10-13]. Carbonized ZIF-derived composites inheriting the merits of rich in nitrogen, polyhedral structures and metallic components exhibit valuable application in preparation of microwave absorbers[14-16]. Among ZIF-based microwave absorbers, cobalt-based ZIF, named as ZIF-67, is the most used template. Additionally, carbon nanotubes[17], polypyrrole[18] metallic oxides[16] and so on also have been utilized to optimize ZIF-67 derived microwave absorbers. Besides cobalt coordination ions, nickel ions also work in ZIF-based microwave absorbers[19]. NiCo alloy with carbon materials has been proved to have favorable performance in absorbing microwave[20]. However, there is no report on preparing ZIFs composed of nickel and cobalt to fabricate eligible microwave absorption materials. We believe Ni/Co bimetallic ZIFs have the research value for developing high-performance microwave absorbers.

For this purpose, in this chapter, we aim to develop a metal organic framework-based magnetic carbon nanomaterial. A template-free strategy is adopted to prepare Ni and Co bimetallic ZIFs derived composites with spontaneous network. It is the first time that Ni/CO bimetallic ZIF is used for preparing microwave absorption materials. The organic ligand acts as carbon and nitrogen sources while Ni^{2+} and Co^{2+} can be reduced into NiCo alloys. By tuning feed ratios of nickel nitrate and cobalt nitrate, composites with different morphology and component were fabricated. The optimization was concluded when molar ratio of Ni^{2+}/Co^{2+} was 1:2. The Ni_1CO_2@C with 3D network structure combined with wax showed admirable microwave absorption performance. The minimum value of reflection loss is -41.9 dB at 12.2 GHz with a thickness of 1.5 mm while the whole X band is covered with thickness of 2.6 mm. The strong microwave behaviors could be attribute to dielectric-magnetic synergistic effect and network structure. The source of dielectric and magnetic loss is specifically investigated and analyzed. These experimental results shed light on rational design of template-free microwave absorption materials.

3.2 Experiment section

3.2.1 Chemicals

Nickel nitrate hexahydrate ($Ni(NO_3)_2{\cdot}6H_2O$), Cobalt nitrate hexahydrate ($Co(NO_3)_2{\cdot}6H_2O$) and 2-Methylimidazole (2-MeIm) were purchased from

Wako Pure Chemical Industries Ltd., Japan. All reagents were analytical grade and employed without further purification. Deionized water was used for all experiments.

3.2.2 Synthesis

3.2.2.1 Synthesis of Ni_xCo_y-ZIFs

All of the chemicals were analytical grade and used without further purification. In a typical synthesis of Ni_1Co_2-ZIF, $Ni(NO_3)_2·6H_2O$ (582 mg, 2 mmol), $Co(NO_3)_2·6H_2O$ (1164 mg, 4 mmol) were dissolved in water (60 mL) and stirring for 30min to form a uniform solution. As-prepared solution was quickly poured into 20 mL aqueous solution where dissolving 2-methylimidazole (1968 mg, 24 mmol). The mixed solution stirred for 10 min and was incubated at room temperature for 24 h. Then the product was washed with ethanol for several time and dried at 60℃ for 12 h. For comparation, ZIFs with different Ni^{2+}/Co^{2+} molar ratios are synthesized. The specific $Ni(NO_3)_2·6H_2O/Co(NO_3)_2·6H_2O$ ratios in Ni_xCo_y-ZIFs are 1164mg/582mg (molar ratio = 2:1), 873mg/873mg (molar ratio = 1:1) and other process conditions are the same as synthesis of Ni_1Co_2-ZIF. The final products are named Ni_2Co_1-ZIF, Ni_1Co_1-ZIF.

3.2.2.2 Preparation of Ni_xCo_y@C composites

The Ni_xCo_y-ZIFs are put in a tube furnace then heated to 700℃ under argon. The heating rate of is 2℃ min^{-1} and annealing time is 2 h. After calcination, products show a color change from purple to black. The

composites made with different ratios of metal salts were named as Ni_2Co_1@C, Ni_1Co_1@C and Ni_1Co_2@C derived from Ni_2Co_1-ZIF, Ni_1Co_1-ZIF and Ni_1Co_2@C, respectively.

3.2.3 Characterization

X-ray diffraction (XRD, MiniFlex 300, Rigaku Corporation, Japan) were employed to examine phase and crystal structure of composites. Field emission scanning electron microscopy (FESEM, Hitachi S-5000, Japan) was applied to observe morphology and structure of composites. X- ray photoelectron spectroscopy (XPS, AXIS-ULTRA DLD, KRATOS) were used to confirm element distribution and chemical composition of composites. Raman spectrometer with 532nm laser excitation (HoloLab series 5000, Kaiser optical system) was utilized to perform Raman spectra of composites.

3.2.4 Electromagnetic measurements

Electromagnetic parameters of composites are measured on the vector network analyzer (37247D, Anritsu Co., Ltd.) between the frequency range of 2-12.4 GHz. A sample containing 40wt% of obtained Ni_xCo_y@C is uniformly mixed with paraffin then compressed into a ring with an outer diameter of 7 mm and an inner diameter of 3.04 mm.

3.3 Result and discussion

Fig. 3.1 demonstrate the preparation process of Ni_xCo_y@C, which

mainly consists of two steps: crystallization and pyrolysis. In crystallization, the Ni_xCo_y-ZIFs are successfully synthesized by reaction of 2-MeIM with Ni^{2+} and Co^{2+}. The 2-MeIM acting as the organic ligand not only produces carbon and nitrogen source, but also provide sites for capturing metal ions (Ni^{2+} and Co^{2+}) to form bimetallic ZIFs. In high-temperature pyrolysis, the 2-MeIM ligands were transformed into N-doped graphitic carbon, while the metal nodes were reduced to CoNi alloy particles distributing in carbon.

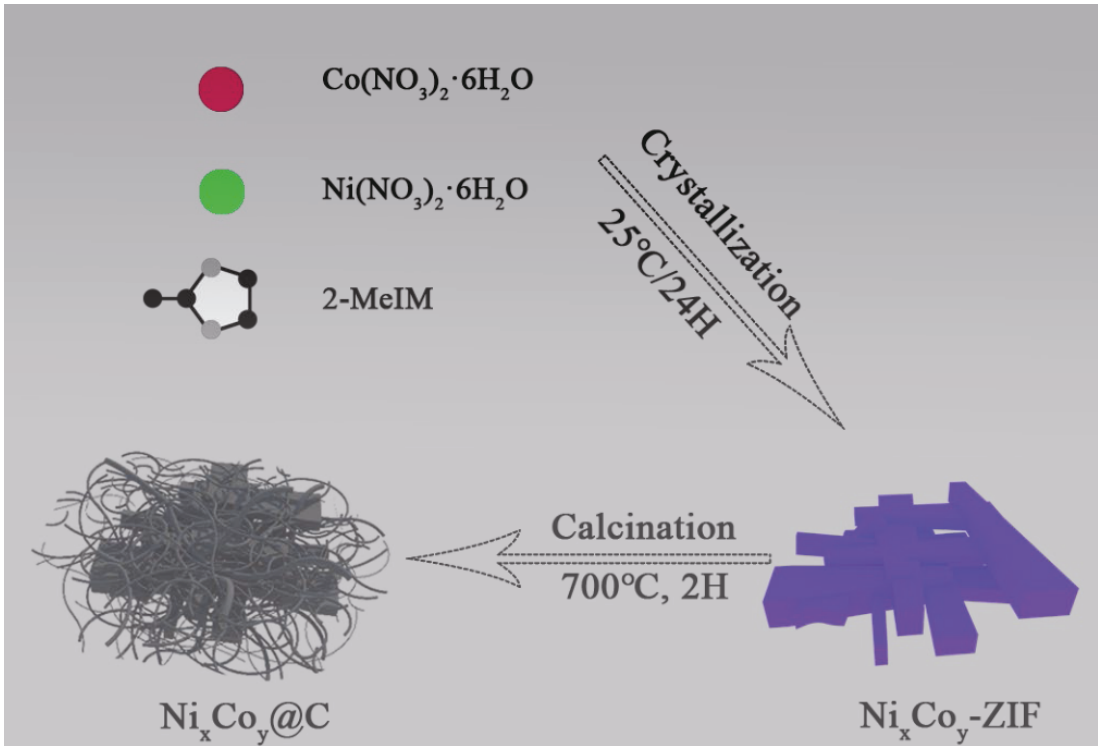

Fig. 3.1. Schematic for synthetic process of Ni_xCo_y@C composites.

The micromorphology of products was observed by FESEM and exhibited in Fig. 3.2. Figs. 3.2a-c exhibit morphology of the as-prepared Ni_xCo_y-ZIF, all of them shows irregular flake-like forms in micron grade. What is worth mentioning is that such form is not similar to neither Ni-

ZIF[19] nor Co-ZIF[21]. It can be concluded that the Ni/Co ratio has an apparent impact on sizes of flakes. The flakes get larger from Ni_2Co_1-ZIF to Ni_1Co_2-ZIF with the ratio of Co^{2+} increasing. Figs. 3.2d-f shows the pyrolysis products of the Ni_xCo_y-ZIF. The Ni_2Co_1@C exhibits the bulk shape where partially isolated particles can be observed. When the Ni/Co ratio is changed to 1:1, it shows some lengthened particles on the bulks' surface of the Ni_1Co_1@C. Further tuning the Ni/Co ratio, the 3D network is constructed in the Ni_1Co_2@C. In view of the uniform experiment condition except the Ni/Co ratio in synthetic process, the different morphology of pyrolysis products may result from catalysis of the NiCo alloy with different proportion[22-24].

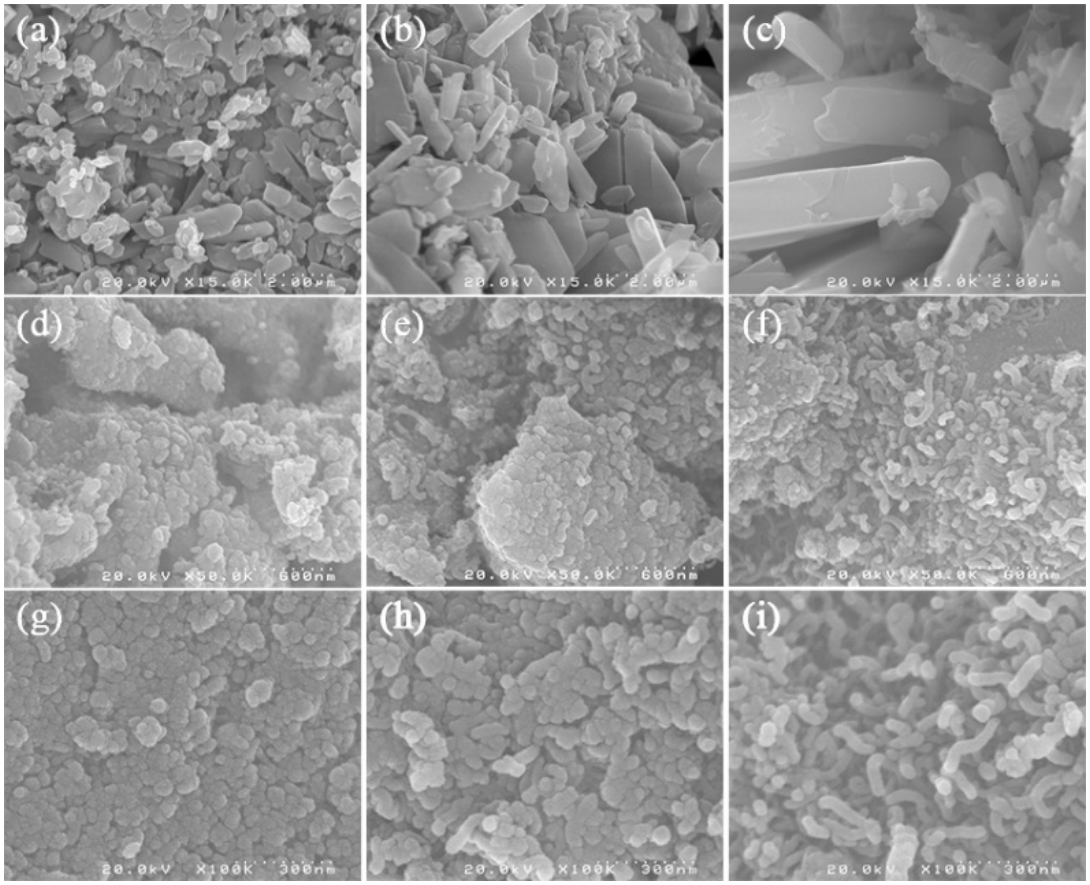

Fig. 3.2. FESEM images of Ni_2Co_1-ZIF (a), Ni_1Co_1-ZIF (b), Ni_1Co_2-ZIF (c), Ni_2Co_1@C (d), Ni_1Co_1@C (e), Ni_1Co_2@C (f), and the high magnification FESEM images of Ni_2Co_1@C (g), Ni_1Co_1@C (h), Ni_1Co_2@C (i).

X-ray Diffraction can be made use of to investigate the characteristics and components of the composites, the result is displayed in Fig. 3.3a. The XRD pattern of Ni_xCo_y@C presents three characteristic peaks at 44.5°, 51.7° and 76.1°, which shows a light shift compared with metallic Ni (JCPDS 01-1260) and Co (JCPDS 15-0806), corresponding to the (111), (200) and (220) planes of metallic NiCo alloy [25]. The wide peak located at around 26° can be attributed to (002) plane of graphitic carbon (JCPDS No.41-1487), suggesting the 2-MeIM organic ligands were totally reduced to carbon. The above patterns prove that all Ni_xCo_y@C composites contain CoNi alloy and carbon matrix.

The component in carbon matrix is further investigated by Raman spectra. Raman spectroscopy is used to evaluate the graphitization degree of the carbon matrixes. As shown in Fig. 3.3b, two characteristic peaks located at around 1350 cm^{-1} and 1580 cm^{-1} can be observed, corresponding to the D band and G band. In general, the D band confirms amorphous carbon and the G band represents graphitized carbon. The obvious peaks of D band and G band sustain the coexistence of amorphous carbon and graphitized carbon. It is accepted that the intensity ratio of I_D/I_G can be regarded as the graphitization degree of in carbon composites[26]. Typically, the I_D/I_G values of Ni_2Co_1-C, Ni_1Co_1-C and Ni_1Co_2-C are 1.02,

1.03, 1.03. It should be pointed out that all values of samples are nearly the same constant, indicating that the carbon in these composites owns similar graphitization degree. It has been proved that Ni and Co can act as catalysts in processing of graphitization, but changing the ratios of Ni and Co shows little effect on enhancing the graphitization degree[27]. Such phenomenon suggests that variation of electromagnetic properties may result from the chemical components rather than the graphitization degree.

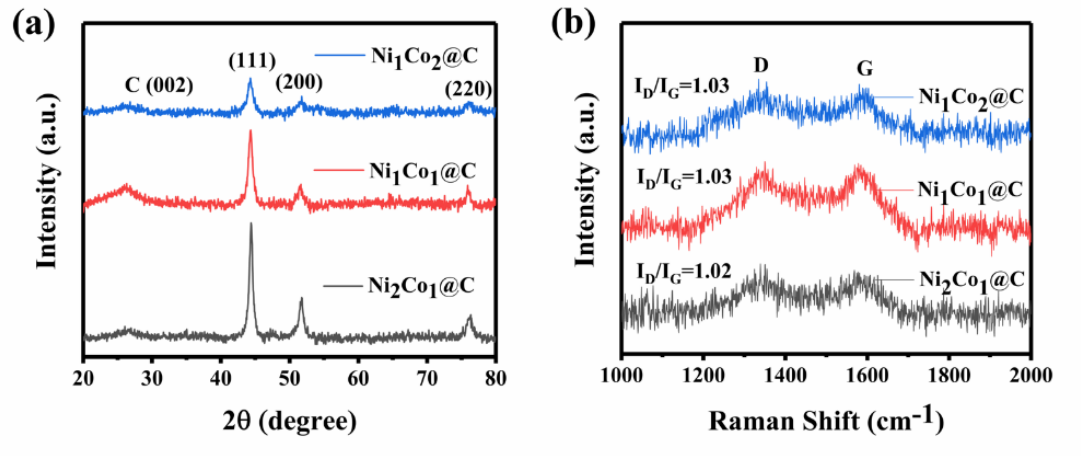

Fig. 3.3. XRD spectra(a), Raman spectra(b) of Ni_xCo_y@C composites.

XPS was employed to examine the surface chemical components of Ni_xCo_y@C. As shown in Fig. 3.4a, the surface XPS spectrum shows the existence of C, N, O, Ni and Co. The engendering of oxygen may be attributed to partial oxidation in air and some O_2 absorption sites in porous structure. For the C 1s XPS spectrum in Fig. 3.4b, it consists three kinds of carbon species. The peaks located at 284.4 eV, 284.8 eV, 288.5 eV can be regarded as C-C. C-O-C, and O=C-O functional groups. The XPS spectrum of N 1s in Fig. 3.4c also has three signals at 398eV, 400eV and 402.5eV,

corresponding to pyridinic-N, pyrrolic-N and graphitic N. This result proves the successful incorporation of N atoms in carbon lattice structures. The spectrums of Ni 2p and Co 2p in Figs. 3.4e and 3.4f confirm existence of high-valence Ni and Co in Ni_xCo_y@C. The metallic Co with binding energies (778.5eV and 793.3eV) exhibits in the Co 2p XPS spectrum, which means the Co^0 is in composites. It also shows the Co^{3+} species (781eV and 796.4eV) and Co^{2+} (779.8 eV and 794.7eV) species with satellites (786.3eV and 802.1eV), respectively. The spectrum of Ni 2p suggests presence of the Ni^{2+} species (854.8eV and 872.3eV). The above analysis proves the composite consists of more than one metal oxide on the surface. According to previous literatures, the various polar groups on the surface of composites are positive for achieving enhanced dipoles polarization and improve microwave absorption properties[28, 29].

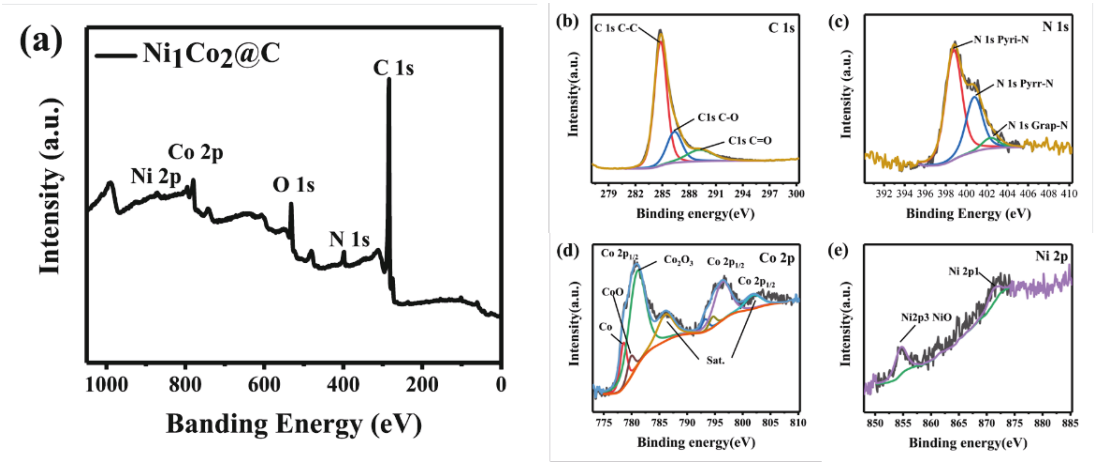

Fig. 3.4. XPS spectra (a), XPS spectra in the C 1s region (b), N 1s region (c), Co 2p region (d), Ni 2p region (e).

The reflection loss (RL) value plays a vital role in evaluation of

microwave absorption performance. According to the linear transmission theory, the RL coefficients of composites are calculated by the complex permittivity (ε_r) and permeability (μ_r) values[30]. The specific formulas are as follows:

$$Z_{\text{in}} = Z_0\sqrt{\mu_r/\varepsilon_r}\, tanh[j(2\pi f d/c)]\sqrt{\mu_r\varepsilon_r} \quad (3\text{-}1)$$

$$RL(dB) = 20\, log|(Z_{in} - Z_0)/(Z_{in} + Z_0)| \quad (3\text{-}2)$$

where Z_{in}, ε_r, μ_r, d is the input impedance, complex permittivity, complex permeability and thickness of the composites, Z_0 represent the free space impedance, c refers to the velocity of the microwave in free space. RL values exceeding -10 dB means that 90% of the incident microwave has been absorbed, which reaches effective absorbing intensity. From Figs 3.5a-f, Ni_xCo_y@C with different Ni/Co molar ratios show various levels of microwave absorption performance in measured frequency range (2-12.4GHz) and at different simulated thickness (1-4mm), indicating that the as-obtained composites' microwave absorption properties could be tuned by adjusting Ni/Co molar ratios. Moreover, the effective absorption regions are encircled by dash line in Figs. 3.5b, 5d and 5f. For Ni_2Co_1@C, the RL_{max} value is -7.1 dB, which is dissatisfied for absorbing microwave. When the Ni/Co ratio is adjusted, the composites' microwave absorption intensity and effective bandwidth show obvious changes. The Ni_1Co_1@C exhibits optimal RL_{min} value of -24.7 dB at 6.9 GHz in 3.5mm and effective absorption band can reach to full X band (8.2-

12.4) in 2.8 mm. Further changing the Ni/Co ratio, the Ni_1Co_2@C shows better absorption ability compared with the other two composites. the Ni_1Co_2@C exhibits an improved RL_{min} value of -41.9 dB at 12.2 GHz in 1.5mm and the effective absorption band covers entire X band in 2.6mm. In a word, it achieves a stronger intensity and the whole X band absorption in a thinner thickness. These comparations confirm Ni_1Co_2@C is more valuable for practical application.

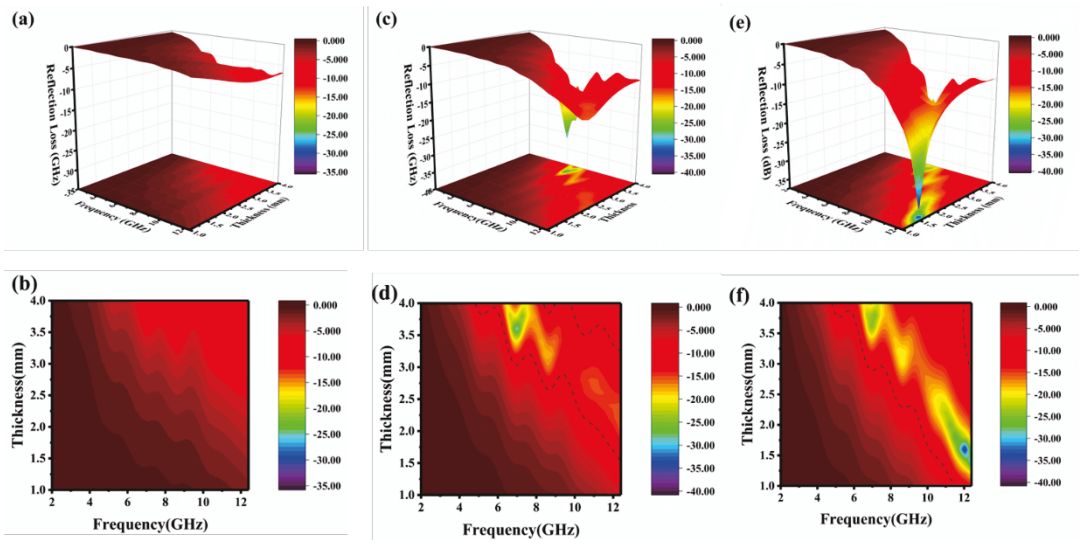

Fig. 3.5. The three-dimensional maps of simulated RL values and contour maps of Ni_2Co_1@C (a, b), Ni_1Co_1@C (c, d), Ni_1Co_2@C (e, f).

To reveal the superior microwave absorption performance of Ni_xCo_y@C, the electromagnetic parameters are supposed to be discussed. The microwave absorption capacity is basically depended on complex permittivity ($\varepsilon_r = \varepsilon' - j\varepsilon''$) and permeability ($\mu_r = \mu' - j\mu''$)[31]. The real part ($\varepsilon'$) and the imaginary part (ε'') of the complex permittivity represent the storage and dissipation capability while the real part μ' and the imaginary part (μ'') of the complex permeability stand for the storage

and dissipation ability of magnetic energy. The dielectric loss tangent ($\tan\delta_\varepsilon=\varepsilon''/\varepsilon'$) and magnetic loss tangent ($\tan\delta_\mu=\mu''/\mu'$) are on behalf of the dielectric and magnetic loss capacity. As shown in Fig. 3.6a, ε' values range from 8.7 to 2.6 for Ni_2Co_1@C, from 15.1 to 3.2 for Ni_1Co_1@C, and 13.2 to 2.9 for Ni_1Co_2@C. The ε'' also displays a decline curve in Fig. 3.6b, decreasing from 2.6 to 0.2 for Ni_2Co_1@C, from 7 to 0.3 for Ni_1Co_1@C and 5.83 to 0.2 for Ni_1Co_2@C. It can be observed that both ε' and ε'' values exhibit decreasing tendencies with increasing frequency. This phenomenon is called frequency dispersion effect and primarily caused by hysteresis of the high-frequency electric field[17]. The values of ε'' in measured frequency could reflect interfacial polarization and dipolar polarization. According to previous literature, interfacial polarization depends on the surface area and heterogeneity of composites, where components with different permittivity would accumulate charge at boundaries. This impact could be enhanced if there are pores and heterogeneous interfacial in composites. Dipoles, limited by defects and residual groups, are the bound charges in dielectric materials. Different from free electrons, they could not move freely in an external electric field. When given a high-frequency alternating electric field, the dipoles could not timely respond to the external electric field, which causes polarization of the diploes. The dipolar polarization is caused by the permanent dipole and is related to aspect ratio. Consequently, typical dispersion behavior

appears in form of decreasing ε' and ε''.

From Figs. 3.6c-d, μ' and μ'' values of the products show different volatility trends. For Ni_2Co_1@C, both μ' and μ'' values show increasing trends from 1.2 to 1.5 and from 0.1 to 0.46, respectively. For Ni_1Co_1@C, the μ' and μ'' values increase from 1.1 to 1.5 and from 0.05 to 1.2, showing the same trends as that of Ni_2Co_1@C, For Ni_1Co_2@C, the μ' first increases from 1.22 to 1.49 then decreases from 1.49 to 0.8 while the μ''climbs up from 0.07 to 2.45 with several fluctuations. Figs. 3.6e-f show the $\tan\delta_\varepsilon$ and $\tan\delta_\mu$ of the Ni_xCo_y@C composites, which can prove the composites have both dielectric and magnetic loss. What's more, it can be demonstrated again the change of Ni/Co ratio can adjust the dielectric and magnetic properties, the close values of complex permittivity and permeability are also useful for tailoring impedance matching[32].

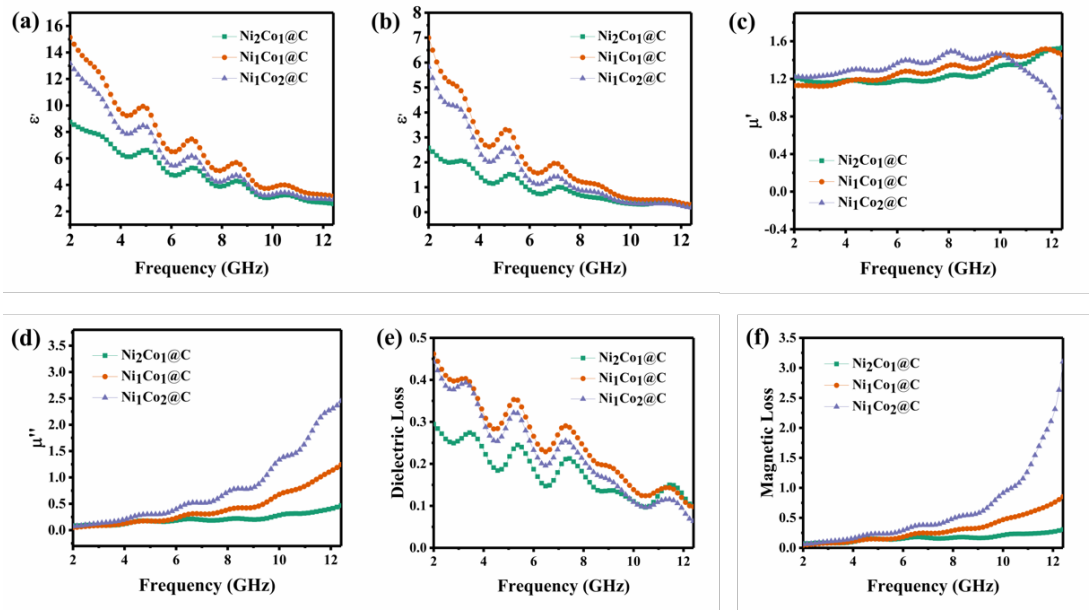

Fig. 3.6. Real part (a) and imaginary part of permittivity, real part (c) and imaginary part (d) of permeability, dielectric loss (e) and magnetic loss (f) of Ni_xCo_y@C

composites.

In order to investigate the relaxation processes which plays an important role in dielectric loss mechanism, Debye relaxation process is analyzed and the relationship between ε' and ε'' is described as follows[33]:

$$\varepsilon_r = \varepsilon_\infty + \frac{\varepsilon_S - \varepsilon_\infty}{1 + j2\pi f\tau} = \varepsilon' - j\varepsilon'' \tag{3-3}$$

And the equation can express relationship between ε' and ε''.

$$\varepsilon' = \varepsilon_\infty + \frac{\varepsilon_S - \varepsilon_\infty}{1 + (2\pi f)^2\tau^2} \tag{3-4}$$

$$\varepsilon'' = \frac{2\pi f\tau(\varepsilon_S - \varepsilon_\infty)}{1 + (2\pi f)^2\tau^2} \tag{3-5}$$

Where f is the frequency, τ represents polarization relaxation time, ε_S and ε_∞ corresponds to static permittivity and high-frequency limit permittivity, respectively. By means of equation, Cole-Cole semicircle can be displayed in the ε'- ε'' curves.

$$\left(\varepsilon' - \frac{\varepsilon_S + \varepsilon_\infty}{2}\right)^2 + \left(\varepsilon''\right)^2 = \left(\frac{\varepsilon_S - \varepsilon_\infty}{2}\right)^2 \tag{3-6}$$

Based on equation, the presence of polarization process could be proved by Cole-Cole semicircle of the ε''-ε'' plots. As illustrated in Figs. 3.7a-c, all composites show more than one Cole-Cole semicircle, which means there are multiply polarization processes in obtained composites. From the XPS result, different oxygen functional groups existed in composites. These chemical bonds bring about different surroundings of the dipoles, which results in the multi-dipoles polarization loss. In addition, the CoNi alloy in carbon matrix possibly cause other polarization loss like interfacial polarization to attenuate incident microwave.

Due to all Ni_xCo_y@C samples show more than one Debye relaxation process, the different dielectric behaviors among three samples need to be investigated further. Generally speaking, the conduction loss and polarization relaxation play indispensable roles in affecting' dielectric behaviors in an electromagnetic field. Dielectric conductivity is a vital factor to evaluate the conduction loss. The following Eq. (3-7) can be used for calculating dielectric conductivity[34]:

$$\sigma = \omega \varepsilon_0 \varepsilon'' \tag{3-7}$$

Where ω is stand for the angular frequency and ε_0 is the permittivity of free space. Fig. 3.7d shows the dielectric conductivity of samples. It is obvious that the Ni_1Co_1@C owns the maximum values and Ni_2Co_1@C exhibits the minimum values in frequency of 2-12.4 GHz, suggesting that the conduction loss contributes most effect to Ni_1Co_1@C and least to Ni_2Co_1@C.

As for polarization relaxation, the relationship between ε' and ε'' can be expressed as following equation by associated with Eqs. (3-4) and (3-5):

$$\varepsilon' = \frac{1}{2\pi\tau}\frac{\varepsilon''}{f} + \varepsilon_\infty \tag{3-8}$$

Theoretically speaking, if dielectric loss is composed of only one type of polarization relaxation, the relationship of ε' versus ε''/f will be a step function[35]. And the slope (k) of the function is used to be calculated for the constant relaxation time and expressed as the following equation:

$$\tau = \frac{1}{2\pi k} \tag{3-9}$$

Fig. 3.7e displays the curve of ε' versus ε''/f. Not surprisingly, the straight line is difficult to be found, implying the polarization relaxation of three samples are all derived from more than one single process. The fit lines are acquired with the help of linear regression analysis, then the relaxation time can be calculated by Eq. (3-9). From Fig. 3.7e, the curve of every sample is able to be matched into three fit lines, named the first, second and third fit line. In Fig. 3.7f, the Ni_1Co_1@C exhibits the longest relaxation time while Ni_2Co_1@C shows the shortest time. The longer relaxation means that it costs more time for dipoles to be synchronous with the external field. The possibility that causes different relaxation time of the Ni_xCo_y@C may attribute to the different Ni/Co ratios in samples. According to the above analysis, the stronger dielectric loss of Ni_1Co_1@C in three samples results from the higher conductivity and longer polarization time. However, the as-obtained Ni_xCo_y@C composites possess dielectric and magnetic properties. The dielectric loss is not the only factor that contributes to enhanced microwave absorption performance.

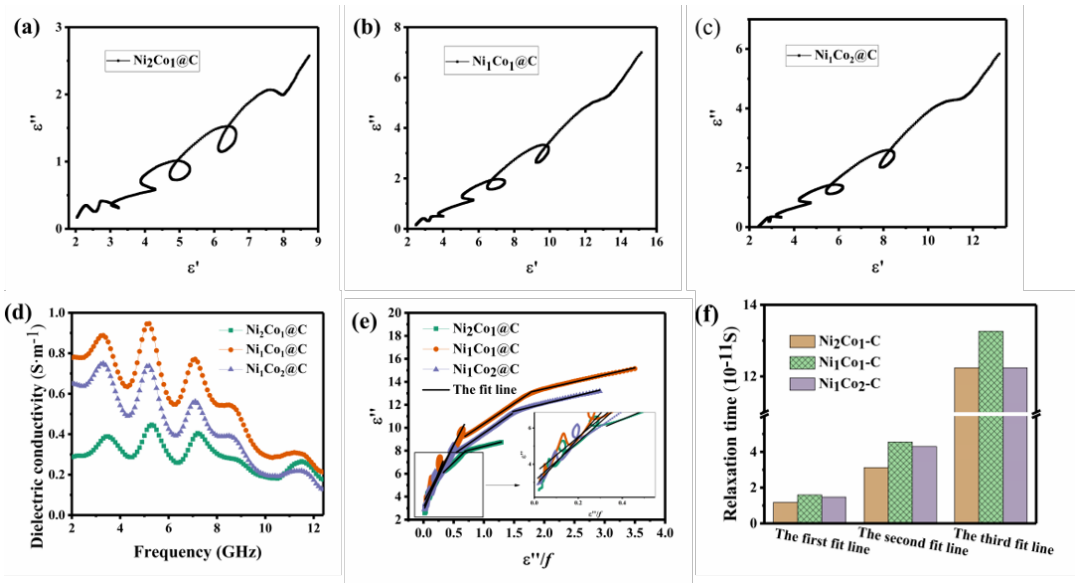

Fig. 3.7. Cole-cole polts (a-c), dielectric conductivity (d), the relationship between ε' and ε''/f (e) and relaxation time (f) of Ni_xCo_y@C composites

Different from dielectric loss, the magnetic loss is mainly caused by the eddy current effect, magnetic resonance (natural resonance and exchange resonance), magnetic hysteresis loss and domain wall resonance. In theory, the eddy current effect and magnetic resonance occur in gigahertz frequency while the magnetic hysteresis loss and the domain wall resonance appears in higher and lower frequency. To be more exact, the natural resonance appears in 2-10 GHz and exchange resonance occurs in 10~ GHz[36]. The magnetic resonance discussed in measured frequency is comprised of natural and exchange resonance. The eddy current loss can be evaluated by following equation.

$$C_0 = \mu''(\mu')^{-2} f^{-1} = 2\pi\mu_0 d^2 \sigma \quad (3\text{-}10)$$

The C_0 would be constant when the magnetic loss is brought about only by the eddy current effect. And if there is magnetic resonance contributing to the magnetic loss, the C_0 will vary with frequency. From Fig. 3.8, the C_0

value of Ni_2Co_1@C exhibits slight fluctuation in 2-9 GHz and keeps constant in 9-12.4 GHz, which means the magnetic loss of Ni_2Co_1@C is eddy current loss in 2-9 GHz and dominated by magnetic loss in 9-12.4 GHz. By contrast, both the C_0 values of Ni_1Co_1@C and Ni_1Co_2@C fluctuate in measured frequency, demonstrating the magnetic loss mechanism of the two samples is composed of eddy current loss and magnetic loss.

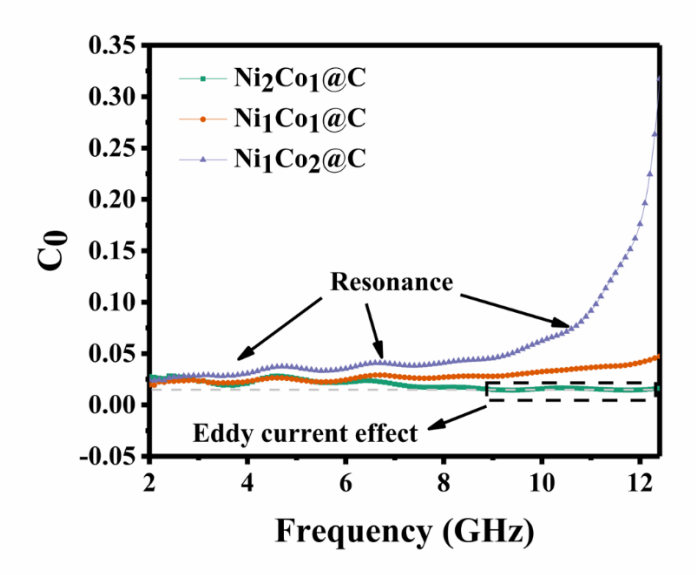

Fig. 3.8. C_0 versus frequency polts of Ni_xCo_y@C.

It is widely accepted that impedance matching and attenuation constant are two main factors to visually explain the microwave absorption mechanism of materials[37, 38]. An excellent microwave absorbing material should own appropriate impedance matching property generally defined as Z, which can be expressed by eq. (11), the closer the Z value is to 1, the more easily microwave can enter composites.

$$Z = \left|\frac{Z_{in}}{Z_0}\right| = \left|\sqrt{\mu_r/\varepsilon_r}\, tanh\left[j(2\pi f d/c)\sqrt{\mu_r \varepsilon_r}\right]\right| \quad (3\text{-}11)$$

The Z values of obtained samples are shown in Fig. 3.9a. It's not hard to find that the Z value of Ni_1Co_2@C is closer to 1 compared with Ni_2Co_1@C and Ni_1Co_1@C in frequency range of 8.2-14.4, indicating more microwave can penetrate the surface of Ni_1Co_2@C rather than the other samples. Besides, the microwave attenuation property, the ability of converting incident microwave into other forms of energy and eliminating transmitted microwave, is also integral for absorbers. It can be evaluated by the attenuation constant (α), which can be presented as the following equation[39]:

$$\alpha = \frac{\sqrt{2}\pi f}{c} \times \sqrt{(\mu''\varepsilon' - \mu'\varepsilon') + \sqrt{(\mu''\varepsilon'' - \mu'\varepsilon') + (\mu'\varepsilon'' + \mu''\varepsilon')}} \quad (3\text{-}12)$$

The calculated attenuation constants (α) of three samples are shown in Fig. 3.9b. All of them display a general trend of increase in measured frequency. It is obviously that the attenuation constant of Ni_1Co_2@C is highest among them especially in frequency range of 8-12.4 GHz, suggesting the strongest microwave attenuation ability of Ni_1Co_2@C. Based on the above analysis, Ni_1Co_2@C owns the excellent microwave absorption performance due to the appropriate impedance and powerful attenuation constant, which means the largest number of microwave can enter composites and be weakened by the strongest attenuation ability compared with the other two samples.

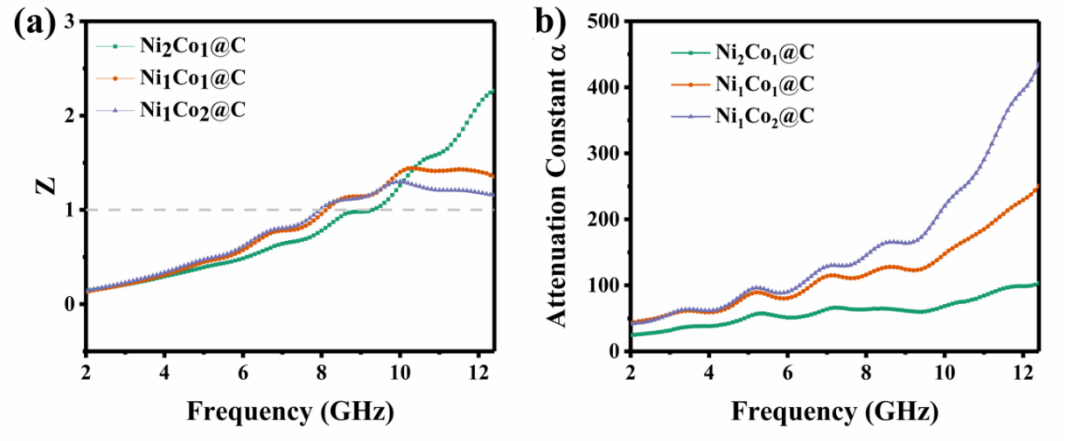

Fig. 3.9. Impedance matching Z at 2.6mm (a) and attenuation constant α (b) of Ni_xCo_y@C.

The possible microwave absorption mechanism of Ni_1Co_2@C discussed in Fig. 3.10. can be ascribed to the following aspects: (1) The 3D network structure has suitable impedance matching. When microwave arrives at the surface of the composites, most of it penetrates into the composites; (2) The microcurrent in 3D conductive structure induced by incident microwave generates conductive loss; (3) the microwave propagation path effected by the 3D network structure causes multiple reflection and scattering, which is helpful to counteract microwave to a degree; (4) The dipole and interfacial polarization originated from heterostructures and defects in composites, which is proved by the XPS and Raman analysis, contribute to polarization relaxation; (5) The NiCo magnetic alloy produces magnetic loss further consumes energy of microwave. In short, 3D network composites with contents of NiCo alloy and carbon show promise to become ideal candidate of microwave absorbing materials as is

expected.

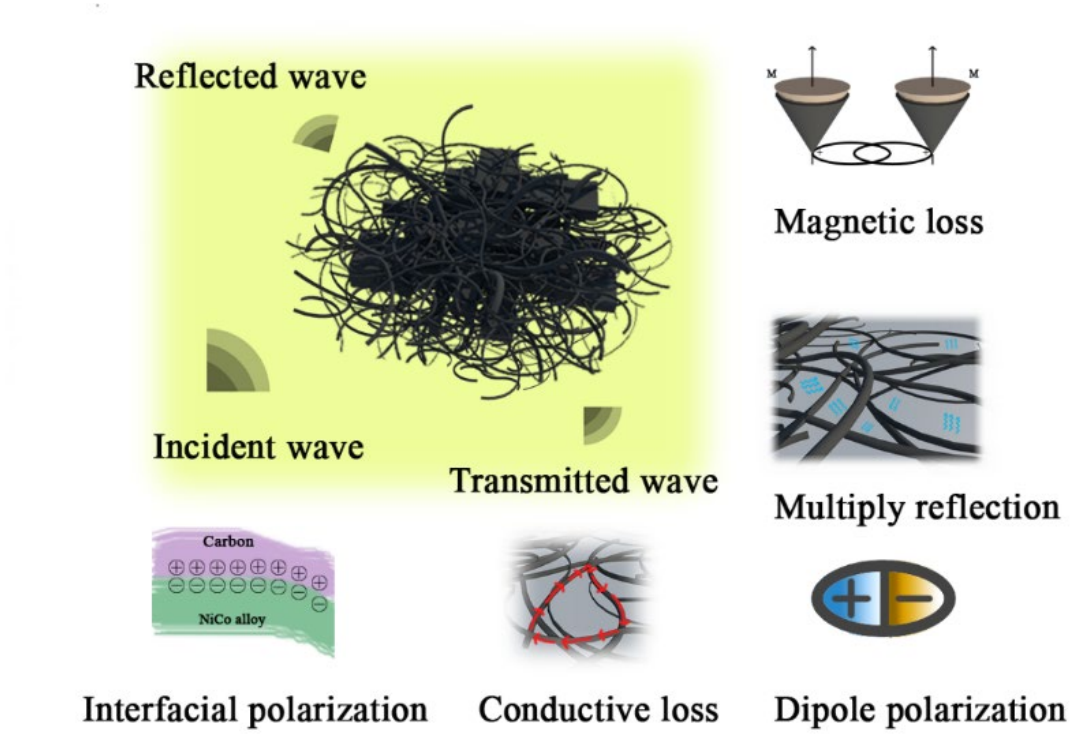

Fig. 3.10. Schematic illustration of microwave absorption mechanism in Ni_xCo_y@C.

3.4 Conclusion

In this chapter, we present a feasible, self-assembled way to successfully fabricate Ni_xCo_y@C microwave absorption materials by directly annealing bimetallic ZIFs precursors. By regulating Ni/Co ratios, the spontaneous network structure is formed when the Ni/Co ratio is 1:2. The optimal Ni_1Co_2@C composites derived from Ni_1Co_2-ZIF shows excellent microwave absorption performance with a RL_{min} value -41.9 dB at 12.2GHz in 1.5 mm and the whole X band (8.2-12.4) is included into the effective absorption band (less than -10 dB) in 2.5 mm. Further investigation confirms Ni/Co ratios has an impact on the dielectric and

magnetic parameters. From discussion of loss mechanism, dielectric loss consisting of polarization relaxation as well as conductive loss is mainly dominated by relaxation time and dielectric conductivity while magnetic loss generated from eddy current effect and resonance. Meanwhile, the impedance matching and attenuation constant offered by 3D network structure with alloy and carbon in Ni_1Co_2@C are also tailored. All of what mentioned above accounts for the outstanding microwave absorption capacity of Ni_1Co_2@C. This result provides a new perspective to construct efficient microwave absorption materials with adjustable morphology and component.

References

[1] Z. Zhao, X. Zhou, K. Kou, H. Wu, PVP-assisted transformation of ZIF-67 into cobalt layered double hydroxide/carbon fiber as electromagnetic wave absorber. Carbon, 173 (2021) 80-90.

[2] F.Y. Ren, J.M. Xue, X.L. Liu, L.F. Cheng, In situ construction of CNWs/SiC-NWs hybrid network reinforced SiCN with excellent electromagnetic wave absorption properties in X band. Carbon, 168 (2020) 278-289.

[3] Y. Fan, H. Yang, M. Li, G. Zou, Evaluation of the microwave absorption property of flake graphite. Materials Chemistry and Physics, 115 (2009) 696-698.

[4] Y.F. Zhu, L. Zhang, T. Natsuki, Y.Q. Fu, Q.Q. Ni, Facile synthesis of BaTiO3 nanotubes and their microwave absorption properties. ACS Appl Mater Interfaces, 4 (2012) 2101-2106.

[5] Z. Li, X. Han, Y. Ma, D. Liu, Y. Wang, P. Xu, C. Li, Y. Du, MOFs-Derived Hollow Co/C Microspheres with Enhanced Microwave Absorption Performance. Acs Sustain Chem Eng, 6 (2018) 8904-8913.

[6] S. Dong, W. Tang, P. Hu, X. Zhao, X. Zhang, J. Han, P. Hu, Achieving Excellent Electromagnetic Wave Absorption Capabilities by Construction of MnO Nanorods on Porous Carbon Composites Derived from Natural Wood via a Simple Route. Acs Sustain Chem

Eng, 7 (2019) 11795-11805.

[7] Y.Q. Fan, Y.H. Li, Y.L. Yao, Y. Sun, B.H. Tong, J. Zhan, Hierarchically porous carbon sheets/Co nanofibers derived from corncobs for enhanced microwave absorbing properties. Appl Surf Sci, 534 (2020).

[8] J.L. Mancuso, A.M. Mroz, K.N. Le, C.H. Hendon, Electronic Structure Modeling of Metal-Organic Frameworks. Chem Rev, 120 (2020) 8641-8715.

[9] J.-C. Shu, X.-Y. Yang, X.-R. Zhang, X.-Y. Huang, M.-S. Cao, L. Li, H.-J. Yang, W.-Q. Cao, Tailoring MOF-based materials to tune electromagnetic property for great microwave absorbers and devices. Carbon, 162 (2020) 157-171.

[10] J. Yan, X. Zheng, C. Wei, Z. Sun, K. Zeng, L. Shen, J. Sun, M.H. Rümmeli, R. Yang, Nitrogen-doped hollow carbon polyhedron derived from salt-encapsulated ZIF-8 for efficient oxygen reduction reaction. Carbon, 171 (2021) 320-328.

[11] S. Gayathri, P. Arunkumar, J.H. Han, Scanty graphene-driven phase control and heteroatom functionalization of ZIF-67-derived CoP-draped N-doped carbon/graphene as a hybrid electrode for high-performance asymmetric supercapacitor. J Colloid Interface Sci, 582 (2021) 1136-1148.

[12] A. Gu, J. Chen, Q. Gao, M.M. Khan, P. Wang, Y. Jiao, Z. Zhang,

Y. Liu, Y. Yang, The preparation of Ag/ZIF-8@ZIF-67 core-shell composites as excellent catalyst for degradation of the nitroaromatic compounds. Appl Surf Sci, 516 (2020).

[13] Q. Li, J. Guo, H. Zhu, F. Yan, Space-Confined Synthesis of ZIF-67 Nanoparticles in Hollow Carbon Nanospheres for CO2 Adsorption. Small, 15 (2019) e1804874.

[14] H. Chen, R. Hong, Q. Liu, S. Li, F. Huang, Y. Lu, L. Wang, K. Li, H. Zhang, CNFs@carbonaceous Co/CoO composite derived from CNFs penetrated through ZIF-67 for high-efficient electromagnetic wave absorption material. J Alloy Compd, 752 (2018) 115-122.

[15] L. Wang, X. Bai, B. Wen, Z. Du, Y. Lin, Honeycomb-like Co/C composites derived from hierarchically nanoporous ZIF-67 as a lightweight and highly efficient microwave absorber. Composites Part B: Engineering, 166 (2019) 464-471.

[16] L. Xu, Y. Xiong, B. Dang, Z. Ye, C. Jin, Q. Sun, X. Yu, In-situ anchoring of Fe3O4/ZIF-67 dodecahedrons in highly compressible wood aerogel with excellent microwave absorption properties. Mater Design, 182 (2019).

[17] X. Zhu, H. Qiu, P. Chen, G. Chen, W. Min, Anemone-shaped ZIF-67@CNTs as effective electromagnetic absorbent covered the whole X-band. Carbon, 173 (2021) 1-10.

[18] S. ur Rehman, M. Sun, M. Xu, J. Liu, R. Ahmed, M.A. Aslam,

R.A. Ahmad, H. Bi, Carbonized zeolitic imidazolate framework-67/polypyrrole: A magnetic-dielectric interface for enhanced microwave absorption properties. Journal of Colloid and Interface Science, 574 (2020) 87-96.

[19] J. Yan, Y. Huang, Y. Yan, L. Ding, P. Liu, High-Performance Electromagnetic Wave Absorbers Based on Two Kinds of Nickel-Based MOF-Derived Ni@C Microspheres. ACS Appl Mater Interfaces, 11 (2019) 40781-40792.

[20] L.-L. Liang, Z. Liu, L.-J. Xie, J.-P. Chen, H. Jia, Q.-Q. Kong, G.-H. Sun, C.-M. Chen, Bamboo-like N-doped carbon tubes encapsulated CoNi nanospheres towards efficient and anticorrosive microwave absorbents. Carbon, 171 (2021) 142-153.

[21] J. Yan, Y. Huang, X. Han, X. Gao, P. Liu, Metal organic framework (ZIF-67)-derived hollow CoS2/N-doped carbon nanotube composites for extraordinary electromagnetic wave absorption. Composites Part B: Engineering, 163 (2019) 67-76.

[22] X.-W. Wei, X.-M. Zhou, K.-L. Wu, Y. Chen, 3-D flower-like NiCo alloy nano/microstructures grown by a surfactant-assisted solvothermal process. CrystEngComm, 13 (2011) 1328-1332.

[23] S. Bai, X. Shen, G. Zhu, M. Li, H. Xi, K. Chen, In situ growth of Ni(x)Co(100-x) nanoparticles on reduced graphene oxide nanosheets and their magnetic and catalytic properties. ACS Appl Mater

Interfaces, 4 (2012) 2378-2386.

[24] B. Quan, X. Liang, G. Ji, Y. Zhang, G. Xu, Y. Du, Cross-Linking-Derived Synthesis of Porous CoxNiy/C Nanocomposites for Excellent Electromagnetic Behaviors. ACS Appl Mater Interfaces, 9 (2017) 38814-38823.

[25] Y.L. Wang, S.H. Yang, H.Y. Wang, G.S. Wang, X.B. Sun, P.G. Yin, Hollow porous CoNi/C composite nanomaterials derived from MOFs for efficient and lightweight electromagnetic wave absorber. Carbon, 167 (2020) 485-494.

[26] L. Wang, M. Huang, X. Yu, W. You, J. Zhang, X. Liu, M. Wang, R. Che, MOF-Derived Ni1−xCox@Carbon with Tunable Nano–Microstructure as Lightweight and Highly Efficient Electromagnetic Wave Absorber. Nano-Micro Letters, 12 (2020).

[27] Y. Cheng, J. Cao, H. Lv, H. Zhao, Y. Zhao, G. Ji, In situ regulating aspect ratio of bamboo-like CNTs via CoxNi1−x-catalyzed growth to pursue superior microwave attenuation in X-band. Inorganic Chemistry Frontiers, 6 (2019) 309-316.

[28] X. Zhou, Z. Jia, A. Feng, J. Kou, H. Cao, X. Liu, G. Wu, Construction of multiple electromagnetic loss mechanism for enhanced electromagnetic absorption performance of fish scale-derived biomass absorber. Composites Part B: Engineering, (2020).

[29] X.J. Zeng, X.Y. Cheng, R.H. Yu, G.D. Stucky, Electromagnetic

microwave absorption theory and recent achievements in microwave absorbers. Carbon, 168 (2020) 606-623.

[30] X. Li, L. Yu, W. Zhao, Y. Shi, L. Yu, Y. Dong, Y. Zhu, Y. Fu, X. Liu, F. Fu, Prism-shaped hollow carbon decorated with polyaniline for microwave absorption. Chem Eng J, 379 (2020).

[31] S. Wei, X. Wang, Y. Zheng, T. Chen, C. Zhou, S. Chen, J. Liu, Facile Preparation of Snowflake-Like MnO2 @NiCo2 O4 Composites for Highly Efficient Electromagnetic Wave Absorption. Chemistry–A European Journal, 25 (2019) 7695-7701.

[32] Y. Li, R. Liu, X. Pang, X. Zhao, Y. Zhang, G. Qin, X. Zhang, Fe@C nanocapsules with substitutional sulfur heteroatoms in graphitic shells for improving microwave absorption at gigahertz frequencies. Carbon, 126 (2018) 372-381.

[33] X. Li, Y. Zhu, X. Liu, B. Bin Xu, Q. Ni, A broadband and tunable microwave absorption technology enabled by VGCFs/PDMS-EP shape memory composites. Compos Struct, 238 (2020).

[34] X. Zhou, B. Wang, Z. Jia, X. Zhang, X. Liu, K. Wang, B. Xu, G. Wu, Dielectric behavior of Fe3N@C composites with green synthesis and their remarkable electromagnetic wave absorption performance. J Colloid Interface Sci, 582 (2020) 515-525.

[35] Y. Duan, Z. Liu, H. Jing, Y. Zhang, S. Li, Novel microwave dielectric response of Ni/Co-doped manganese dioxides and their

microwave absorbing properties. Journal of Materials Chemistry, 22 (2012).

[36] X. Wang, F. Pan, Z. Xiang, Q. Zeng, K. Pei, R. Che, W. Lu, Magnetic vortex core-shell Fe3O4@C nanorings with enhanced microwave absorption performance. Carbon, 157 (2020) 130-139.

[37] H. Zhang, Z. Jia, A. Feng, Z. Zhou, C. Zhang, K. Wang, N. Liu, G. Wu, Enhanced microwave absorption performance of sulfur-doped hollow carbon microspheres with mesoporous shell as a broadband absorber. Composites Communications, 19 (2020) 42-50.

[38] P.B. Liu, S. Gao, Y. Wang, F.T. Zhou, Y. Huang, J.H. Luo, Metal-organic polymer coordination materials derived Co/N-doped porous carbon composites for frequency-selective microwave absorption. Compos Part B-Eng, 202 (2020).

[39] Y. Zhang, Z. Yang, M. Li, L. Yang, J. Liu, Y. Ha, R. Wu, Heterostructured CoFe@C@MnO2 nanocubes for efficient microwave absorption. Chem Eng J, 382 (2020).

Chapter 4: Design of multilayer composites for microwave absorption

4.1 Introduction

The multilayer structure design of microwave absorption materials is to find materials, order, thickness and other parameters with required microwave absorption performance in a specific frequency band[1-5]. The performance of multilayer composites can be evaluated under selected parameters[6]. With known parameters, reflection loss at a certain frequency point or a certain band is calculated by transmission line theory[7]. Therefore, how to find optimal parameters efficiently and accurately to calculate the absorption performance is significant for design of multilayer composites.

The traditional optimization design methods of multilayer materials include conjugate gradient method, Newton iteration method, simplex method, penalty function method and simulated annealing method[8-11]. Although these methods have achieved some results in the optimization of microwave absorption materials, they still have obvious shortcomings such as long iteration time, local convergence and other phenomena are formed in the iterative process[12-14]. It not only reduces the computing efficiency, but also hard to obtain the optimal parameter solution. In response to these

problems, application of new global optimization algorithms in composites fields has emerged in recent years, such as genetic algorithm and particle swarm algorithm[15-18]. Genetic algorithm is a kind of search algorithm with features random, highly parallel, adaptive search. It was founded by the team of Professor Jhon H. Holland in the University of Michigan, a bionic optimization algorithm based on Darwin's theory of biological evolution and Mendel's genetic variation theory to solve complex global optimization problems[19-21]. According to biological evolution, every species on earth has to undergo the process of natural selection for survival of the fittest since its birth. Individuals with strong survivability are more likely to survive and have more chances to produce offspring, otherwise they will be eliminated. Due to the group search strategy and the information exchange between individuals in the group, the search hardly depends on gradient information[22-24]. So, it has advantages of stability and high efficiency which is suitable for dealing with complex system design problems with many parameters. Compared with traditional optimization algorithm, the genetic algorithm can significantly improve the optimization efficiency of material parameters. Therefore, it has been widely used and continuously developed in the process optimization of composites research.

Besides, computer-assisted analysis is also an efficient way to figure out influence of structures on multilayer composites. The research and

development of microwave absorption materials under computer-assisted design can greatly improve the research efficiency and reduce the cost of exploratory experiments. CST, HFSS and COMSOL are commonly used in electromagnetic research, which establish physical models to reflect various relationship between relevant parameters in visual forms[25-29]. Researchers can analyze experimental results by electromagnetic field, energy loss and radar cross section. Finite element analysis has been widely used in structural optimization of frequency-selective surfaces but slowly applied in field of nanocomposites for microwave absorption in recent years[30-32].

Herein, in order to effectively improve design and analysis efficiency of multilayer composites, two materials (EWC-1 and Ni_1Co_2@C) synthesized in previous two chapters are used as a database to design a whole C-band absorption composite. To better explain the follow-up process, the mathematical model of multilayer composites for microwave absorption is introduced primarily. Then, multilayer composites with a single material in the database is established and its performance is analyzed. The effect of material types, thickness and layer number and interval distance on microwave absorption performance is verified, which emphasizes the limitation of single factor variable analysis in multilayer composites design. After that, the structural parameters are optimized by genetic algorithm, and the best parameters of C-band absorption are obtained. Finally, the

model is established by the optimized parameters, and the finite element method is used to analyze attenuation mechanism of multilayer composites.

4.2 Mathematical model of multilayer structures for microwave absorption

Transmission line theory is a circuit system capable of transmitting microwave, which is of great fundamentality and importance in the study of electromagnetics technology[33-35]. The transmission line equation can be obtained from the basic circuit theory and Maxwell's equation shown as follows:

$$\begin{cases} \frac{\partial_u}{\partial_z} + \left(r + L\frac{\partial}{\partial_t}\right) i = 0 \\ \frac{\partial_i}{\partial_z} + \left(g + C\frac{\partial}{\partial_t}\right) u = 0 \end{cases} \tag{4-1}$$

If the voltage and current on the transmission line are sinusoidal AC voltage and current, here are the formulas of voltage and current:

$$\begin{cases} u(z,t) = U(z)e^{j\omega t} \\ u(z,t) = I(z)e^{j\omega t} \end{cases} \tag{4-2}$$

Then, the equation (4-1) can be changed into the following equation:

$$\begin{cases} \frac{dU}{dz} = -ZI \\ \frac{dI}{dz} = -YU \end{cases} \tag{4-3}$$

Where $Z = r + j\omega L$ represents the impedance per unit length and $Y = g + j\omega C$ represents admittance per unit length. When taking the derivative of z, the equation (4-3) can be changed into the following expression:

$$\begin{cases} \dfrac{d^2U}{dz^2} = \gamma^2 U \\ \dfrac{d^2I}{dz^2} = \gamma^2 I \end{cases} \tag{4-4}$$

The propagation constant γ representing the propagation and loss of waves can be expressed as follows:

$$\gamma = \sqrt{ZY} = \sqrt{(r + j\omega L)(g + j\omega C)} = \alpha + j\beta \tag{4-5}$$

α

$$= \sqrt{\frac{1}{2}(rg - \omega^2 LC) + \frac{1}{2}\sqrt{(r^2 + \omega^2 L^2)(g^2 + \omega^2 C^2)}} \tag{4-6}$$

β

$$= \sqrt{\frac{1}{2}(\omega^2 LC - rg) + \frac{1}{2}\sqrt{(r^2 + \omega^2 L^2)(g^2 + \omega^2 C^2)}} \tag{4-7}$$

The real part of the propagation constant α is attenuation constant, which represents attenuation of wave amplitude per unit length along the propagation direction. β represents the phase shift constant. The solution of equation (4-4) is shown as following:

$$U(z) = a_1 e^{-\gamma z} + b_1 e^{\gamma z} \tag{4-8}$$

$$U(z) = \frac{a_1}{Z_0} e^{-\gamma z} - \frac{b_1}{Z_0} e^{\gamma z} \tag{4-9}$$

Z_0 is the characteristic impedance of the transmission line, the physical meaning of which is ratio of traveling wave voltage to traveling wave current. The calculation equation of the characteristic impedance Z_0 is shown as following:

$$Z_0 = \sqrt{\frac{r + j\omega L}{g + j\omega C}} \tag{4-10}$$

Obviously, for lossy transmission lines or for low frequency transmission

lines, the characteristic impedance is frequency dependent with a complex number. When the transmission line has no loss or frequency is high, $r \ll \omega L$, $g \ll \omega C$, the equation can be changed into as following:

$$Z_0 = \sqrt{\frac{L}{C}} \tag{4-11}$$

Thus, when transmission line has no loss or frequency is high enough, characteristic impedance is independent of frequency. Here we use U_0 to represent the voltage at z=0, and I_0 to represent the current at z=0. According to equation (4-8) and (4-9), the following equation can be obtained:

$$U_0 = a_1 + b_1 \tag{4-12}$$

$$U_0 = \frac{a_1 - b_1}{Z_0} \tag{4-13}$$

The expression of a_1 and b_1 are as following:

$$a_1 = \frac{U_0 + I_0 Z_0}{2} \tag{4-14}$$

$$b_1 = \frac{U_0 - I_0 Z_0}{2} \tag{4-15}$$

Then steady state equation of transmission line with Z coordinate can be obtained as following:

$$U(z) = U_0 \cosh \gamma z - I_0 Z_0 \sinh \gamma z \tag{4-16}$$

$$I(z) = U_0 \cosh \gamma z - \frac{U_0}{I_0} \sinh \gamma z \tag{4-17}$$

When using terminal voltage U_1 and terminal current I_1 to represent the transmission line steady-state equation, the result can be as following:

$$U(z) = U_1 \cosh \gamma (l - z) - I_1 Z_0 \sinh \gamma (l - z) \tag{4-18}$$

$$I(z) = I_1 \cosh \gamma (l - z) - \frac{U_1}{Z_0} \sinh \gamma (l - z) \tag{4-19}$$

The input impedance Z_{in} at any point of the transmission line is defined as following:

$$Z_{in} = \frac{U(z)}{I(z)} = \frac{U_1 \cosh \gamma(l-z) - I_1 Z_0 \sinh \gamma(l-z)}{I_1 \cosh \gamma(l-z) - \frac{U_1}{Z_0} \sinh \gamma(l-z)} \quad (4\text{-}20)$$

According to $U_l = I_l Z_l$, the equation (4-20) can be changed into as following:

$$Z_{in} = Z_0 \frac{\tanh \gamma(l-z) + \frac{Z_l}{Z_0}}{1 + \frac{Z_l}{Z_0} \tanh \gamma(l-z)} \quad (4\text{-}21)$$

If $\tanh n = \frac{Z_l}{Z_0}$, the input impedance Z_{in} can be expressed as following:

$$Z_{in} = Z_0 \tanh(\gamma(l-x) + n) \quad (4\text{-}22)$$

When z = 0, the equation 4-21 can be expressed as following:

$$Z_{in} = Z_0 \tanh(\gamma l + n) = Z_0 \frac{Z_l + Z_0 \tanh \gamma l}{Z_0 + Z_l \tanh \gamma l} \quad (4\text{-}23)$$

When the layer number is n, the impedance of n-th can be expressed as following:

$$Z_n = \eta_n \frac{Z_{n-1} + \eta_n \tanh(\gamma l)}{Z_n + \eta_{n-1} \tanh(\gamma l)} \quad (4\text{-}24)$$

Then the reflection loss can be expressed as:

$$RL = RL = 20 \log_{10} \left| \frac{Z_n - Z_0}{Z_n + Z_0} \right| \quad (4\text{-}25)$$

It can be seen from the above formula that microwave absorption performance can be changed by regulating the electromagnetic parameters, the thickness of each layer and materials used in multilayer structure. By optimization, multilayer structures with best performance can be selected by calculating different parameters.

4.3 Design method

As can be seen from the Figs.4.1a and b, both the materials EWC-1 and Ni_1Co_2@C generate absorption performance in C band at 3-5mm, but hardly absorb microwave of the whole C band. A large number of research results show that a single material is limited by non-adjustable electromagnetic parameters and propagation paths, poor matching impedance and other reasons, and there is little room for performance improvement. So multilayer composites with different structures need to be discussed here.

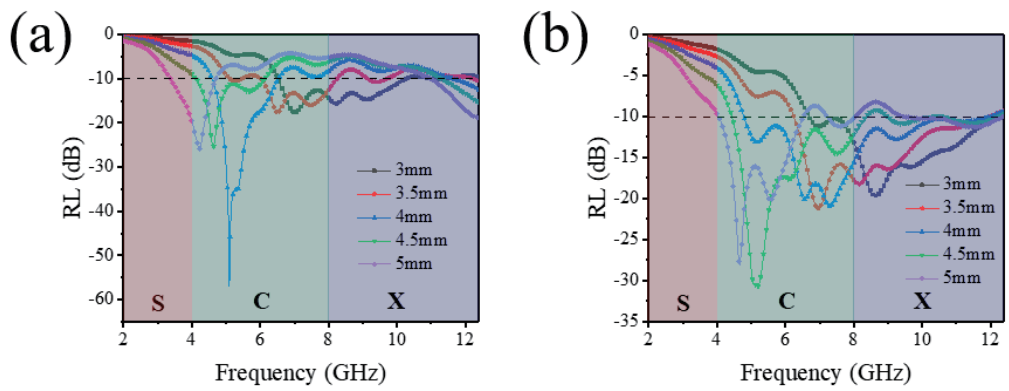

Fig. 4.1. RL values of (a) EWC-1 and (b) Ni_1Co_2@C in 3-5mm.

4.3.1 Design on multilayer composites with a single material

Herein we build a multilayer model with a single material as shown in the Figs. 4.2a and b to discuss the effect of thickness, interval distance and number of layers on microwave absorption performance. The multilayer composites are coating onto the reflective substrate with a perfect electric conductor (PEC). To be specific, EWC-1 or Ni_1Co_2@C are used as the

single material for multilayer composites and adding interval distance as air layers. By individually changing the thickness S of single-layer material, number of layers L_n and thickness of the interval distance T, the effects of these parameters on microwave absorption properties of single-material multilayer structures are analyzed. The specific calculation is carried out by equations 4-24 and 4-25.

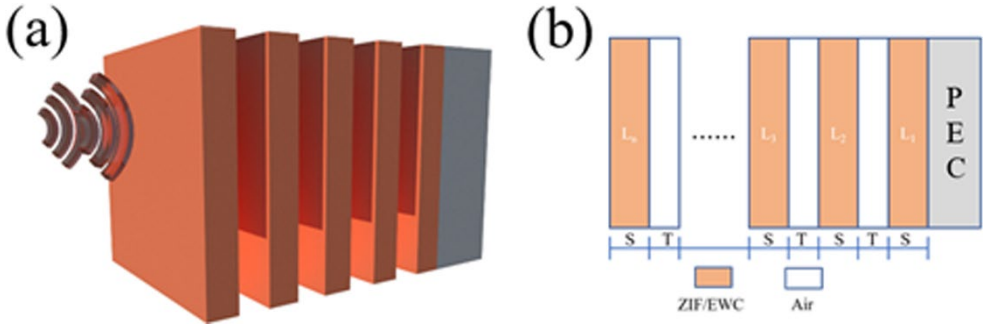

Fig. 4.2. (a) 3D model and (b) cross-section drawn of multilayer composites

4.3.2 Design on multilayer composites with double materials

According to calculation results of multilayer composites with the single material, the efficient multilayer design is carried out to improve structural parameters of multilayer composites. The genetic algorithm is used to optimize parameters. The optimization variables are ordering, thickness, material layers number and interval distance while the aim is to achieve the whole C-band absorption. The specific process is as follows:

The first step is the parameter encoding process, referring to the chromosome encoding scheme, encoding each parameter is basic for multiple chromosomes[36-38]. There are three variables in this

optimization process. Sort of material {· · · 1, 3, 2, 3, 1 · · ·} , {· · · 1, 3, 1, 3, 1 · · ·} or {· · · 2, 3, 2, 3, 2 · · ·} (To code the materials more conveniently, EWC-1, Ni_1Co_2@C and air layers are defined as 1, 2, 3 respectively), thickness of a single layer of multilayer composites {d_1, d_2, d_3 · · ·d_n}, and interval distance of air layers {m1, m2, m3 · · ·m_n}, where n represents the total number of design layers.

In order to simplify the difficulty of structural processing and ensure that the thickness of the multilayer structure in specific range (0-L), the constraints of thickness are dynamically adjusted when thickness is decoded, and the result of the adjustment is that the thickness constraints of the i-th layer are:$d_i < L - \sum_{j=1}^{j-1} d_j$.

Algorithm parameter settings for optimal design: the maximum number of iterations of the algorithm T=100, the crossover probability P_c=0.9, the mutation probability P_m=0.1, the population size N=100, and the optimal preservation individual=30. The specific process is shown in Fig.4.3.

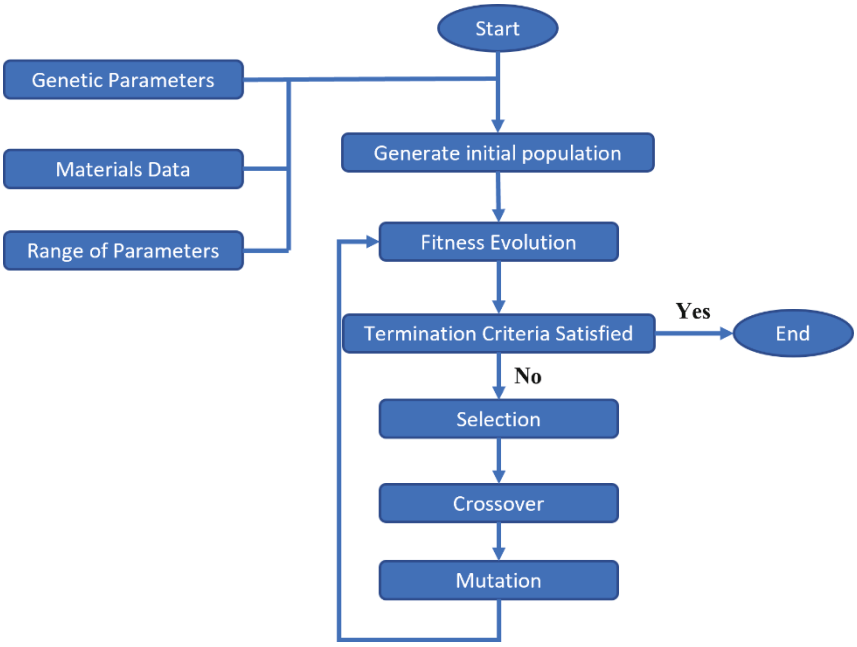

Fig. 4.3. Flowchart of the basic genetic algorithm optimizer

In view of design complexity, the layers are set as 9 layers. As contrasted with 9-layers structures, structures without interval distance are set as 5 layers. The thickness of each layer is limited in 3mm. The orders of selected composites are in Table.4.1. For easy identification of samples, EWC-1 is named as W, interval distance is named as A and Ni_1Co_2@C is named as Z. The labels from L1 to L9 means layers from the surface layer to innermost layer. And 0 means that there is no interval distance in structures. According to naming rule, the samples of WAW, ZAZ, WAZ and ZAW are 9-layer composites while samples of WZ and ZW are 5-layer composites.

Table 4.1

Layer/Sample	WAW	ZAZ	WAZ	ZAW	WZ	ZW
L1	W	Z	W	Z	W	Z
L2	A	A	A	A	0	0
L3	W	Z	Z	W	Z	W
L4	A	A	A	A	0	0
L5	W	Z	W	Z	W	Z
L6	A	A	A	A	0	0
L7	W	Z	Z	W	Z	W
L8	A	A	A	A	0	0
L9	W	Z	W	Z	W	Z

Finally, COMSOL is carried out for visualization analysis of multilayer structures according to GJB2038-94. The dimensions of model are 180*180 mm^2. Then the model is put into the pattern of finite difference time domain numerical technique. To monitor electromagnetic field and power loss, waveguide port is used to excite the signal in the far-field region. The specific boundary condition of x-axis, y-axis, positive z-axis is set as E-field = 0, H-field = 0, and the path of EM wave propagation toward the negative z-axis direction conditions. The COMSOL's result is compared with the result calculated by transmission line theory to prove the accuracy.

4.4 Analysis on multilayer composites with the single material

4.4.1 Effect of interval distance on microwave absorption performance

First interval distance is discussed here. The total thickness of EWC-1 and Ni_1Co_2@C material are set to be 3 mm and 2.6 mm, respectively, and the number of layers is 5. The interval distance in 0.1mm, 0.2mm, 0.3mm, 0.4mm, 0.5mm is set and the corresponding performance for EWC-1 and Ni_1Co_2@C is shown in Fig. 4.4(a) and (b).

With increase of interval distance, the RL_{min} of EWC-1 decreases from -18 dB to-8.5dB at 7GHz while enhances from -6dB to 13.8dB at 5.2GH. And Ni_1Co_2@C shows degraded performance from -15.8dB to -10.4dB at 10.5GHz when increasing distance. Meanwhile, microwave absorption capability of Ni_1Co_2@C (from -8dB to -10.8dB) at 7GHz is shown. From the result of multilayer structures with single material, it can be concluded that at relatively high frequency band, although the performance decreases with increase of interval distance, the performance in relatively low frequency shows better. Such condition indicates that increasing interval distance individually can improve absorption performance at low frequency but weaken performance at high frequency, so interval distance combined with other parameters needs to be optimized further.

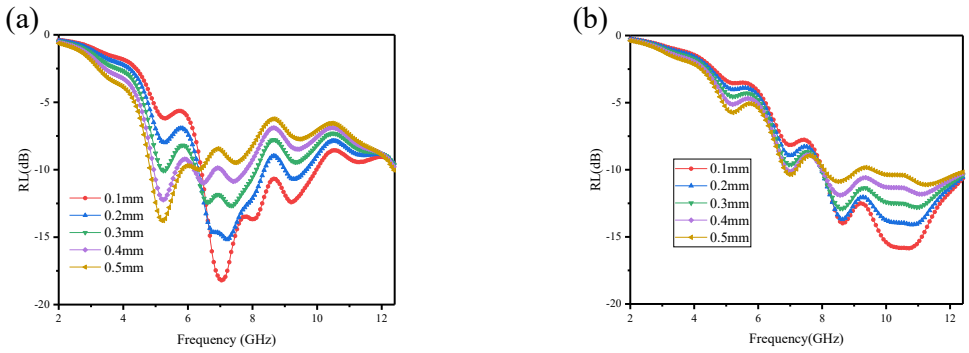

Fig. 4.4. RL values of (a) EWC-1 and (b) Ni_1Co_2@C in different interval distance.

4.4.2 Effect of layer number on microwave absorption performance

As for multilayer composites, the number of layers also is an important parameter for microwave absorption. Herein, effect of layer number on microwave performance of EWC-1 and Ni_1Co_2@C is discussed. Thickness of total material layers and interval distance is set as 3mm and 0.1mm, then effect of layer number (from 1 to 5 layers) on performance of multilayer composites is discussed in Fig. 4.5a and b respectively.

For EWC-1, as the number of layers increases, RL_{min} decreases from -13dB to -10dB at 8.7GHz while RL_{min} values increase from -5dB to -7dB at 5GHz. It indicates that increasing number of layers can decrease performance at relatively high frequency band but improve performance at relatively low frequency. Different from EWC-1, RL_{min} values of Ni_1Co_2@C decreases from -18dB to -10dB at 10.5GHz with the increase of the number of layers but the RL_{min} values increases from -7dB to -10dB

and from -3dB to -6dB at 7 and 5.2 GHz, respectively. Both the results of two materials demonstrate that increasing the number of layers decreases performance at relatively high frequency but increases performance at relatively low frequency simultaneously. In order to ensure the performance while taking absorption bandwidth into consideration, it is also necessary to optimize the number of layers in the multilayer composites.

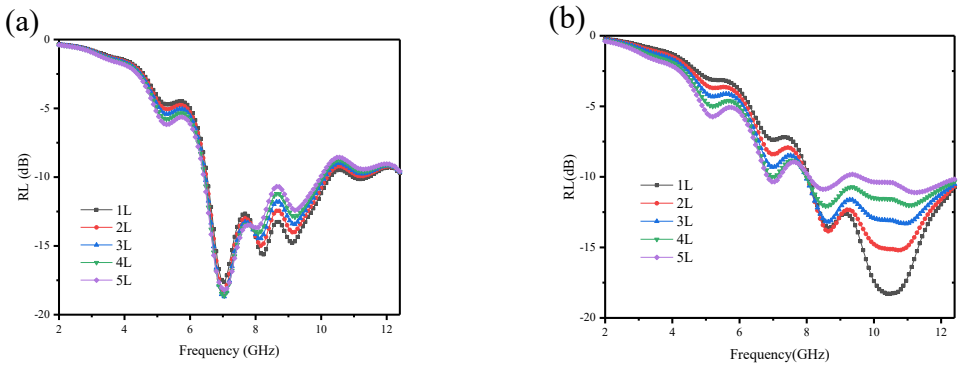

Fig. 4.5. RL values of (a) EWC-1 and (b) Ni_1Co_2@C in different layer number.

4.4.3 Effect of layer thickness on microwave absorption performance

The above analysis has verified effect of interval distance and layer number on the performance of multilayer composites. Here the single-layer thickness of multilayer composites is discussed. The interval distance and layer number are set as 0.5mm 5 layers. The single layer is set as 0.2mm, 0.4mm, 0.6mm, 0.8mm, 1mm, 1.2mm and the corresponding performance is shown in Fig. 4.6a and b. On the one hand, EWC-1 achieves the

maximum absorption performance -54dB at 3.2GHz while the single layer is 1mm and the Ni_1Co_2@C reaches RL_{min} -36dB at 3GHz while the single layer is 1mm. Besides, different structures in both materials show that absorption peaks shift to lower frequency as the thickness increases. That is to say, the increase of the thickness of the single layer can improve the absorption performance at low frequencies. This can be attribute to the quarter-wavelength theory. What's more, increasing single layer thickness also makes the composites show better absorption capability at relative higher frequency. For example, EWC-1 has an absorption peak of -29.3dB at 12GHz at 1mm and Ni_1Co_2@C shows a broadband absorption performance of 9.3-12.4GHz at ZIF at 1.2mm. In short, changing thickness of single layer can also affect microwave absorption properties of multilayer composites, while increasing thickness of the single layer has potential to prepare broadband absorption composites. Therefore, the thickness of single layer is also one of factors for developing multilayer microwave absorption composites.

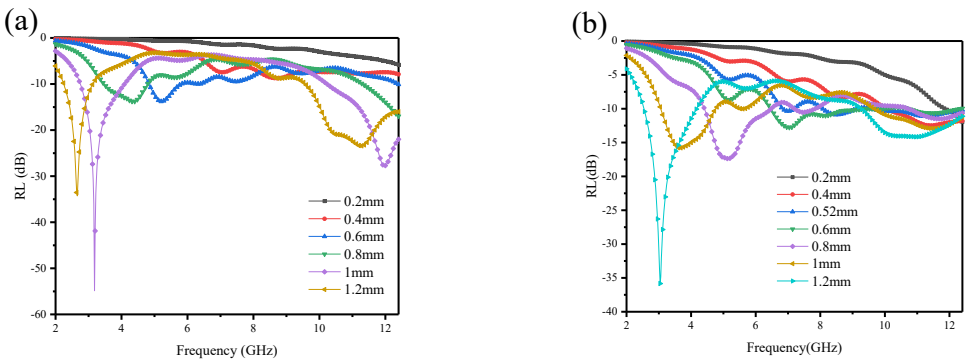

Fig. 4.6. RL values of (a) EWC-1 and (b) Ni_1Co_2@C in different layer thickness.

4.4.4 Effect of layer number on microwave absorption performance with limited thickness

Although increase of layer thickness can significantly improve absorption performance, considering that the excessive thickness will limit the practical application, layers in limited thickness also needs to be discussed. Here interval distance and total thickness of multilayer composites is set as 0.5mm, and 6mm. respectively. Fig. 4.7a and b show performance of EWC-1 and Ni_1Co_2@C with layers changing from 2 to 6 layers. For both two materials, the increase in the number of layers resulted in that composites achieve different RL_{min} values. To be specific, absorption peak of EWC-1 shifts from 3.3GHz to 4.8GHz and reaches RL_{min} -50dB at 3.7GHz while the number of layers is 3. Absorption peak of Ni_1Co_2@C shift from 4.2GHz to 5.2GHz and reaches RL_{min} value -28.9dB at 4.3GHz while the number of layers is 2. In a word, microwave absorption performance of multilayer composites also can be optimized by adjusting the number of layers when the total thickness is limited.

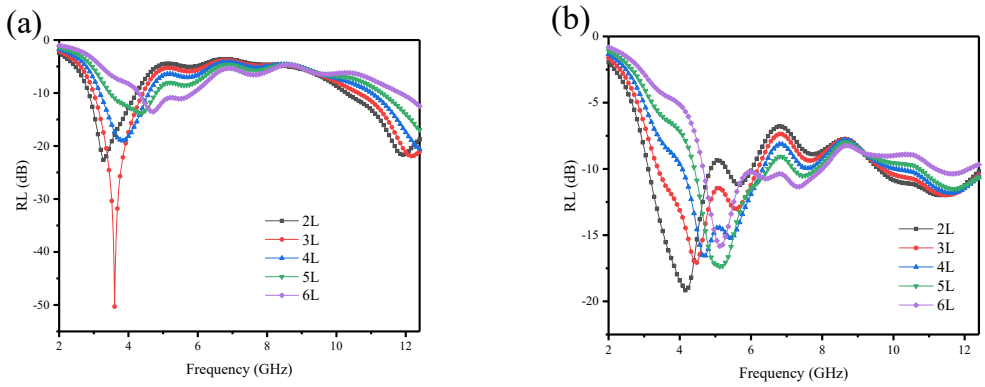

Fig. 4.7. RL values of (a) EWC-1 and (b) Ni_1Co_2@C in different layer number with limited thickness.

4.5 The results of genetic algorithm optimization

From the derivation of the above equations, it can be seen that the objective function with the characteristics of high nonlinearity, multi-parameter and multi-peak is one of the obstacles to optimize many complex electromagnetic optimization problems, which makes the calculation take a long time. The intelligent algorithm has irreplaceable advantages for optimizing complex problems, the most representative of which is the genetic algorithm[39-41].

According to the genetic algorithms, the optimized thickness of layers is shown in Table 4.2. As for using a single material, although WAW and ZAZ can achieve the whole C-band absorption it requires high thickness of 13.29mm and 11.4211mm. As for multilayer composites composed of two materials, WAZ and ZAW can show the whole C-band absorption in thickness of 12.5346mm and 17.4938mm. However, WZ and ZW show

required performance in thickness of 4.71687mm and 5.38125mm. Obviously, WZ show significantly thinner thickness comparing with other samples. From above analysis, it can be concluded that the changes of the number of layers, thickness of the single layer and air interval can indeed optimize microwave absorption properties of multilayer composites, but the overall thickness is too thick. Compared with multilayer structures with air spacer added as interval layers, WZ and ZW without interval distance can achieve the whole C-band absorption at a thinner thickness. What's more, WZ can achieve C-band absorption at the thinnest thickness. and addition of interval layers shows no advantage in optimization process.

From table 4.2, to achieve C-band absorption, the thickness of WAW, ZAZ, WAZ and ZAW is obviously thicker than that of WZ and ZW. Such phenomenon means that for attenuation of microwave, contribution caused by selected materials is much greater than that of scattering microwave between layers. Compared with the ZW, the WZ, where EWC-1 as the surface layer, can generate the whole C-band absorption in a thinner thickness. So, the 5-layer WZ is the best optimized composites for C-band microwave absorption.

Table 4.2

Layer(mm)	WAW	ZAZ	WAZ	ZAW	WZ	ZW
L1	1.11236	1.43225	1.93125	1.40625	0.737	0.88125
L2	2.00257	0.43561	1.5034	2.83125	0	0
L3	1.38376	1.76933	1.19422	2.98125	0.8278	2.08125
L4	1.27681	0.91874	2.18372	0.39375	0	0
L5	1.66924	1.98144	0.91875	1.70625	1.8091	0.05625
L6	2.28612	1.46488	2.79375	0.46875	0	0
L7	0.02028	0.08859	0.07851	2.19375	1.30384	0.35625
L8	2.96381	2.46464	1.55625	2.79375	0	0
L9	0.57503	0.86562	0.37474	2.71875	0.03913	2.00625
$L_{composites}$	13.29	11.4211	12.5346	17.4938	4.71687	5.38125

4.6 Comparison between experimental and analysis

The results calculation and simulation for microwave performance of the WZ multilayer composite is shown in Fig. 4.8a. It is obvious that the simulation result is agreed with the calculation result well, which confirms that the model set by COMSOL is reliable. Then electromagnetic field and power loss analysis are carried out to figure out the absorption mechanism in the optimized multilayer structure.

Electric field distribution, magnetic field distribution and power loss are simulated for 5 peaks in C band (4 GHz, 5GHz, 6GHz, 7GHz, 8GHz). As

shown in Fig. 4.8b, the multilayer structures respond differently to electric field at selected frequency points. The electric field concentrates on surface of composites and generates the maximum electric field intensity at 4 GHz. Then both surface electric field strength and depth tend to be weaker at 5 GHz. As the frequency continues to increase, the surface electric field has a weakening trend, electric field responses gradually shift to inner layer while the depth gradually expands. Therefore, in low frequency point, the electric field is mainly concentrated on the surface. In high frequency point, the response of the composite to the electric field is mainly concentrated inside the material, indicating that microwave can penetrate composites and form an electric field inside.

For the magnetic field, the structure also shows different responses at different frequencies, and the internal response of the structure is more sensitive to the magnetic field. The strongest magnetic field is generated inside the material at 5GHz. Unlike the electric field distribution, the magnetic fields at all five frequency points are concentrated inside the material and weak magnetic field strength on the surface is benefit to appropriate impedance matching. In addition, responses to magnetic fields are stronger than that to electric field. It proves that the materials selected here are dominated by magnetic loss, which is similar to the conclusion in previous 2 chapters.

When it comes to the power loss in Fig. 4.8b, no strong loss is formed

on the surface at the five frequency points, which proves that the role of the surface layer plays is not to attenuate microwave. However, the loss is concentrated near the surface of the material, which proves that the front part of the multilayer structure mainly plays the role of attenuating microwave energy. The reason why the loss at 4GHz is significantly lower than other selected frequency points may result from that a strong electric field is formed here, which negatively affects the impedance matching, result in that effective loss can not be generated. Considering the results of finite element analysis for five frequency points, the power loss at the position near the front of the composite. According to the results of optimal design of the structure of the multilayer composite, the front part is Ni_1Co_2@C material, which indicates that the material that plays the role of attenuation is Ni_1Co_2@C. This result also can be explained by attenuation constants. From comparation in Fig. 4.8c, the values of Ni_1Co_2@C are greater than that of EWC-1 from 4GHz, which is easier to attenuate microwave as a lossy layer.

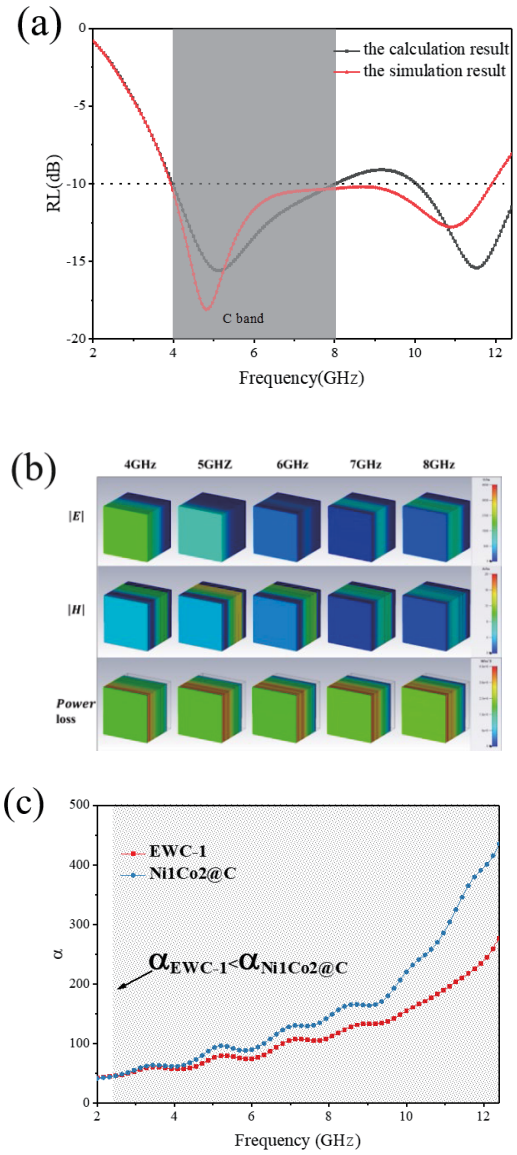

Fig. 4.8. (a) Comparison of RL values between the genetic algorithm design and the simulation results, (b)Simulated electric field, magnetic field and power loss distribution of the optimal multilayer composite, (b) attenuation constant of EWC-1 and Ni_1Co_2@C.

4.7 Conclusion

In this chapter, genetic algorithm and finite element analysis are used to design and optimize multilayer composites. Considering design principle of multilayer composites, the materials EWC-1 and Ni_1Co_2@C synthesized

in above chapters are used as material database of microwave absorption. Firstly, the microwave absorption formula of multilayer structures is obtained according to transmission line theory. By using control variable method, the effect of materials, layer number, thickness and interval distance on the performance of multilayer composites is studied separately. All the parameters are effective for regulating absorption performance in low frequency or broaden absorption band. Then, selected materials and structures are calculated by genetic algorithm to obtain the optimal structure thickness under the condition of full C-band absorption. When EWC-1 is set as front layer for 5-layers structure without interval distance, the composites show whole C-band absorption in 4.71687mm. Finally, the finite element method is used to establish microwave absorption model and the result is consistent with the calculation result. In analysis of electric fields magnetic fields and power loss inside the multilayer material, the results show that the front layers play roles in transmitting and attenuating microwave. Such phenomenon demonstrates that by optimizing the layers and thicknesses of materials with different electromagnetic properties, the composites with whole C-band absorption can be prepared. In a word, it proves that genetic algorithm and computer-assisted method are efficient ways for developing and analyzing multilayer composites in microwave absorption field.

References

[1] Y. Huang, D. Wu, M. Chen, K. Zhang, D. Fang, Evolutionary Optimization Design of Honeycomb Metastructure with Effective Mechanical Resistance and Broadband Microwave Absorption. Carbon, (2021).

[2] Z. Liu, Y. Wang, K. Li, S. Ding, F. Wang, P. Zhang, W. Yang, S. Liu, J. Han, C. Wang, H. Du, J. Yang, Broadband microwave absorber composed of sandwich structure with a lossless medium as the intermediate layer. J Magn Magn Mater, 548 (2022).

[3] S. Ghosh, S. Bhattacharyya, K.V. Srivastava, Design, characterisation and fabrication of a broadband polarisation - insensitive multi - layer circuit analogue absorber. IET Microwaves, Antennas & Propagation, 10 (2016) 850-855.

[4] X. Chen, Z. Wu, Z. Zhang, Y. Zou, Ultra-broadband and wide-angle absorption based on 3D-printed pyramid. Optics & Laser Technology, 124 (2020).

[5] L. Huang, Y. Duan, J. Liu, Y. Zeng, G. Ma, H. Pang, S. Gao, W. Zhang, Bioinspired Gyrotropic Metamaterials with Multifarious Wave Adaptability and Multifunctionality. Advanced Optical Materials, 8 (2020).

[6] F. Luo, D. Liu, T. Cao, H. Cheng, J. Kuang, Y. Deng, W. Xie, Study

on broadband microwave absorbing performance of gradient porous structure. Advanced Composites and Hybrid Materials, 4 (2021) 591-601.

[7] Y. Qing, H. Nan, L. Ma, F. Luo, W. Zhou, Double-layer structure combined with FSS design for the improvement of microwave absorption of BaTiO3 particles and graphene nanoplatelets filled epoxy coating. J Alloy Compd, 739 (2018) 47-51.

[8] J. Zhang, G. Wang, T. Wang, F. Li, Genetic Algorithms to Automate the Design of Metasurfaces for Absorption Bandwidth Broadening. ACS Appl Mater Interfaces, 13 (2021) 7792-7800.

[9] R. Nie, B. He, S. Yan, X. Ma, Optimization design method for the cable network of mesh reflector antennas considering space thermal effects. Aerospace Science and Technology, 94 (2019).

[10] A. Codrignani, D. Savio, L. Pastewka, B. Frohnapfel, R. van Ostayen, Optimization of surface textures in hydrodynamic lubrication through the adjoint method. Tribology International, 148 (2020).

[11] X. Zhu, D. Fan, Z. Xiang, L. Quan, W. Hua, M. Cheng, Systematic multi-level optimization design and dynamic control of less-rare-earth hybrid permanent magnet motor for all-climatic electric vehicles. Applied Energy, 253 (2019).

[12] D. Micheli, R. Pastore, A. Vricella, M. Marchetti, Matter's

Electromagnetic Signature Reproduction by Graded-Dielectric Multilayer Assembly. IEEE Transactions on Microwave Theory and Techniques, 65 (2017) 2801-2809.

[13] D. Micheli, R. Pastore, A. Delfini, A. Giusti, A. Vricella, F. Santoni, M. Marchetti, O. Tolochko, E. Vasilyeva, Electromagnetic characterization of advanced nanostructured materials and multilayer design optimization for metrological and low radar observability applications. Acta Astronautica, 134 (2017) 33-40.

[14] D. Micheli, A. Vricella, R. Pastore, M. Marchetti, Synthesis and electromagnetic characterization of frequency selective radar absorbing materials using carbon nanopowders. Carbon, 77 (2014) 756-774.

[15] T. Liu, P. Zhang, G. Cui, X. Yue, Fracture performance prediction of polyvinyl alcohol fiber-reinforced cementitious composites containing nano-SiO2 using least-squares support vector machine optimized with quantum-behaved particle swarm optimization algorithm. Theoretical and Applied Fracture Mechanics, 115 (2021).

[16] S.O. Fadlallah, T.N. Anderson, R.J. Nates, Artificial Neural Network–Particle Swarm Optimization (ANN-PSO) Approach for Behaviour Prediction and Structural Optimization of Lightweight Sandwich Composite Heliostats. Arabian Journal for Science and Engineering, 46 (2021) 12721-12742.

[17] P. Antil, S. Singh, A. Manna, N. Katal, C. Pruncu, An improvement in drilling of SiCp/glass fiber - reinforced polymer matrix composites using response surface methodology and multi-objective particle swarm optimization. Polymer Composites, 42 (2021) 5051-5064.

[18] X. Ma, K. Tian, H. Li, Y. Zhou, P. Hao, B. Wang, Concurrent multi-scale optimization of hybrid composite plates and shells for vibration. Compos Struct, 233 (2020).

[19] S. Mirjalili, J. Song Dong, A.S. Sadiq, H. Faris, Genetic Algorithm: Theory, Literature Review, and Application in Image Reconstruction, in: Nature-Inspired Optimizers, 2020, pp. 69-85.

[20] H. Eroğlu, M. Aydin, Solving power transmission line routing problem using improved genetic and artificial bee colony algorithms. Electrical Engineering, 100 (2018) 2103-2116.

[21] W. Hou, X. Xu, X. Han, H. Wang, L. Tong, Multi-objective and multi-constraint design optimization for hat-shaped composite T-joints in automobiles. Thin-Walled Structures, 143 (2019).

[22] N.P. Raut, A.B. Kolekar, S.L. Gombi, Optimization techniques for damage detection of composite structure: A review. Materials Today: Proceedings, 45 (2021) 4830-4834.

[23] Z. Ciğeroğlu, G. Küçükyıldız, B. Erim, E. Alp, Easy preparation of magnetic nanoparticles-rGO-chitosan composite beads:

Optimization study on cefixime removal based on RSM and ANN by using Genetic Algorithm Approach. Journal of Molecular Structure, 1224 (2021).

[24] S. Srinivasan, S. Thirumurugaveerakumar, N. Nagarajan, N. Mohammed Raffic, K. Ganesh Babu, A review of optimization techniques in machining of composite materials. Materials Today: Proceedings, 47 (2021) 6811-6814.

[25] H. Luo, F. Chen, X. Wang, W. Dai, Y. Xiong, J. Yang, R. Gong, A novel two-layer honeycomb sandwich structure absorber with high-performance microwave absorption. Composites Part A: Applied Science and Manufacturing, 119 (2019) 1-7.

[26] A. Sotiropoulos, S. Koulouridis, A. Masouras, V. Kostopoulos, H.T. Anastassiu, Carbon nanotubes films in glass fiber polymer matrix forming structures with high absorption and shielding performance in X-Band. Composites Part B: Engineering, 217 (2021).

[27] A. Kasgoz, M. Korkmaz, A. Durmus, Compositional and structural design of thermoplastic polyurethane/carbon based single and multi-layer composite sheets for high-performance X-band microwave absorbing applications. Polymer, 180 (2019).

[28] A. Toktas, D. Ustun, A Triple-Objective Optimization Scheme Using Butterfly-Integrated ABC Algorithm for Design of Multilayer RAM. Ieee T Antenn Propag, 68 (2020) 5602-5612.

[29] J. Chen, J. Zheng, F. Wang, Q. Huang, G. Ji, Carbon fibers embedded with FeIII-MOF-5-derived composites for enhanced microwave absorption. Carbon, 174 (2021) 509-517.

[30] S. Kundu, A. Chatterjee, A compact super wideband antenna with stable and improved radiation using super wideband frequency selective surface. AEU - International Journal of Electronics and Communications, 150 (2022).

[31] M. Rahzaani, G. Dadashzadeh, M. Khorshidi, New technique for designing wideband one layer frequency selective surface in X-band with stable angular response. Microwave and Optical Technology Letters, 60 (2018) 2133-2139.

[32] Q. Zhou, P. Liu, K. Wang, H. Liu, D. Yu, Absorptive frequency selective surface with switchable passband. AEU - International Journal of Electronics and Communications, 89 (2018) 160-166.

[33] K.M. Krishna, A. Jain, H.S. Kang, M. Venkatesan, A. Shrivastava, S.K. Singh, M. Arif, Development of the Broadband Multilayer Absorption Materials with Genetic Algorithm up to 8 GHz Frequency. Security and Communication Networks, 2022 (2022) 1-12.

[34] Y. Liu, R. Tai, M.G.B. Drew, Y. Liu, Several Theoretical Perspectives of Ferrite-Based Materials—Part 1: Transmission Line Theory and Microwave Absorption. J Supercond Nov Magn, 30 (2017) 2489-2504.

[35] B. Bowen, L. Xiaoping, X. Jin, L. Yanming, Reflections of Electromagnetic Waves Obliquely Incident on a Multilayer Stealth Structure With Plasma and Radar Absorbing Material. IEEE Transactions on Plasma Science, 43 (2015) 2588-2597.

[36] J.H.S. Almeida, M.L. Ribeiro, V. Tita, S.C. Amico, Stacking sequence optimization in composite tubes under internal pressure based on genetic algorithm accounting for progressive damage. Compos Struct, 178 (2017) 20-26.

[37] M.V. Pathan, S. Patsias, V.L. Tagarielli, A real-coded genetic algorithm for optimizing the damping response of composite laminates. Computers & Structures, 198 (2018) 51-60.

[38] M.T. Bhoskar, M.O.K. Kulkarni, M.N.K. Kulkarni, M.S.L. Patekar, G.M. Kakandikar, V.M. Nandedkar, Genetic Algorithm and its Applications to Mechanical Engineering: A Review. Materials Today: Proceedings, 2 (2015) 2624-2630.

[39] T. Liu, G. Zou, Evaluation of Mechanical Properties of Materials Based on Genetic Algorithm Optimizing BP Neural Network. Comput Intell Neurosci, 2021 (2021) 2115653.

[40] T.-W. Liu, J.-B. Bai, N. Fantuzzi, G.-Y. Bu, D. Li, Multi-objective optimisation designs for thin-walled deployable composite hinges using surrogate models and Genetic Algorithms. Compos Struct, 280 (2022).

[41] J.-B. Bai, T.-W. Liu, Z.-Z. Wang, Q.-H. Lin, Q. Cong, Y.-F. Wang, J.-N. Ran, D. Li, G.-Y. Bu, Determining the best practice – Optimal designs of composite helical structures using Genetic Algorithms. Compos Struct, 268 (2021).

Chapter 5: Conclusion

Electromagnetic radiation is a common phenomenon in operation of electronic equipment, but it has also become one of serious pollution, causing unpredictable harm to device and life. In recent years, taking advantage of electromagnetic theory and material science knowledge to solve the electromagnetic radiation problem has become one of the research hotspots. Compared with electromagnetic shielding materials, microwave absorption materials can directly absorb microwave and avoid secondary radiation. However, development of communication equipment also needs higher requirements for microwave absorption materials, so traditional materials can not meet requirement. As a kind of dielectric material with light weight and good stability, carbon material shows great potential for absorbing materials. But how to use carbon materials to develop low cost, simple synthesis, wide absorption band, thin thickness and strong absorption capacity of materials still remains a certain challenge. Although the multilayer-structure design is a useful strategy to provide excellent microwave absorption materials, the optimization process is complicated requires high computer performance. In view of these problems, the finding and research results in this dissertation can be remarked as following:

In chapter 1, an overview of development of microwave absorption materials, including definition, analysis theory and carbon materials has been present. Meanwhile, design and simulation on multilayer composites also have been reviewed.

In chapter 2, the magnetic carbon material is prepared by using egg white as carbon and sulfur source while ferric nitrate, cobalt nitrate, nickel nitrate is for alloy source. Samples with different metallic salt content were prepared by mixing, freeze-drying and pyrolysis. According to the measured electromagnetic parameters, microwave absorption properties of samples were calculated by transmission line theory. In comparison, it can be concluded that EWC-1 shows excellent microwave absorption performance (−47.09 dB at 13.8 GHz) at a ultra-thin thickness (1mm)。The analysis of dielectric loss and magnetic loss demonstrates that the sulfur-doped carbon and trimetallic alloy optimize the impedance matching of EWC-1 and provide a strong attenuation capability as well. In a word, egg white is a potential biomass to provide high-performance microwave absorption materials.

In chapter 3, the magnetic carbon materials with different morphologies are prepared by pyrolysis of ZIF materials using a metal-organic framework derivative synthesis method. By changing Ni/Co ratio, microwave absorption properties of samples with different morphologies and compositions are compared. The RL_{min} value -41.9 dB at 12.2 GHz in

1.5 mm and the whole X-band absorption in 2.5 mm can be generated in Ni_1Co_2@C. Finally, the microwave absorption mechanism analyzed by transmission line theory indicates polarization relaxation, conductive loss, eddy current effect and resonance all work in microwave attenuation process. The results indicate that ZIF materials can provide efficient way for development of broadband absorption microwave materials.

In chapter 4, considering that working band of microwave absorption materials is hard to be regulated and optimization is complicated, genetic algorithm is used to select material parameters and analyze attenuation mechanism in multilayer structure with finite element method. Firstly, the effect of single layer thickness, layer number, interval distance and total thickness on microwave absorption property of multilayer structure with the single material are researched. Then genetic algorithm is used to optimize design of nine-layers composites. The optimization results of the whole C-band absorption show that interval distance hardly works. In structures without interval distance, the composite with EWC-1 as the surface layer can achieve the whole C-band absorption at 4.71687mm. Due to the similar results between the model set by COMSOL and the calculation of transmission line theory, the model is used to analyze attenuation mechanism of the multilayer composite. In electromagnetic field analysis, it can be concluded that magnetic field responses are stronger than electric field responses which proves that magnetic loss of

two materials larger than dielectric loss. And the power loss results shows that Ni_1Co_2@C exhibits greater attenuating capability than that of EWC-1. The above results prove that genetic algorithm and finite element method are efficient ways for research and development on novel multilayer microwave absorption composites.

In summary, egg white derived materials and ZIF derived materials has potential to be developed for microwave absorption. The genetic algorithm and finite element analysis are efficient ways to be applied in developing required microwave absorption materials. More efforts should be taken to solve problems existed in microwave absorption field.

List of publication

Li F, Xia H, Ni Q Q. Egg-white-derived magnetic carbon flakes with enhanced microwave absorption properties[J]. Synthetic Metals, 2021, 278: 116827.

Li F, Xia H, Ni Q Q. Co, Ni-coordinated ZIF derived nitrogen doped carbon network with encapsulated alloy for microwave absorption[J]. Diamond and Related Materials, 2021, 120: 108669.

Scientific presentation

Fengyu Li, Hong Xia, Qing-Qing Ni, Egg-white-derived magnetic carbon flakes with enhanced microwave absorption properties. China-Japan Composite Materials Academic and Technology Exchange Conference, Wuhu, China.

Acknowledgements

During the preparation of the doctoral thesis, I have received a lot of invaluable helps from many people. Their comments and advice contribute to the accomplishment of the thesis.

First of all, the profound gratitude should go to my supervisor Professor Qing-Qing Ni. He offered me numerous valuable comments and suggestions with incomparable patience and encouraged me profoundly throughout my doctoral study. Without his painstaking teaching and insightful advice, the completion of this thesis would have been impossible. Meanwhile I also want to thank Dr. Hong Xia giving me help in study and life.

I owe many thanks to Prof. Toshiaki Natsuki, Prof. Yoshio Hashimoto, Prof. Musubu Ichikawa. Their extensive advice and guidance broadened the scope of my knowledge in various research fields.

I greatly appreciate Prof. Weilai Chen, Prof. Yaqin Fu, Prof. Zhu Yaofeng, Prof. Xiaoxi Liu, Prof. Ick-Soo Kim, Prof. chunhong Zhu, Prof. Heng Zhang, Prof. Wei Li for leading me into a challenging but fascinating field of academic research and provide various support. The profit that I gained from them will be of everlasting significance to my future research.

I gratefully thank the support received from technicians in Shinshu University for their help.

Support from my Colleague and friends, Xiaoyu Guan, Jun Hong, Hairong Chen, Yaonan Yu, Baoji Hu, Guangyu Su, Hao Wang, Zhuojun Chen, Zhifeng Sun and Chengbin Gao, help me a lot no matter in research or in life.

Finally, I would like to thank my family especially my parents. They support me all the time at every period of school life.